Receive and Transmit Spatial Modulation Techniques for Low Complexity Devices

Ali Mokh

UNIVERSITE BRETAGNE LOIRE / MATHSTIC

INSA RENNES

THESE DE DOCTORAT DE

L'INSA RENNES

COMUE UNIVERSITE BRETAGNE LOIRE

ECOLE DOCTORALE N° 601
Mathématiques et Sciences et Technologies de l'Information et de la Communication
Spécialité : *Télécommunications*

Par

Ali MOKH

Receive and Transmit Spatial Modulation Techniques for Low Complexity Devices

Unité de recherche : IETR – UMR CNRS 6164

Rapporteurs avant soutenance :

Geneviève Baudoin	Professeur, ESIEE, Paris
Laurent Ros	Maître de conférences, HDR INP, Grenoble

Composition du Jury :

Jean-Pierre Cances	Professeur, ENSIL, Limoges / Président
Geneviève Baudoin	Professeur, ESIEE, Paris / Rapporteur
Laurent Ros	Maître de conférences, HDR, INP, Grenoble / Rapporteur
Marco Di Renzo	Chargé de Recherche, HDR, CNRS CentraleSupelec/ Examinateur
Michel Terré	Professeur, CNAM, Paris / Examinateur
Matthieu Crussière	Maître de conférences, HDR, INSA, Rennes / Co-encadrant
Maryline Hélard	Professeur, INSA, Rennes / Directrice de thèse
Invité	
Dinh-Thuy Phan Huy	Ingénieur, Orange, Châtillon

UNIVERSITE BRETAGNE LOIRE / MATHSTIC

INSA RENNES

Intitulé de la thèse :

Receive and Transmit Spatial Modulation Techniques for Low Complexity Devices

Ali MOKH

En partenariat avec :

"To Find Your Self, Think for Yourself."

Socrates

"They did'nt know it was impossible, so they did it."

Mark Twain

"The most subversive people are those who ask questions."

Jostein Gaarder, Sophie's World

DEDICATION

To my Parents, Wife, Daughter and my friends,

To Hussein Ahmad Akhdar

Declaration of Originality

I, Ali MOKH, declare that this thesis titled, "Receive and Transmit Spatial Modulation Techniques for Low Complexity Devices" and the work presented in it are my own. I confirm that:

- This work was done wholly or mainly while in candidature for a Doctoral degree at the Institut National des Sciences Appliqués de Rennes.
- Where I have consulted the published work of others, this is always clearly attributed.
- Where I have quoted from the work of others, the source is always given. With the exception of such quotations, this thesis is entirely my own work.
- I have acknowledged all main sources of help.
- Where the thesis is based on work done by myself jointly with others, I have made clear exactly what was done by others and what I have contributed myself.

Ali MOKH
Date: 15/11/2018

RÉSUME EN FRANÇAIS

Introduction

Dans la quatrième génération de réseaux cellulaires (4G), le Long-Term Evolution (LTE) et son extension, les systèmes LTE-Advanced, avec une interface radio avancée, comprenant du Multiple-Input Multiple-Output (MIMO), de l'Orthogonal Frequency-Division Multiplexing (OFDM) et des technologies d'ada-ptation de liens, ont été adoptés. Les architectures 4G offrent, en plus des applications voix et données, un accès Internet à très haut débit. De cette manière, des applications exigeant un débit de données élevé sont fournies, telles que les jeux, la télévision haute définition et le cloud computing. Cependant, il y a toujours une augmentation spectaculaire du nombre d'utilisateurs qui s'abonnent chaque année aux systèmes mobiles à haut débit. De plus en plus de personnes recherchent un accès Internet plus rapide en mobilité, des téléphones portables plus modernes et, en général, une communication instantanée avec les autres ou un accès à l'information. Les smartphones et les ordinateurs portables plus puissants sont de plus en plus populaires de nos jours, exigeant des capacités multimédia avancées. D'un autre côté, les réseaux 4G ont pratiquement atteint la limite théorique du débit de données avec les technologies actuelles et ne sont donc pas suffisants pour répondre aux défis susmentionnés. La cinquième génération de réseaux cellulaires (5G) devrait commencer à être deployé vers 2020 et, compte tenu de l'énorme demande de transmission de données entre un grand nombre de périphériques connectés, il est largement admis que, comparé au réseau 4G, le réseau 5G devrait augmenter l'efficacité spectrale, l'efficacité énergétique, le débit de données, et le débit cellulaire moyen [1]. Le but est de connecter le monde entier et d'obtenir des communications transparentes et omniprésentes entre tous (personnes et à personnes), entre tout type de support (machine à machine), où qu'elles soient (n'importe où), à tout moment. L'un des grands défis de la prochaine 5G consiste alors à intégrer le futur réseau cellulaire un trafic de données massif issu de la communication entre les objets.

L'Internet des objets (IoT) est un des mots-clés qui représente une des évolutions de la 5G afin de connecter les objets connectés (CD) au réseau. On s'attend à ce que ces CD soient adaptés et activés avec un comportement autonome et une interconnexion sécurisée, afin d'atteindre le plus haut degré d'intelligence et d'assurer une interopérabilité totale. De plus, les éléments composant l'IoT seront caractérisés par de faibles ressources en termes de calcul et de capacité énergétique [2]. Donc, il est important de prendre en compte la complexité des opérations qui effectuent la transmission entre le CD et le réseau. Ainsi, l'augmentation du débit de données et de l'efficacité spectrale,

tout en minimisant la consommation d'énergie, comptent parmi les éléments clés de conception de futurs systèmes de communication sans fil.

Les coûts élevés du spectre radioélectrique, d'une part, et la consommation de bande passante par les services nécessitant un débit de données élevé, d'autre part, nécessitent des recherches sur des techniques qui augmentent l'efficacité spectrale. Ainsi, ces dernières années, l'exploitation de la dimension spatiale (antennes multiples au niveau du récepteur et /ou de l'émetteur) dans les systèmes radioélectriques a fait l'objet de nombreuses recherches. En ajoutant plusieurs antennes, un degré de liberté supplémentaire (en plus des dimensions temporelle et fréquentielle) dans la transmission sans fil peut être offert pour permettre de transférer davantage de données d'informations. Par conséquent, une amélioration significative des performances peut être obtenue en termes de fiabilité, efficacité spectrale et efficacité énergétique.

Depuis le début des années 2000, la modulation spatiale (SM) s'est imposé comme un principe de transmission prometteur pour les appareils de faible complexité et à faible consommation d'énergie [2]. Les SM exploitent l'index de l'antenne d'émission ou des antennes de réception pour transmettre des bits d'information supplémentaires communément appelés bits spatiaux et symboles spatiaux [3]–[6]. Les premiers schémas SM proposés concernaient les systèmes en boucle ouverte car ils ne nécessitaient aucune connaissance de canal au niveau de l'émetteur (CSIT). Ce sont les schémas de SM à l'émission (TSM). Ils s'appuient principalement sur la stratégie de Space Shift Keying (SSK) [7]. On considère par défaut un système MIMO fortement asymétrique en SM, entre un objet et un station de base. Cette technique pourrait être utilisée pour la transmission de la liaison montante en raison de sa simplicité au niveau de l'émetteur et offre une bonne efficacité spectrale en comparaison des autres schémas de transmission de type Single-Input Single-Output (SISO).

D'autre part, les principes SM peuvent être également transposés du côté du récepteur, ce qui conduit au principe de Receive Spatial Modulation (RSM). Comme introduit dans [8], RSM peut aussi être appelé Transmit Precoding Spatial Modulation (TPSM) car il repose sur une opération de prétraitement ou de pré-codage spatial qui exploite la connaissance du canal à l'émission, afin de cibler une des antennes du récepteur. Par conséquent, contrairement à TSM, qui utilise le concept SSK pour associer les bits d'information aux indices d'antenne d'émission, le RSM effectue une opération pré-SSK pour effectuer l'association sur les indices de l'antenne de réception visée. Une détection très simple est possible au niveau de récepteur pour détecter le symbole spatial [9], [10].

Inspirée par cette technologie, le projet "Modulation Spatiale" est lancé par l'Agence nationale de la recherche (ANR) dont l'objectif est de "concevoir une nouvelle interface d'air pour Internet-des-objets mobile à intégrer dans les interfaces air futures pour les réseaux mobiles (5G) et les WLAN". cette thèse qui fait parti de ce projet, prend en compte une de la partie traitement de signal, et a étudié les performances des schémas SM côté émetteur et récepteur, dans la perspective d'offrir un système de transmission de liaison montante et descendante complet entre la station de base et le CD. Un tel système offre l'avantage d'une complexité de calcul réduite au niveau du CD, et la complexité la plus importante au niveau de la BS, avec une bonne efficacité spectrale.

Chapitre 1 : Etat de l'art

Dans ce chapitre, un bref historique de l'évolution des communications sans fil est présenté. On explique comment l'exploitation de la dimension spatiale permet d'améliorer les performances des systèmes sans fil, ce qui a conduit les chercheurs à s'intéresser aux systèmes de communication MIMO au cours des deux dernières décennies. Le concept des systèmes MIMO et ses avantages sont présentés. Par la suite, en raison du gain de multiplexage en diversité, le concept de Spatial Modulation (SM) est présenté et il est expliqué que celui-ci fournit une transmission économe en énergie en exploitant à la fois la diversité et le gain de multiplexage. Ainsi, l'état de l'art des systèmes SM est structuré en deux parties. Dans la première partie, la technique TSM est présentée, lorsque le principe de SM est utilisé avec ou sans symboles IQ supplémentaires. Un diagramme permet de fournir un aperçu des différents schémas basés sur ce concept et leurs études de performance. Les avantages et les inconvénients de techniques TSM ont également été fournis dans ce chapitre. Dans la deuxième partie, le principe SM de réception est présenté, avec différentes méthodes de précodage. En outre, comme dans le cas TSM, une vue d'ensemble de la recherche publiée sur différents systèmes basés sur le concept de réception SM est fournie.

Chapitre 2 : Receive Antenna Shift Keying

Dans ce chapitre, le schéma de transmission Receive Antenna Shift Keying (RASK) basé sur le concept SM à la réception est évalué. Ici, l'émetteur effectue une étape de prétraitement pour cibler une antenne de réception, résultant en une efficacité spectrale égal : $\log_2(N_r)$, dont l'efficacité spectrale est defini ici d'être le nombre de bit par symbol. Deux méthodes de précodage sont utilisées et comparées : le Zero-Forcing (ZF) et le Maximum Ratio Transmission (MRT). Du côté du récepteur, différents schémas de détection sont proposés pour chaque méthode de précodage et peuvent être classés en deux catégories : détection cohérente et non cohérente. Le premier estime le signal et sa phase, et une synchronisation de la phase entre les antennes est nécessaire, tandis que le second estime uniquement la puissance reçue.

Pour le ZF-RASK tout d'abord, i.e. un système RASK avec un précodage ZF, nous avons démontré de manière analytique que le récepteur optimal peut être réduit à un comparateur, en raison de l'absence d'interférences entre les antennes. En outre, les résultats montrent que la détection cohérente a de meilleures performances mais au prix d'une complexité matérielle supplémentaire au niveau du récepteur, car une chaîne RF complète avec transition en bande de base et conversion analogique numérique est nécessaire pour chaque antenne de réception.

Dans le cas du MRT-RASK, le détecteur ML reste plus complexe et nécessitent une estimation de canal. Nous avons proposé différents détecteurs pour le système MRT-RASK qui ne nécessitent pas d'estimation de canal. La complexité de calcul a été étudiée et comparée, et les dérivations analytiques de la BEP théorique pour certains détecteurs ont été fournies et validées par des simulations. Afin de réduire la complexité matérielle du détecteur cohérent, nous avons proposé d'utiliser des commutateurs sur le récepteur, de sorte que plusieurs antennes de réception soient connectées à une même chaîne RF. Cette méthode entraîne une dégradation du SNR effectif et donc une dégra-

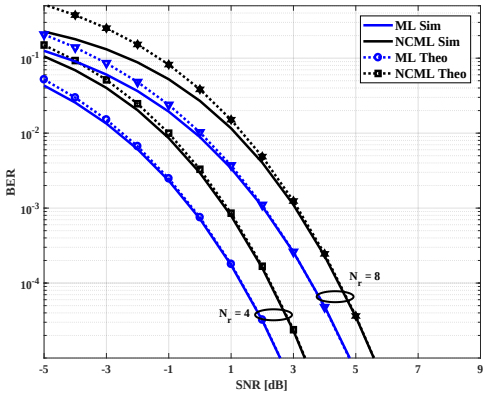

BER performance of 16×4 and 16×8 ZF-RASK systems using CML and NCML detectors over Rayleigh channel, simulated and theoretical results

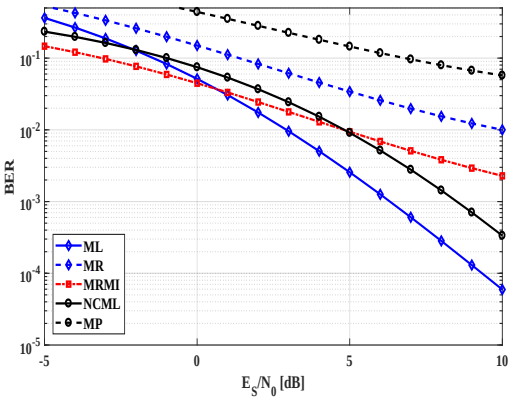

BER performance of 8×4 MRT-RASK systems using all detectors over Rayleigh channel

dation des performances. Ainsi, en fonction du rapport entre le nombre de chaînes RF et le nombre d'antennes de réception, le détecteur non cohérent pourrait surpasser le détecteur cohérent lorsque des commutateurs sont utilisés. Nous avons donc calculé le point d'équivalence qui donne le nombre minimum de chaînes RF nécessaires pour que le détecteur cohérent reste plus performant que le non cohérent. Enfin, le schéma RASK avec pré-codage MRT a été étudié de manière analytique dans un scénario de canal LOS. Les résultats ont été validés par des simulations et une mise en œuvre pratique sur plate-forme radio-logicielle.

Chapitre 3 : Extended Receive Antenna Shift Keying

Dans ce chapitre, nous avons proposé d'augmenter l'efficacité spectrale du RASK. Au lieu de cibler une seule antenne de réception, un nombre variable d'antennes de réception est ciblé pour chaque durée de symbole. Ce nouveau système s'appelle ERASK. Tout d'abord, nous avons présenté le principe du schéma lorsque le précodage ZF est utilisé. Nous avons démontré que le détecteur ML peut être réduit à un détecteur de seuil d'amplitude. Un autre détecteur basé sur un seuil de puissance a également été présenté. Les dérivations analytiques du BEP pour les deux détecteurs sont fournies et validées par des simulations. Par la suite, nous avons étudié l'effet des erreurs d'estimation des canaux et de la corrélation entre les antennes sur les performances de ZF-ERASK, par des dérivations analytiques du BEP et des simulations. De plus, les performances étudiées de l'ERASK lors du précodage MRT sont comparées à celles du ZF-ERASK. Ici, le seuil d'amplitude n'est plus le détecteur optimal, et les résultats montrent que le ZF-ERASK surpasse le MRT-ERASK lorsque le même détecteur est utilisé. En outre, il est montré que plus le nombre d'antennes émettrices est élevé, plus les performances de MRT-ERASK et celle du ZF-ERASK sont proches.

Enfin, nous avons proposé de transmettre des symboles IQ supplémentaires avec le symbole spatial d'ERASK, dans un système appelé Extended Receive Spatial Modulation (ERSM). Comme le système ERASK utilise toutes les combinaisons possibles

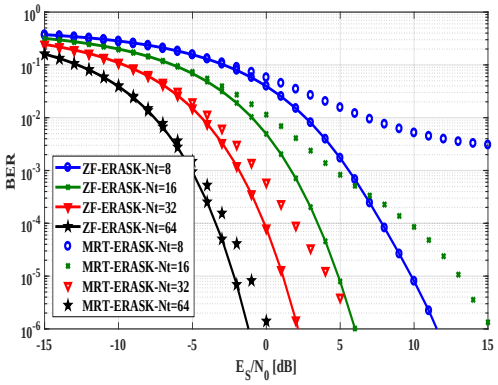

Comparison of the BER performance of MRT-ERASK and ZF-ERASK over a Rayleigh fading channel, N_r=2

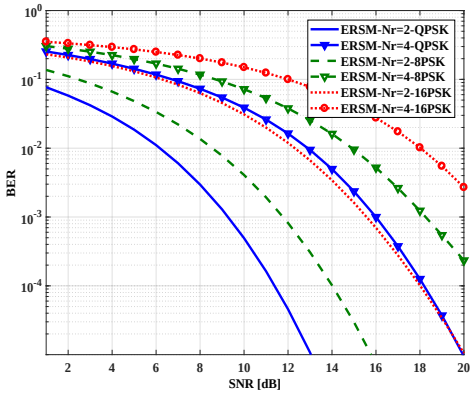

BER vs SNR for a 8×2 and 8×4 MIMO ERSM, for QPSK, 8-PSK, and 16-PSK with Rayleigh fading

d'antennes ciblés, l'une d'entre elles étant de ne pas cibler une antenne de réception, dans ce cas, il est impossible d'envoyer le symbole IQ. Nous avons donc proposé d'utiliser deux niveaux de puissance pour transmettre les deux symboles (symboles spatial et IQ). Nous avons également calculé les performances analytiques du BEP. Un rapport de puissance optimal entre les deux niveaux de puissance minimisant le BEP total a été calculé analytiquement et validé par des simulations. Les résultats montrent que lorsque le rapport optimal est utilisé, les performances de l'ERSM restent les mêmes si nous modifions la configuration du symbole, en modifiant l'ordre de la modulation IQ ou le nombre d'antennes de réception ciblées, tout en conservant la même efficacité spectrale.

Chapitre 4 : Extended Space Shift Keying

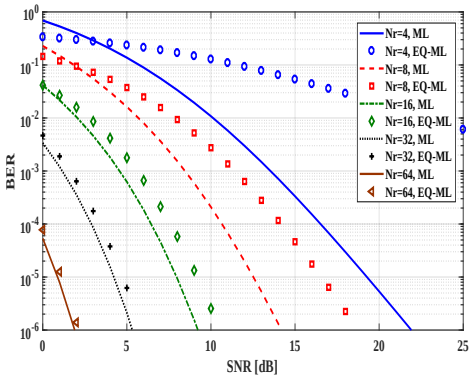

BER performance of 2x8 ESSK system, using ML and EQ-ML detection, theoretical and simulation comparison

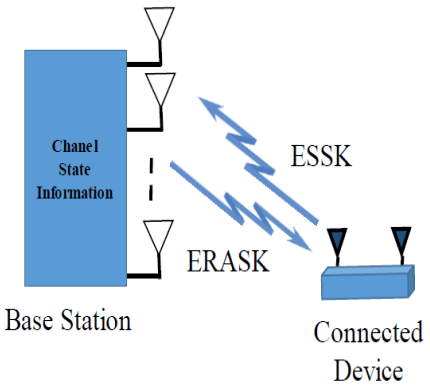

Visualization of the transmission between Base Station and Connected Device

Dans ce chapitre, nous avons proposé un schéma TSM appelé ESSK et analogue au

système ERASK mais appliqué à l'émetteur pour la transmission de liaison montante entre l'objet et la station de base. Un nombre variable d'antennes d'émission est activé afin d'augmenter l'efficacité spectrale globale. Nous avons étudié les performances du schéma dans le canal de Rayleigh en dérivant le BEP analytique lorsque le détecteur ML est utilisé. En outre, nous avons proposé d'implémenter une égalisation au niveau du récepteur pour détecter le symbole, en utilisant la même matrice de précodage dans la transmission descendante pour ERASK. Le résultat montre que le détecteur ML surpasse le détecteur avec égalisation, mais que plus le nombre d'antennes de réception est élevé, plus les performances du détecteur avec égalisation et celles du détecteur ML sont proches. Enfin, nous avons vérifié la dualité d'ESSK et ERASK en liaison montante et descendante, lorsque le détecteur avec égalisation est utilisé. À la fin de ce chapitre, on a proposé un système de transmission entre une station de base et un objet connecté, basé sur le concept de la modulation spatiale, dont la complexité est réduite au niveau de l'objet.

Chapitre 5 : Beamforming Hybrid Pour Receive Antenna Shift Keying en mmWaves

Dans ce dernier chapitre, une étude détaillée de RASK dans les systèmes mmWave a été réalisée, couvrant tous les scénarios possibles analytiquement et numériquement par rapport aux travaux existants dans la littérature. Nous avons proposé d'utiliser un beamformer hybride comprenant un beamformer analogique et un beamformer numérique. Dans le formateur de faisceau analogique, la méthode de formation de faisceaux LoS et la méthode de formation de faisceaux Equal Gain Transmission (EGT) ont été proposées et étudiées, tandis que le précodeur numérique est toujours le précodeur ZF. Nous avons dérivé des expressions pour l'efficacité spectrale dans le cas d'environne-

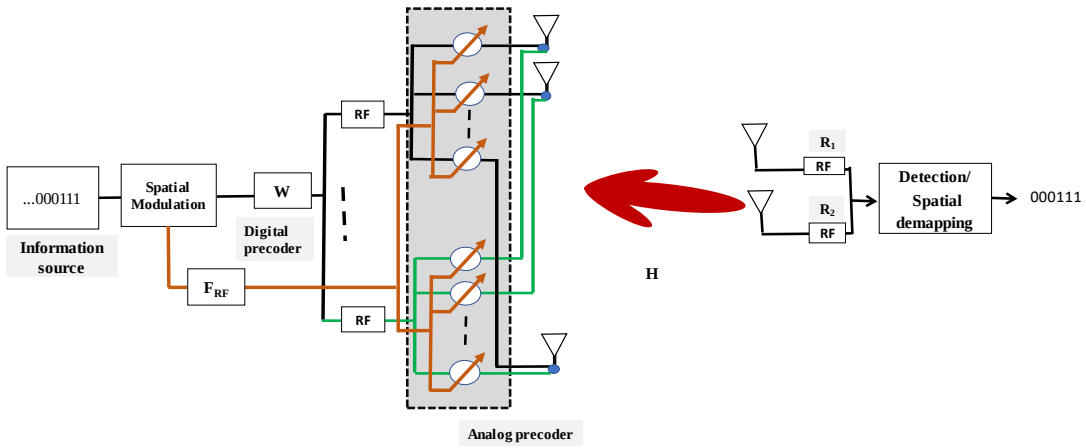

Block Diagram of RASK with Hybrid beamforming

ments de canaux LoS purs pour tout scénario de déploiement possible, étant donné que deux antennes de réception existent et que l'optimisation optimale du déploiement du réseau de transmission est appliquée à la minimisation de corrélation. De même, nous

avons dérivé des expressions pour le BEP dans le cas d'environnements de canaux de type LoS purs pour tout scénario de déploiement possible, étant donné que le récepteur a deux antennes de réception, et qu'un déploiement optimal du réseau de transmission est appliqué pour la minimisation de corrélation. De plus, une expression pour le BEP a été dérivée pour les environnements à trajets multiples rares ainsi qu'une analyse complète des performances réalisables du RASK dans les systèmes mmWave. Tous les modèles introduits ont été validés par analyse numérique.

Conclusion

Dans cette thèse, nous avons évalué les performances des modulations spatiales pour des transmissions vers des objets peu complexes. Des schémas de transmission en liaison montante et en liaison descendante ont été proposés et étudiés sur la base du principe SM. L'objectif principal était de minimiser la complexité de l'appareil connecté tout en offrant de bonnes performances en terme d'efficacité spectrale et de BEP. Plus spécifiquement, nous avons évalué les performances du schéma RASK en utilisant différentes méthodes de précodage et différents schémas de détection. En outre, le système RASK a été étudié pour des transmissions sur canaux de Rayleigh, de type LoS, ainsi que dans un environnement mmWave en utilisant la formation de faisceau hybride. De plus, un schéma étendu de RASK appelé ERASK a été proposé et étudié dans le but d'augmenter l'efficacité spectrale tout en conservant une détection de faible complexité sur l'objet connecté. En outre, un schéma analogue au système ERASK pour la transmission en liaison montante, appelé ESSK, a été proposé et étudié. Dans la suite, un résumé des principales contributions et conclusions de la thèse est fourni. Enfin, nous avons proposé de transmettre des symboles IQ supplémentaires avec le symbole spatial d'ERASK, appelé ERSM. Mais comme l'ERASK utilise toutes les combinaisons possibles d'antennes cibles, l'une d'entre elles étant de ne pas cibler une antenne de réception, dans ce cas, il est impossible d'envoyer le symbole IQ. Nous avons donc proposé d'utiliser deux niveaux de puissance pour transmettre les deux symboles (symboles spatial et IQ). Nous avons également calculé les performances analytiques du BEP. Un rapport de puissance optimal entre les deux niveaux de puissance minimisant le BEP total a été calculé analytiquement et validé par des simulations. Les résultats montrent que lorsque le rapport optimal est utilisé, les performances de l'ERSM restent les mêmes si nous modifions la configuration du symbole, en modifiant l'ordre de la modulation IQ ou le nombre d'antennes de réception ciblées, tout en conservant la même efficacité spectrale.

Acknowledgments

Firstly and foremost, I would like to express my sincere thanks, appreciation, and deepest gratitude to the supervisors of my PhD studies, Professor Maryline Helard and Dr. Matthieu Crussiere.

They gave me the opportunity to pursue my PhD degree, which had been one of my most desirable dreams until this moment. Therefore, the volume of my gratitude for this is unlimited. During my PhD studies, Prof Helard and Dr Crussiere were the best example of academic excellence who inspired me the most. Their insightful advice and technical guidance have shaped the way of my thinking in the most positive direction. Thank you for everything.

I am really grateful to my research coauthors during my PhD studies, Dr. Marco Di Renzo, Dr. Yvan Kokar, and Dr. Mohammad Shehata. Each one of them helped me in the most valuable way. Marco helped me to increase my research level ta a higher level thanks to his advice and technical support. Yvan simplified the way to understand some technical limitations of the implementation, and we had a great collaboration using his platform and my theoretical results. Shehata really helped me in the last stage of my PhD. Our discussions enabled me to produce the best results. My research would not be the same without them. Thank you for this.

Many thanks to Mr. Francois Yven and my fellow intern Mr. Mohammad Alawieh for helping me in evaluating my work with a practical implementation. Francois worked hard to get the platform to our lab, and Mohammad did a wondefull job in 6 months to provide a successful proof of concept. Thank you guys!

A special thanks to Saja Takache, my wife's sister, for proofreading parts of my publication. She positively affected my style of writing in an invaluable way. Thank you very much Saja.

Furthermore, I would like to acknowledge the nancial support of the French National Agency of Research. The work presented in this thesis was supported by the ANR's project "Spatial Modulation". In addition, I would like to thank all the people of the Spatial Modulation project for our three-year fruitful collaboration. The ofce hours during the past years have been uncountable. However, due to my ofce friends, Ahmad Shokair, Ahmad Jabban, Yehya Nasser, Wael Ayyoub, Maryam Al Hassan, Marwan Hajj, Ferdaous Mattusi, Hassan Haddad, Samara Gharbieh and Mohammad Rihani. With them, I have some really nice memories. In addition to this, they were always available for short or even longer technical discussions. Thank you all. Furthermore, many special thanks go to my Rennes friends, Mohammad Amhaz, Ali El Amine, Rachelle Hazimeh, Alaa Kobeissy, Ali Fahs, Adham Gamal, Alaa Noureddine, and Abass Madi.

Their presence made the already beautiful Rennes even more beautiful.

Last but not least, I would like to express my gratitude and love to the most valuable people of my life, my family. Starting with my parents in law, who came from Lebanon to support me in my PhD defense and took care of my wife and newborn daughter during my preparation of the manuscript. Thank you very much! For my parents, they provided me with love and support in every possible way. I could never succeed in anything without them. They really shaped my values, character and ethics. What I feel and what I owe to them cannot be expressed with minor things like words. Finally, a big and special thanks to the loves of my life, my wife Sakina and my daughter Fatima. In addition to your support all the time, technically and emotionally, I should say that because of you I am so happy to have this work done. Thank you darlings.

To anyone I may have missed in these acknowledgments, it is the mild weather that often misses the news, despite how much it comforts us, and how necessary it is for our functionality. To the pleasant breezes and soft rays of sun, I also owe a great thank you.

Contents

List of Figures

List of Tables

Notations

Nomenclature

- $\mathbf{A}$: matrix
- $\mathbf{a}$: vector
- a_i : $i-th$ element of $\mathbf{a}$
- a : scalar

Operators

- $Q(.)$: Gaussian distribution function
- $[\mathbf{A}]^H$: Trans-conjugate of the matrix $\mathbf{A}$
- $[\mathbf{A}]^T$: Transpose of the matrix $\mathbf{A}$
- $[\mathbf{A}]^*$: Conjugate of the matrix $\mathbf{A}$
- $\mathrm{Tr}[\mathbf{A}]$: Trace of the matrix $\mathbf{A}$
- $\mathbb{E}_k$: Expectation over k
- $\lceil a \rceil$: Ceil of a
- $\lfloor a \rfloor$: Floor of a
- $\Re\{.\}$: Real part
- $\Im\{.\}$: Imaginary part
- Arg : Argument
- det(.) : determinant
- $\mathcal{CN}(.,.)$: Complex Gaussian distribution
- $d(\mathbf{x}_k, \mathbf{x}_j)$: Hamming distance between $\mathbf{x}_k$ and $\mathbf{x}_j$

Symbols

- m : number of bits per symbol
- k : index of targeted antenna
- f : normalization factor
- M : order of M-order modulation
- I : number of paths
- γ : Power Ratio
- $\bar{\tau}$: Switching factor
- E_s : Symbol energy
- N_r : Number of receive antennas
- N_t : Number of transmit antennas
- N_a : Number of active or targeted antennas
- N_S : Number of switches
- N_{RF} : Number of RF chains
- σ_n : standard deviation of noise
- σ_H : standard deviation of channel estimation error
- σ_I : standard deviation of interference
- $\mathcal{C}$: capacity
- P_t : total transmit power
- $\mathbf{P}_k$: Power allocation vector to send the *k-th* spatial symbol
- $p_{i,k}$: power allocation level to the *i-th* receive antenna when the *k-th* symbol is transmitted
- $\bar{\Lambda}$: transmit spatial correlation
- d_t : inter-element antenna spacing at the transmitter
- d_r : inter-element antenna spacing at the receiver
- D : Distance between the transmitter and the receiver
- D_s : Symbol rate
- B : Bandwidth
- T_i : i-th transmission antenna

- R_j : j-th receive antenna
- $h_{j,i}$: complex channel coefficient
- $w_{j,i}$: complex precoding matrix coefficient
- λ_j : *j-th* eigenvalue of the channel matrix
- λ_j^H : *j-th* eigenvalue of the channel matrix $\mathbf{H}$
- $\lambda_j^{H_e}$: *j-th* eigenvalue of the equivalent channel matrix $\mathbf{H}_e$
- λ_{max} : the maximum eigenvalue of the channel matrix
- λ^w : the wavelength
- y_j : The received baseband signal at the j-th receive antenna
- r : The received baseband signal in SISO
- α_i : complex gain associated with the *i-th* path in SISO
- $\alpha_{k,i}$: complex gain associated with the *i-th* path received by the *k-th* receive antenna
- η_j : complex Gaussian noise at receive antenna j
- $\theta_{k,p}$: angle of departure for path p of receive antenna R_k
- $\Delta\theta$: angular difference between two paths
- ρ : received SNR
- ρ_t : transmit spatial correlation factor
- ρ_r : receive spatial correlation factor
- ϕ : phase of received signal
- ν : Detection threshold
- $\mathcal{P}_e$: Binary error probability
- $\mathcal{P}(x)$: Probability of x
- $\mathbf{s}$: The transmitted baseband signal
- $\mathbf{z}$: vector of equalized received signal
- $\mathbf{s}_k$: The transmitted baseband signal when sending *k-th* spatial symbol
- $\mathbf{y}$: The receive baseband signal vector
- $\mathbf{x}$: symbol vector
- $\mathbf{x}_k$: symbol vector when sending *k-th* spatial symbol

- $\mathbf{h}_k$: channel vector associated to the *k-th* receive antenna
- $\mathbf{f}_k$: Analog beamforming vector associated to the *k-th* receive antenna
- $\mathbf{f}_{LoS}$: Analog LoS beamforming vector
- $\mathbf{f}_{EGT}$: Analog Equal Gain Transmission beamforming vector
- $\mathbf{n}$: complex Gaussian noise vector
- $\mathbf{a}_t$: transmit array steering vector
- $\mathbf{H}$: MIMO baseband channel matrix
- $\bar{\mathbf{H}}$: average long term CSI that is accuratly estimated at the transmitter
- $\tilde{\mathbf{H}}$: instantaneous CSI deviation matrix
- $\mathbf{H}_I$: Channel matrix with independent entries
- $\mathbf{R}_t$: transmit spatial correlation matrix
- $\mathbf{R}_r$: receive spatial correlation matrix
- $\mathbf{H}_e$: MIMO baseband equivalent channel matrix after analog beamforming
- $\mathbf{P}$: MIMO hybrid beamforming matrix
- $\mathbf{W}$: MIMO baseband precoding matrix
- $\mathbf{F}_{RF}$: analog beamformer
- $\mathbf{I}_{N_r}$: $N_r \times N_r$ identity matrix
- $\mathbf{U}$: unitary matrix for SVD precoding in channel $\mathbf{H}$
- $\mathbf{V}$: unitary matrix for SVD postcoding in channel $\mathbf{H}$
- $\mathbf{\Lambda}$: Diagonal matrix of eigenvalues of the channel matrix $\mathbf{H}$
- $\mathbf{U}_e$: unitary matrix for SVD precoding in equivalent channel $\mathbf{H}_e$
- $\mathbf{V}_e$: unitary matrix for SVD postcoding in equivalent channel $\mathbf{H}_e$
- $\mathbf{\Lambda}_e$: Diagonal matrix of eigenvalues of the equivalent channel matrix $\mathbf{H}_e$

List of Abreviations

- **2G** : Second Generation of cellular network
- **3G** : Third Generation of cellular network
- **4G** : Fourth Generation of cellular network
- **5G** : Fifth Generation of cellular network
- **ABEP** : Average Bit Error Probability
- **AM** : Amplitude Modulation
- **AoD** : Angle of Departure
- **AWGN** : additive white Gaussian noise
- **BB** : Base Band
- **BEP** : Bit Error Probability
- **BER** : Bit Error Rate
- **BIM** : Beam Index Modulation
- **BS** : Base Station
- **CD** : Connected Device
- **CDMA** : Code-Division Multiple Access
- **CSI** : Channel State Information
- **CSIR** : Channel State Information at the Receiver
- **CSIT** : Channel State Information at the Transmitter
- **DFT** : Discrete Fourier Transform
- **EE** : Energy Efficiency
- **EGT** : Equal Gain Transmission
- **ERASK** : Extended Receive Antenna Shift Keying

- **ERSM** : Extended Receive Spatial Modulation
- **ESNR** : Effective Signal to Noise Ratio
- **ESSK** : Extended Space Shift Keying
- **FDM** : Frequency-division multiplexing
- **FDMA** : Frequency-Division Multiple Access
- **FFT**: Fast Fourier Transform
- **FM** : Frequency Modulation
- **GPSM** : Generalised Precoding Spatial Modulation
- **GRASK** : Generalised Receive Antenna Shift Keying
- **GSM** : Generalised Spatial Modulation
- **GSSK** : Generalised Space Shift Keying
- **IAI** : Inter-Antenna Interference
- **ICI** : Inter-Carrier Interference
- **IMT-A** : International Mobile Telecommunications-Advanced
- **IoT** : Internet-of-Things
- **ISI** : Inter-Symbol Interference
- **LoS** : Line of Sight
- **LTE** : Long-Term Evolution
- **MIMO** : Multiple-Input Multiple-Output
- **MISO** : Multiple-Input Single-Output
- **ML** : Maximum Likelihood
- **MMSE** : Minimum Mean Square Error
- **mmWave** : Millimeter Wave
- **MRC** : Maximum Ratio Combining
- **MRMI** : Maximum Real Minimum Imaginary
- **MRT** : Maximum Ratio Transmission
- **MTs** : Mobile Terminals
- **MU** : Multiuser
- **OFDMA** : Orthogonal Frequency-Division Multiple Access

- **OFDM** : Orthogonal Frequency-Division Multiplexing
- **PEP** : Pairwise Error Probability
- **PSK** : Phase Shift Keying
- **PT** : Power Threshold
- **RASK** : Receive Antenna Shift Keying
- **RAT** : Real Amplitude Threshold
- **RF** : Radio Frequency
- **RSM** : Receive Spatial Modulation
- **SDM** : Space-division multiplexing
- **SDMA** : Space-Division Multiple Access
- **SE** : Spectral Efficiency
- **SEP** : Symbol Error Probability
- **SER** : Symbol Error Rate
- **SISO** : Single-Input Single-Output
- **SM** : Spatial Modulation
- **SMX** : Spatial Multiplexing
- **SNR** : Signal to Noise Ratio
- **SSK** : Space Shift Keying
- **STBC** : Space-Time Bloc Coding
- **STC** : Space-Time Coding
- **SVD** : Singular Value Decomposition
- **TDD** : Time-Division Duplexing
- **TDM** : Time-Division Multiplexing
- **TDMA** : Time-Division Multiple Access
- **TPSM** : Transmit Precoding Spatial Modulation
- **TR** : Time Reversal
- **TSM** : Transmit Spatial Modulation
- **ULA** : Uniform Linear Array
- **ZF** : Zero-Forcing

Chapter 1

General Introduction

1.1 Introduction

Passing from Base Band (BB) communication to higher frequency modulated signals, was the first major evolution in wireless communications in 1933. The reason was to avoid the interference and band limitation when multiple ends to end communications are implemented. Each user can have its own frequency band. In the Second Generation of cellular network (2G), one of the main difference was the use of digital communication in 1991. This evolution enables the transmission of data services such as text messages and pictures, as well as the digital encryption. The Code-Division Multiple Access (CDMA) and Time-Division Multiple Access (TDMA) are used to multiplex signals of different users. In the Third Generation of cellular network (3G), released in 2001, the wireless mobile network has transformed from a pure telephony system to a network that can transport rich multimedia contents. Especially for data services, the aim of 3G is to accommodate high data rate demanding applications such as mobile and fixed Internet access, video calls, and mobile television. Also, TDMA and CDMA are still used for user multiplexing in 3G, in addition to Frequency-Division Multiple Access (FDMA) and Orthogonal Frequency-Division Multiple Access (OFDMA).

In the Fourth Generation of cellular network (4G), the wireless systems were designed to fulfill the requirements of International Mobile Telecommunications-Advanced (IMT-A) using IP for all services [11]. The adopted system for the 4G is the Long-Term Evolution (LTE) and its extension, LTE-Advanced systems, with an advanced radio interface, OFDM, MIMO, and link adaptation technologies. The 4G architectures offer, in addition to the existing voice and data applications of 3G, ultra-broadband Internet access. In this way, high data rate demanding applications are provided, such as gaming, high-definition television, and cloud computing.

However, there is still a dramatic increase in the number of users who subscribe to mobile broadband systems every year. More and more people crave faster Internet access on the move, trendier mobiles, and, in general, instant communication with others or access to information. More powerful smartphones and laptops are becoming more popular nowadays, demanding advanced multimedia capabilities.

On the other hand, 4G networks have just about reached the theoretical limit on the data rate with current technologies and therefore are not sufficient to accommodate the above challenges. The Fifth Generation of cellular network (5G) network is expected

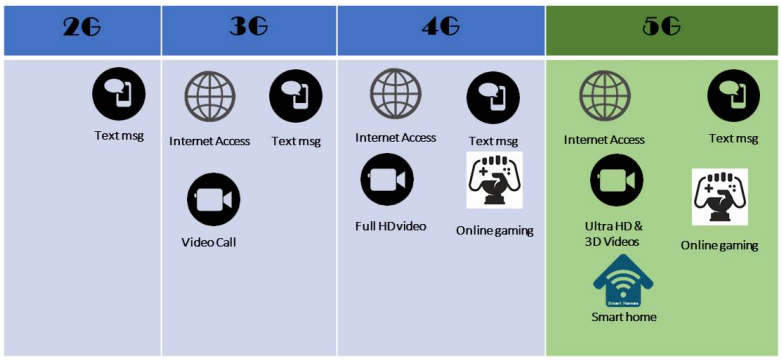

Figure 1.1 – Evolution of cellular networks generations

to be standardized around 2020, and regarding the huge demand of data transmission between a large number of connected devices, it is widely agreed that compared to the 4G network, the 5G network should achieve 1000 times the system capacity, 10 times the spectral efficiency, energy efficiency and data rate, and 25 times the average cell throughput [1]. The aim is to connect the entire world, and achieve seamless and ubiquitous communications between anybody (people to people), anything (people to machine, machine to machine), wherever they are (anywhere), whenever they need (anytime), by whatever electronic devices/services/networks they wish (anyhow). Figure 1.1 shows a part of the evolution of services provided by different cellular network generation. One big challenge of the next 5G is then to accommodate the future cellular network with massive data traffic issued from machine type communication.

Internet-of-Things (IoT) is the keyword that represents the evolution in 5G that is able to connect the so-called Connected Device (CD) to the network. It is expected that those CD are adapted and enabled with autonomous behavior, and secure interconnection, to achieve the higher degree of smartness making a full interoperability.

Moreover, things composing the IoT will be characterized by low resources in terms of both computation and energy capacity [2]. Accordingly, it is important to pay attention to the complexity of operations that are making the transmission between the CD and the network.

As result, increasing the data rate and the Spectral Efficiency (SE), whilst minimizing energy consumption, are some of the key elements that drive research for designing future wireless communication systems.

The high costs for radio spectrum, on the one hand, and the bandwidth-consuming by services that need high data rate, on the other hand, require research in techniques that improve the SE considerably. Therefore, in recent years, the exploitation of the spatial dimension (multiple antennas at the receiver and/or multiple antennas at the transmitter) in radio systems have been subject to investigation by many researchers [12].

MIMO systems consist of multiple antennas at both the transmitter and/or receiver. By adding multiple antennas, a greater degree of freedom (in addition to time and frequency dimensions) in wireless channels can be offered to accommodate more information data. Hence, a significant performance improvement can be obtained in terms of reliability, SE, and Energy Efficiency (EE). In massive MIMO systems, the transmitter

and/or receiver are equipped with a large number of antenna elements (typically tens or even hundreds). The enormous number of receive antennas can be possessed by one device or distributed to many devices. Besides inheriting the benefits of conventional MIMO systems, a massive MIMO system can also significantly enhance both SE and EE. Furthermore, in massive MIMO systems, the effects of noise and fast fading vanish, and intracell interference can be mitigated using simple linear precoding and detection methods.

Since the early 2000s, SM has established itself as a promising transmission concept for low complexity devices and low power consumption [2]. SM exploits the index of transmit antenna or receive antennas to transmit additional information bits commonly referred to as spatial bits and spatial symbols [3]–[6].

The first proposed SM schemes concerned open loop systems because they required no Channel State Information at the Transmitter (CSIT). They are called Transmit Spatial Modulation (TSM) schemes and mainly relies on Space Shift Keying (SSK) strategies [7]. This technique could be used for uplink transmission because of its simplicity and offers a good SE compared to the other SISO transmission schemes. On the other side, when MIMO system has more transmit antennas than receive antennas, just like the downlink transmission between Base Station (BS) and the user, then, its capacity when operated under the CSIT mode may be much higher than that when operated under the Channel State Information at the Receiver (CSIR) mode [13]. For this reason, SM principles can be transposed at the receiver side, leading to the RSM concept. As introduced in [8], RSM can also be referred to as TPSM since it relies on a preprocessing or spatial pre-coding operation that exploits the CSIT, so as to target one of the antennas of the receiver. Hence, in contrast to TSM, which uses the SSK concept to map the information bits to the transmit antenna indices, RSM carries out a kind of pre-SSK operation to map them to the indices of the receive antenna. A very simple detection is needed at the receiver to detect the spatial symbol [9], [10]. Inspired by this technology, the project "Space Modulation" is launched by the National Research Agency (ANR) whose objective is "to design a new air interface for mobile Internet-of-the-objects to be integrated into future air interfaces for networks mobiles (5G) and WLANs". This thesis, which is part of this project, takes into account one of the signal processing part, and studied the performance of SM schemes at the transmitter and receiver side, that could offer a complete uplink and downlink transmission system between the BS and CD that provide a low computation complexity at the CD while it is maintained at the BS, with good SE.

1.2 Contributions

Different contributions have been made in this thesis in order to evaluate the performance of the SM to be used for low complexity devices in uplink and downlink transmission. In general, We focused on the performance of different schemes with different detection algorithms, and in multiple channel scenarios. The computational complexity has been also taken into account.

In the first contribution, we started with the SM at the receiver, with an existing scheme called RASK to be evaluated. Here, the transmitter performs a preprocessing step to target one receive antennas, resulting in an SE equal to $\log_2(N_r)$. Two precoding

methods are used and compared in our framework that is ZF and MRT. At the receiver side, different detection schemes are proposed, for each precoding method, and could be categorized into two categories: coherent and non-coherent detection. The first one estimates the signal and its phase, and so a phase synchronization between antennas is needed, while the second one only estimates the received power. We derived the theoretical BEP conditioned by the channel for some detectors, to evaluate its performance. For ZF RASK, we demonstrated analytically that the optimal receiver can be reduced to a single tap detector, because of the interference cancellation. Also, results show that the coherent detection has better performance but in the cost of additional hardware complexity at the receiver, since a down converter is needed for each receive antenna. In order to reduce the hardware complexity of the coherent detector, we proposed to use switches at the receiver, so that multiple receive antenna are connected to one RF chain. This method leads to a degradation in the effective SNR, and so a degradation in performance. Thus, depending on the ratio of the number of RF chain to the number of the receive antenna, the non-coherent detector could outperform the coherent detector when switches are used. So, we calculated the equivalence point that gives the minimum number of RF chains needed so that the coherent detector stay more performante than the non-coherent one. For MRT RASK, the ML detector remains more complex and needs channel estimation. We proposed different detectors for MRT RASK that doesn't need channel estimation. The computation complexity was studied and compared, and analytical derivations the theoretical BEP for some detectors was provided and validated through simulations. Finally, the RASK scheme with MRT precoding was analytically studied under LOS channel scenario. Results were validated through simulations and practical implementation.

In the second contribution, we proposed to increase the SE of the RASK, so instead of targetting one receive antenna, a variable number of receive antenna are targeted each symbol duration. This novel scheme is called ERASK. First, we presented the concept of the scheme, when the ZF precoding is used. We demonstrated that the ML detector is reduced to an amplitude threshold detector. With the ML, another detector that is based on a power threshold was also presented. The analytical derivations of the BEP for the two detectors are provided and validated through simulations. Afterward, we studied the effect of error in channel estimation and the correlation between antennas on the performance of ZF ERASK, by analytical derivations of the BEP and simulations. Moreover, the studied the performance of the ERASK when the MRT precoding is used, to be compared with the ZF ERASK. Here, the amplitude threshold is no more the optimal detector, and results show that the ZF ERASK outperforms the MRT ERASK when the same detector is used. Also, it is showed that the more the number of transmit antennas is, the closer the performance of MRT ERASK to ZF ERASK is. Finally, we proposed to transmit additional IQ symbools with the spatial symbol of ERASK, called ERSM. But since ERASK use all possible combinations of targetting antennas, and one of them is to not targetting any receive antenna, in this case, it is impossible to send the IQ symbol. So we proposed to use two power levels to transmit the two symbols (spatial and IQ symbols). we derived also the analytical performance of the BEP. An optimal power ratio between the two power levels that minimize the total BEP, was derived analytically and validated by simulations. Results show that when the optimal ratio is used, the performance of ERSM remains the same if we change the configuration of the symbol, by changing the order of IQ modulation or the number of

targeted receive antennas, but keeping the same SE.

In the third contribution, we proposed an analog scheme to ERASK at the transmitter for the uplink transmission, called ESSK. A variable number of transmit antennas is activated in order to increase the overall SE. We studied the performance of the scheme in Rayleigh channel by deriving the analytical BEP when ML detector is used. Also, we proposed to implement an equalization at the receiver to detect the symbol, by using the same matrix of precoding in the downlink transmission for ERASK. The result shows that ML detector outperforms the equalized detector, but the more the number of receive antennas, the closer the performance of equalized detector to the ML is. Finally, we proofed the duality of ESSK and ERASK in uplink and downlink, when the equalized detector is used.

In the fourth and last contribution, a detailed study for RASK in mmWave systems was given, covering all possible scenarios analytically, and numerically compared to the existing work in the literature. We proposed to use hybrid beamformer with analog and digital beamformer. In analog beamformer, LoS beamsteering and EGT beamforming method where proposed and studied, while the digital precoder is always the ZF precoder. We derived closed-form solutions for the SE in case of pure LoS channel environments for any possible deployment scenario, given that two receive antennas exist, and optimal transmit array deployment optimization is applied for correlation minimization. Similarly, we derived closed-form solutions for the BEP in case of pure LoS channel environments for any possible deployment scenario, given that two receive antennas exist, and optimal transmit array deployment is applied for correlation minimization. Moreover, a closed form solution for the BEP was derived for sparse multipath environments as well to have a complete analysis for the achievable performance of the RASK in mmWave systems. All the introduced models were validated with numerical analysis.

1.3 Thesis Outline

In this section, we will give the outline of this thesis. In **Chapter 2**, a brief history of the evolution of wireless communication is provided. It is explained why the exploitation of the spatial dimension to enhance the performance of wireless systems leads the researches to be interested in MIMO communication systems during the last decades. The concept of MIMO systems and its advantages are presented. Afterward, because of the trade-off diversity-multiplexing gain, the concept SM scheme is presented, and it is explained why SM provide an energy efficient transmission because of the exploitation of both diversity and multiplexing gain. Thus, the state of art of SM was given in two part. The first one talk about the transmit SM, where the concept of SM with or without additional IQ symbols is presented, as well as the block diagram, with an overview on different schemes that are based on this concept with their performance studies. Advantages and disadvantages of SM were also provided in this chapter. In the second part, the receive SM is presented, with different precoding methods. Also, as for transmit SM, an overview of the published research of different schemes that are based on receive SM concept are provided.

In **Chapter 3**, the RASK scheme is studied using ZF and MRT precoding. Different detection scheme associated with each precoding method are provided. Performance

analysis of the BEP is provided for some detectors, and confirmed by simulations. The computational complexity was also studied to classify different detectors. We also proposed to use switches at the receiver in order to reduce the hardware complexity when a coherent detector is used. Analytical derivations showed that for ZF RASK, the ML detector could be reduced to a Single Tap detector. Also, it is shown that the coherent detection has lower BER than the non-coherent, but when switches are used for the coherent detector, its performance degrades. Finally, the performance of MRT RASK was analytically studied under LOS channel scenario and validated through simulations and practical implementation.

In **Chapter 4**, the novel scheme ERASK that was proposed to improve the SE of spatial modulation at the receiver side to N_r, by allowing a transmission towards a variable number of receive antennas simultaneously, was presented. It is demonstrated that when the ZF precoding is used, the ML detection is reduced to a simple amplitude threshold. A power threshold detector was also presented with the ML. The expected theoretical performance of the two detectors is provided. Also, the effect of error in channel estimation and the effect of correlation between antenna where studied. In addition, the ERASK with MRT precoding was presented and compared to the ZF ERASK. Finally, the ERSM scheme, that allows the transmission of ERASK and IQ symbols simultaneously, was studied, and the optimal ratio of power levels was calculated, to give the better performance.

In **Chapter 5**, the novel scheme Extended Space Shift Keying (ESSK) that is analog to the ERASK at the transmitter for the uplink transmission of a device connected to a base station was presented. It is demonstrated how the ESSK provides an SE equal to N_t, which is the number of receive antennas in downlink when ERASK is implemented. Two detection strategies are presented, the ML detector and the ZF equalized ML. Theoretical performance of the two detectors is provided. Results show that the ML detector outperforms the equalized detector, but the more the number of transmit antennas increases, the smaller the difference in performance is. Thus, we demonstrated the duality in performance between ERASK, and ESSK such that the equalized detector is implemented. Finally, an Uplink and Downlink transmission system between a base station and a connected device based on the extended SM has been proposed, and we showed how the computational complexity is reduced at the connected device.

In **Chapter 6**, a novel framework considering the RASK technique with hybrid beamforming in a Millimeter Wave (mmWave) propagation environment is presented. The channel model was described, followed by the beamforming strategies, where a combination of analog beamforming and digital precoding is performed. A closed-form solution for the SE in case of pure LoS channel environments for any possible deployment scenario is derived, given that two receive antennas exist, and optimal transmit array deployment optimization is applied for correlation minimization. Moreover, the BEP performance of the framework is analytically and numerically studied with a maximum likelihood detector. All the theoretical and numerical analyses are done for the pure Line of Sight (LoS) channel environment and sparse multi-path channels in order to fully characterize high-frequency environments such as mmWave systems. All the introduced models were validated with numerical analysis.

Finally, in **Chapter 7**, summury of all contributions in this thesis with results is provided. We presented also some propositions to be provided in future works.

1.4 List of Publications

Journal Paper

1. **A. Mokh**, M. Crussiere, M. Helard, and M. D. Renzo, “Theoreticalperformance of coherent and incoherent detection for zero-forcingreceive antenna shift keying”,IEEE Access, 2018.

International Conferences

2. **A. Mokh**, Maryline Helard, and Matthieu Crussiere. "Space Shift Keying Modulations for Low Complexity Internet-of-Things Devices." GLOBECOM 2017-2017 IEEE Global Communications Conference. IEEE, 2017.

3. **A. Mokh**, Maryline Hélard, and Matthieu Crussiere. "Extended Receive Spatial Modulation MIMO scheme for Higher Spectral Efficiency." 2018 IEEE 87th Vehicular Technology Conference. 2018.

4. **A. Mokh**, Matthieu Crussière, and Maryline Hélard. "Performance analysis of extended RASK under imperfect channel estimation and antenna correlation." Wireless Communications and Networking Conference (WCNC), 2018 IEEE. IEEE, 2018.

5. **A. Mokh**, Maryline Hélard, and Matthieu Crussière. "Extended receive antenna shift keying." International Conference on Telecommunications. 2017.

6. **A. Mokh**, Matthieu Crussière, and Maryline Hélard. "Performance analysis of the maximum ratio transmission preprocessing for extended receive antenna shift keying." Wireless Personal Multimedia Communications (WPMC), 2017 20th International Symposium on. IEEE, 2017.

7. **A. Mokh**, Y. Kokar, M. Hélard et M. Crussière, Time reversal receive antenna shift keying on MIMO LOS channel, Sensors Networks Smart and Emerging Technologies (SENSET), 2017.

Patents

8. **A. Mokh**, M. Hélard, M. Crussière, Y. Kokar, J.-C. Prévotet, Technique de modulation spatiale et dispositif de réception associé, déposé le 5 février 2016, FR 3047621. Ext. PCT WO2017134403 le 10/08/2017.

9. **A. Mokh**, M. Hélard, M. Crussière, Y. Kokar, J.-C. Prévotet, Technique de modulation spatiale, déposé le 13 septembre 2016, FR16/01344.

10. **A. Mokh**, M. Hélard, M. Diallo, Methode de transmission sans fil et dispositif associé, déposée le 01 octobre 2018, FR18/01026.

Chapter 2

State of Art

2.1 Introduction

Increasing the data rate and the SE, or minimizing the energy consumption, are the key elements that drive research in future wireless communication systems. Recent advances have demonstrated that MIMO wireless systems can achieve impressive increases in overall system performance. The potential to provide the next major leap forward for wireless communications has led this technology to become the next frontier of wireless communications [14]. In MIMO technology, multiple channels are considered to transmit the symbol vectors and they are detected considering the interference among multiple spatial channels, which necessitates a complicated signal processing for symbol detection and multiple RF fronts end at the transmitter or receiver. Using antenna diversity for space digital modulation was proposed as a novel scheme for MIMO systems with single-Radio Frequency (RF), which is termed as Spatial Modulation [7].

2.2 Evolution of wireless communication systems

2.2.1 History

The first wireless transmission of information was implemented in 1887 by Rodulf Hertz. Based on the theoretical results of Maxwell's equations, Hertz was able to transmit and receive a radio pulse. From this demonstration, the evolution of wireless communications began, using the baseband frequencies for the transmission. Afterward, the range of baseband frequencies was shifted to other frequency ranges suitable for transmission, to avoid interference and band limitation, and a corresponding shift back to the original frequency range at the reception was also implemented. This mechanism is called modulation and demodulation.

Analog modulation started with Amplitude Modulation (AM) with the same concept used for telegraphy, and afterward, Edwin Armstrong invented Frequency Modulation in 1933. The well-known frequency-modulated or FM radio managed to dominate the world of music and public broadcasting, especially during the late 1970s. The reason was that the newly improved signal was less susceptible to noise, static, and electrical or atmospheric interference.

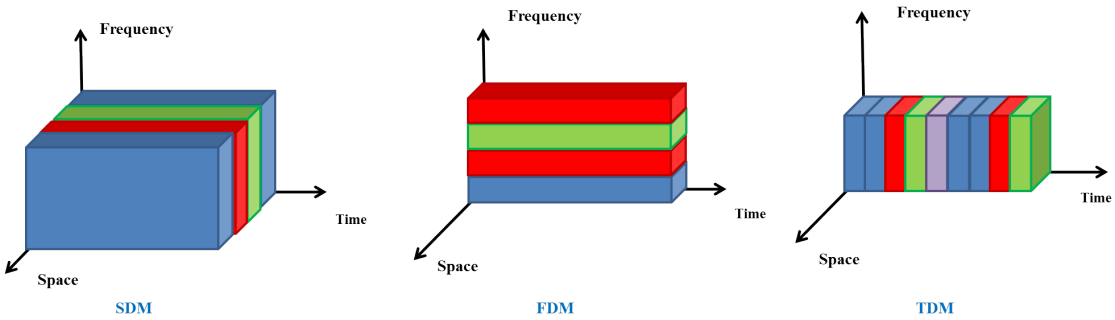

Figure 2.1 – Time, frequency and space multiplexing

In 1948, Claude Shannon proposed the Information Theory to find fundamental limits on digital signal processing and communication operations [15] and calculated the entropy in information sources that will be used further for lossless data compression. The concepts of information theory are based on the smallest data size, the "bit". In analog communication, we cannot exploit the signal structure. However, digital communication based on binary information overcomes this limitation, and more efficient transmission is achieved. Digital communications have, in large part, replaced analog communication as the form of transmitting information through computer and mobile technologies. With digital communications, it is possible to have error correction codes that can bring us close to error-free transmission in noisy channels, and the bandwidth is used more efficiently compared to analog transmission.

2.2.2 Three dimension division

To transmit the digital information, the signal is allocated using different parameters and multiplexed with different manners. A channel access method or multiple access methods allow the transmission between multiple connected terminals in the same transmission medium by sharing its capacity. The three main resources that can be used to multiplex the data, or for multiple access transmission, are time, frequency and space (Figure (2.1)).

Time Division

Time-Division Multiplexing (TDM) was first developed in the 1870s, by Emile Baudot, for applications in telegraphy to route multiple transmissions simultaneously over a single transmission line. The time resources is divided into several recurrent time slots of fixed length, one for each sub-channel. A sample byte or data block of sub-channel 1 is transmitted during time slot 1, sub-channel 2 during time slot 2, etc, so that each signal appears on the line only a fraction of time in an alternating pattern. TDM can be further extended into the TDMA scheme, where several stations connected to the same physical medium, for example sharing the same frequency channel, can communicate, as in GSM telephone systems.

Frequency Division

Thus to increase the bit rate on a multipath channel, the use of a single carrier with a wide band can cause a Inter-Symbol Interference (ISI) problem. One proposed solution is to divide the frequency-selective channel into a large number of flat subchannels to make the receiver simpler [16]. Frequency-division multiplexing (FDM) is a technique by which the total bandwidth available in a communication medium is divided into a series of non-overlapping frequency bands, each of which is used to carry a separate signal. The idea of multicarrier modulations dates back to the 1950s and 1960s for military uses. Each subchannel is modulated with a symbol, and then all the N subchannels are frequency-wise divided. But this method is not effective for band use since subbands must be separated to eliminate ICI [17].

In 1966, Robert Chang [18] proposed a method to reduce the spectral loss by the development of FDM to have well-arranged subchannels without ICI. To have such an arrangement, it is necessary to use orthogonal carriers between them, hence the notion of OFDM. FDMA and OFDMA are two channel access methods that have been developed based on the frequency division criteria.

Space Division

Information theory has revealed that the multipath wireless channel is capable of providing a dramatic increase in capacity, provided that the multipath scattering is sufficiently rich [19]. For this reason, the interest in MIMO systems for wireless communication has taken a lot of interest. In Space-division multiplexing (SDM), and Space-Division Multiple Access (SDMA), both time and frequency can be reused, by transmitting the information along parallel channels, that results from the different positions in space, as for multiuser transmission where each user has a different position, or in multi-antenna transmission, or even for base stations in different cities.

Such technology is a channel access method based on creating parallel spatial pipes next to higher capacity pipes through spatial multiplexing and/or diversity, by which it is able to offer superior performance in radio multiple access communication systems.

2.3 MIMO systems

A MIMO wireless system is a system that has multiple antennas at transmitter and receiver. Indeed, MIMO technology represents today one of the major steps in the enhancement of many wireless communication systems [14]. As any wireless system, MIMO systems could be categorized as "open-loop" and "closed-loop". In open-loop systems, the receiver and transmitter do not communicate back and forth for feedback, and only the receiver is figuring out the channel information to decodes the streams. Here, the complexity is more concentrated on the receiver, and the system is prevented from fully utilizing channel diversity or capacity.

In contrast, if a feedback channel is allocated between the receiver and the transmitter, the system becomes closed-loop. This feedback channel can be used for many purposes, especially for sending information about the channel state back to the transmitter. The information about the channel enables simple spatial diversity, precoding and multiplexing techniques for more effective transmissions. An optimal transmission

performance can be acheived in closed-loop systems with the use of Singular Value Decomposition (SVD) of the channel [13].

2.3.1 Advantages of MIMO systems

The interest in MIMO systems has exploded because of multiple benefits. First, starting with the benefits of a general MIMO system, i.e. in open-loop and closed-loop systems:

- they allow impressive increase in system capacity in the presence of multipath fading environments [13], [19]–[21],
- they provide higher data rate, because the more antennas, the more independent data stream can be sent [22],
- they improve the secrecy capacity of transmission system, due to the existance of multiple link channels with fading [23]–[25],
- they provide diversity because of the larger number of distinct paths [26][27].

In addition of all these benefits, closed-loop MIMO system has more benefits such as:

- they provides energy efficient transmission because of the focusing toward the receiver[22],
- the use of SVD to acheive optimal performance [28].

2.3.2 MIMO Channel Modeling

In wireless communication systems, the propagating wave between a transmitter and a receiver, interacts with the environment and is affected by various physical phenomena. For radio channel communications, the two important aspects that we take into account are:

- Multi-path propagation: when the wave takes multiple different paths to reach the receiver. On the small scale, the phenomena that result this interaction is called "fading", where the principle mechanisms that are characterizing these interactions are: reflection, diffraction, and scattering (diffusion) [29]. Each path has a different delay, and the delay between the first and last path is called delay spread. The inverse of the delay spread is related to the "coherence bandwidth". The larger the coherence bandwidth compared to the signal bandwidth is (i.e. the smaller the delay spread is), the more the channel in this bandwidth is considered as "flat fading channel", otherwise it is called "frequency selective channel".
- Mobility: when the transmitter, the channel, or the receiver is moving during the transmission. These phenomena describe if the channel is slow or fast fading. The higher the mobility is, i.e. the higher the speed of moving, the more the channel is fast fading.

Considering a mobile-radio channel where the impulse response is composed of I paths, with different attenuation and delays, the base band input output equation writes:

$$r(t) = \sum_{i=1}^{I} \alpha_i(t) s(t - \tau_i) + \eta(t) \tag{2.1}$$

where $s(t)$ is the emitted signal, $\eta(t)$ is an additive white noise, $r(t)$ the received signal and $\alpha_i(t)$ is the complex gain associated with the i-th path delayed of τ_i.

Rayleigh Fading

When the symbol duration is higher than the channel delay spread, those paths will be summed. If there is sufficiently much scatter with small delays (rich scattering model), all the scattered paths with different amplitude and phase can be modeled as a complex Gaussian process, because of the central limit theorem. If there is no dominant component to the scatter, then such a process will have zero mean and phase evenly distributed between 0 and 2π radians. The envelope of the channel response will therefore be Rayleigh distributed [30][31]. If the channel is considered to be a Rayleigh flat-fading channel, then the link between single antenna transmitter and single antenna receiver is modeled by one complex coefficient following the complex Gaussian process.

Single User MIMO System Model

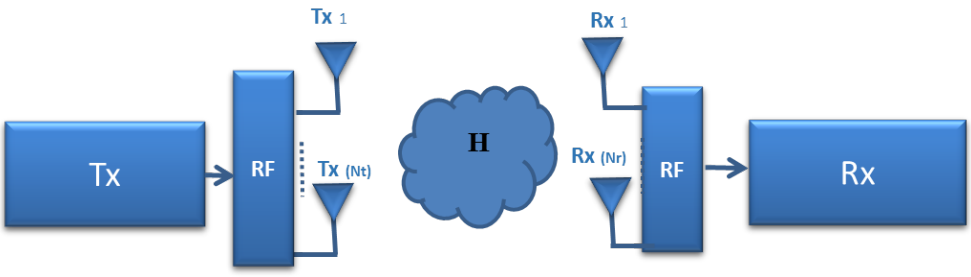

Figure 2.2 – MIMO transmission system

Considering the MIMO transmission system in Figure 2.2, with N_t transmit antennas and N_r receive antennas, and a flat fading channel, the equation of the received signal vector is:

$$\mathbf{y} = \mathbf{H}.\mathbf{s} + \mathbf{n} \tag{2.2}$$

where $\mathbf{H} \in \mathbb{C}^{N_r \times N_t}$ is the "Single User" MIMO "flat fading" channel matrix with element $h_{j,i}$ representing the complex channel coefficient between the i-th transmit antenna, denoted by T_i, and the j-th receive antenna, denoted by R_j. $\mathbf{y} \in \mathbb{C}^{N_r \times 1}$ is the vector of the received signals at all the receive antennas, $\mathbf{s} \in \mathbb{C}^{N_t \times 1}$ is the vector of the transmitted signals by all the transmit antennas, and $\mathbf{n} \in \mathbb{C}^{N_r \times 1}$ is the vector of additive white Gaussian noise (AWGN) samples η_j such that $\eta_j \sim \mathcal{CN}(0, \sigma_n^2)$.

2.3.3 Capacity of MIMO

The MIMO systems can be studied by the evaluation of the information-theoretic (Shannon) capacity. Considering the same MIMO system in Figure 2.2, the capacity of such system for a flat fading channel **H** is given by:

$$\mathcal{C} = \log_2 \left[\det \left(I + \frac{P}{N_0} \mathbf{H}\mathbf{Q}\mathbf{H}^H \right) \right] \tag{2.3}$$

where $\mathbf{Q} \in \mathbb{C}^{N_t \times N_t} = \mathbb{E}\{\mathbf{s}\mathbf{s}^H\}$, P is the total transmitter power, I is a $N_r \times N_r$ identity matrix, and N_0 is the noise spectral density. The analysis of MIMO systems in block Rayleigh-fading channels is presented in [32], and a Gaussian approximation to the capacity distribution is investigated in [33]. All of these analyses show that MIMO systems in uncorrelated Rayleigh-fading environments can potentially provide enormous Shannon capacities. A spatially correlated MIMO channel capacity distribution was also investigated in [34]. The capacity of deterministic MIMO channels with memory and full channel knowledge at the transmitter and the receiver was derived in [35]. Also, authors in [36] deal with the capacity behavior of wireless OFDM-based spatial multiplexing systems in broadband fading environments for the case where the channel is unknown at the transmitter and perfectly known at the receiver.

2.3.4 Energy efficiency improvement

Traditionally, multiple antennas have been used to increase diversity exploitation to combat channel fading. A signal path is provided between the transmitter and the receiver between each two transmit and receive antennas, and so multiple replicas of data with independent fading are obtained by sending signals that carry the same information through different paths. Hence, more reliable reception, or more diversity gain, is achieved.

Also, in general, MIMO schemes improve energy efficiency when the transmitter can focus its emitted energy into the spatial directions where it knows that the receiver is located.

2.3.5 Trade off Diversity-Multiplexing gain

With MIMO transmissions, there is a fundamental trade-off between the diversity gain and the multiplexing gain [37].

In [38], authors analyze the energy efficiency of MIMO transmissions in wireless sensor networks based on the trade-off between the diversity gain and the multiplexing gain. They show that the energy efficiency of MIMO transmissions can be higher than that of the traditional SISO transmissions. The optimal energy efficiency is usually achieved when both the diversity gain and the multiplexing gain are used, which means it is suboptimal if only the diversity gain is considered.

In [26], an elegant mathematical solution for providing full diversity over the flat-fading channels is proposed for the multi-antenna system, called Space-Time Bloc Coding (STBC). But it has been proven in [39] that when the number of transmit antennas is more than two, STBC incurs a loss in capacity, since the equivalent code rate of STBC can not achieve the maximum possible transmission rate for more than two transmit antennas.

2.4 Transmit Spatial Modulation

SM schemes based on MIMO wireless systems appeared in the early 2000s consisting of exploiting the index of the transmit antennas or receive antennas to transmit information bits. In such techniques, location-dependent spatial information is utilized to carry additional information bits to the classical IQ symbols, thereby boosting the overall SE and overcoming Inter-Antenna Interference (IAI), and the information is coded in two symbols: a spatial symbol that is related to the index of antenna, and an IQ symbol. The SE of the system is calculated as to be the number of bits per symbol m. In SM, $m = m_1 + m_2$ where m_1 is the number of bits transmitted by the spatial symbol and m_2 is the number of bits transmitted by an IQ symbol.

2.4.1 Principle

The main concept of the SM is to transmit the data using the index of antennas. When the index of transmit antennas is used, we call it transmit SM, that is based on open loop MIMO systems, where only the receiver estimates the channel at the biginning of transmission to be used for detection. Otherwise, in closed-loop MIMO the spatial symbol could be mapped to the index of receive antennas in the so called Receive SM. In transmit SM, when only the spatial dimension is used to transmit the information, i.e. the spatial bit, the scheme is called SSK.

Without additional IQ

In SSK transmission, only one transmit antenna is activated during each symbol duration, i.e. $m = m_1$, with a total number of combinations equal to N_t, resulting $m = \log_2(N_t)$. Figure (2.3) illustrates an SSK transmission, with $N_t = 4$, i.e. in which $m = 2$ bit per spatial symbol are transmitted. The corresponding spatial mapping table is given as follows:

Activated antenna T_i	T_1	T_2	T_3	T_4
Spatial symbol mapping	00	01	11	10

Figure 2.3 considers the transmission of a sequence of 4 bits, or equivalently of two consecutive spatial symbols. For this considered sequence and according to the above mapping, the active antennas are T_1 first, and T_4 next.

At the receiver side, the receiver should first estimate the channel at the beginning of the transmission. Afterward, the detector uses the channel estimation to determine the active antenna index each symbol duration from the received signal.

With additional IQ

In SM, the transmission schemes also allow for simultaneously transmitting two types of symbols: 1- classical IQ-symbols of a M-order modulation, 2- spatial bits or symbols related to the index of the transmit antenna(s), like SSK modulation [40]. So SM is simply a SSK modulation with additional IQ symbols. Figure 2.4 illustrates a SM constellation, where the information is mapped to a 4 transmit antennas SSK and a 4-QAM modulated signal, capable to transmit 4 bits per SM symbol. In such scheme, the total

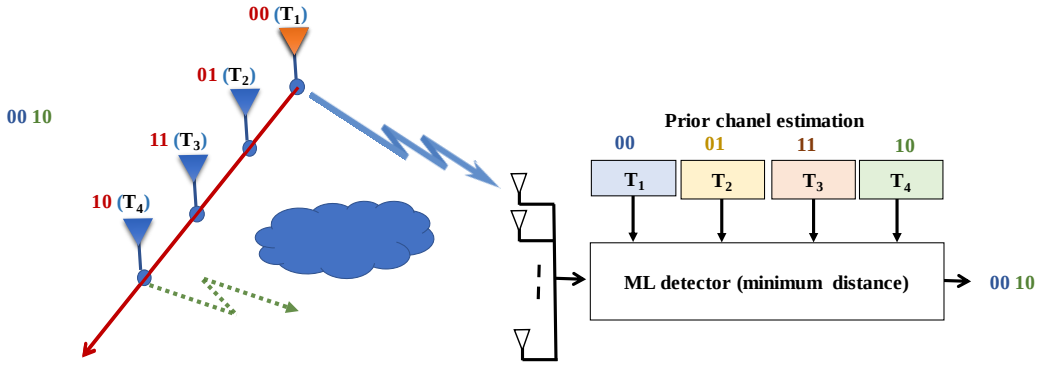

Figure 2.3 – SSK concept illustration

number of transmitted bits per each SM symbol for a system of N_t transmit antennas and M-QAM modulation is

$$m = \log_2(N_t M) \text{ bit/symbol.} \tag{2.4}$$

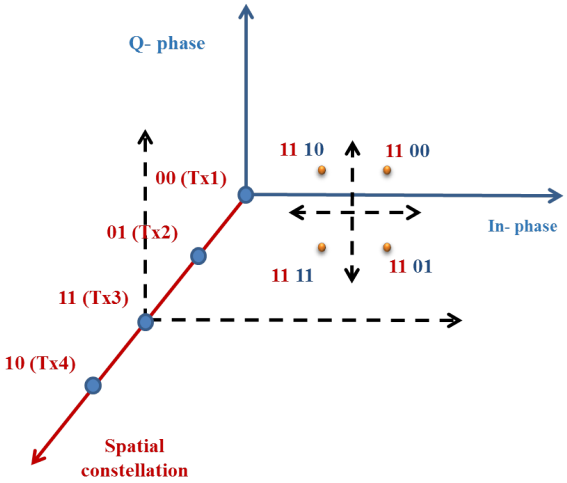

Figure 2.4 – Spatial Modulation Concept illustration

2.4.2 General System Model

A $N_t \times N_r$ MIMO transmission system in flat fading channel is considered. Let M be the size of the M-QAM signal modulation. One of N_t transmit antennas will be activated during each symbol duration depending on the binary information and the spatial mapping of the antenna index to code the spatial constellation of $m_1 = \log_2(N_t)$ bits, as a part of the information block. The other $m_2 = \log_2(M)$ bits are mapped into a constellation point in the signal domain, that will be send by the activated antenna.

A block of m-bits $(m = m_1 + m_2)$ is mapped into a constellation vector $\mathbf{x}^b(i) \in \mathbb{C}^{N_t}$, i.e., $\mathbf{x}^b(i) = [x_1\ x_2\ ...\ x_{N_t}]^T$ by sending the m-th QAM symbol using the i-th antenna. So that the signal to be emitted is

$$\mathbf{x}^b(i) = \Big[0 \quad ... \quad \underbrace{x^b}_{i-\text{th position}} \quad 0\Big]^T \tag{2.5}$$

where $x^b = 1$ for SSK modulation. The signal vector $\mathbf{x}^b(i)$ is transmitted over the wireless channel $\mathbf{H}$. The received signal $\mathbf{y} \in \mathbb{C}^{N_r}$ experiences complex zero-mean additive white Gaussian noise vector $\mathbf{n}$, with a variance σ_n^2. So $\mathbf{y}$ is given by

$$\mathbf{y} = \sqrt{E_s}\mathbf{H}\mathbf{x}^b(i) + \mathbf{n} \tag{2.6}$$

where $\mathbf{y}$ denotes the received signal vector, and E_s denotes the transmitted signal energy. For simplicity, the transmitted power is considered to be normalized to 1, so also the symbol energy is equal to 1.

At the receiver, $\tilde{\mathbf{H}}$ is the estimated channel, so the transmitted M-QAM symbols and spatial symbols are jointly detected using the ML optimal detector as:

$$[\hat{i} \quad \hat{b}] = \text{Arg} \min_{\substack{i\in\{1:N_t\} \\ b\in\{1:M\}}} \left\|\mathbf{y} - \tilde{\mathbf{H}}\mathbf{x}^b(i)\right\|^2, \tag{2.7}$$

where Arg is the argument, min is the minimum operator, and $\|.\|$ is the norm operator. The block diagram of the SM scheme is depicted in Figure 2.5, where an example of transmitting 4 bits using 4 transmit antennas and QPSK SM system. The 4 bits 0111 are first segmented into 2 groups of 2 bits each: 01 are mapped to a QPSK symbol and 11 to a spatial symbol. Considering the same constellation in Figure 2.4, the SM symbol is transmitted by sending the $1 - j$ constellation by the $3rd$ TA. At the receiver side, the N_r receive antennas will exploit the received signal, and so the receiver will estimate which was the active antenna and the QPSK symbol to demapp the SM symbol, and then decode it to the considered binary information.

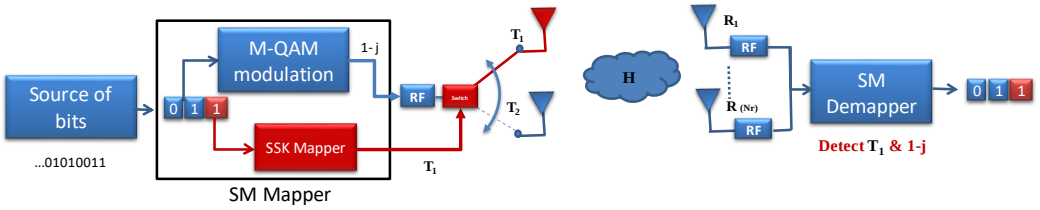

Figure 2.5 – Spatial Modulation Block Diagram

2.4.3 History, Advantages, and Disadvantages

History

SSK was proposed for the first time in [7], where the idea of detecting the transmitted information by exploiting the differences in the signals received, in wireless fading

channels, from two transmit antennas using one receive antenna was first described. One bit is transmitted spatially each symbol duration, and it was extended to a variable number of transmit antennas for reaching higher SE in [41]. The principle of allocating the information to the index of the transmit antenna was exploited in [12]. More studies on the performance of the SSK were later published [42][43][44].

In order to increase the SE of the transmission, the SSK can be combined with other types of modulations (IQ), as was proposed in [45], where the term SM appears for the first time.

Comparing with STBC, SM offers a better capacity gain over Rayleigh fading channels if the number of transmit antennas is greater than two, as proved in [46], but called "Information Guided Channel Hopping" instead of SM.

Numerous research works have been conducted concerning this scheme, starting with [40], where the authors demonstrated that SM outperforms V-BLAST and STBC schemes in error rate, for the same SE, with a lower complexity receiver. A sub-optimal detector based on Maximum Ratio Combining (MRC) detection is used to detect the bits conveyed by the two information carrying units, spatial and M-QAM symbols, independently. The optimal receiver based on Maximum Likelihood (ML) detection was developed and studied in [6], and a reduced complexity sphere decoder for the ML detector is presented in [47].

Performance evaluation of SM scheme has also been published. In [48], the Average Bit Error Rate (ABER) of SM in correlated Nakagami fading channels is computed. Moreover, the effect of imperfect channel estimation over generalized fading channels is studied in [49]. In addition, the performance of SM, compared with Spatial Multiplexing (SMX), using real-world channel estimation, in correlated and uncorrelated channels are studied in [50], and a practical implementation using NI PXI instrument is published in [51]. Furthermore, the effect of antenna switching in band-limited SM is investigated in [52], using realistic shaping pulse for the SM, and they demonstrate that the SM will outperform the classic MIMO systems if the number of transmit antennas is greater than M^{2K-1}, where M is the order of M-ary QAM modulation, and K is the effective length of the pulse shaping filter. In [53], an optimal antenna selection for spatial modulation is given to maximize the total capacity. Otherwise, an energy efficiency evaluation of SM under a different type of BS (macro, micro, pico, and femtocell) is studied in [54]. Authors showed that for all types of BS, SM achieves a range of average data rates with significantly less power consumption compared to Multiple-Input Single-Output (MISO) with only transmit diversity, STBC, and MIMO and that the benchmark systems are up to 67% less energy efficient compared to SM.

Finally, new modulation concepts, based on SM scheme, has been proposed, either to reduce the effect of channel correlation on the performance of SM like the "Trellis-Coded SM" like in [55]–[57], or to enhance the overall throughput with performance enhancement like in [58]–[60].

Advantages and Disadvantages

From [61] and [3], we can specify multiple advantages for the SM. Compared with SISO transmission, SM offers a higher SE, because of the spatial multiplexing gain, that is equal to $\log_2(N_t)$ bit/symbol. Also, compared with MIMO scheme with low complexity coding that is used to exploit the spatial diversity, such as the STBC, the

SM provides a larger capacity because of the spatial multiplexing gain. On the other hand, since the concept of SM is based on activating only one transmit antenna each symbol duration, the transmitter could be reduced to a single RF transmitter. This can be seen as a simple transmitter design compared with conventional MIMO schemes, where a lower power supply is needed at the transmitter. Moreover, activating only one transmit antenna avoid the Inter-Carrier Interference (ICI) and IAI, which compared to the V-BLAST scheme, makes the SM receiver simpler since no interference cancellation algorithms are required. And since the receive antennas are used for exploiting the diversity gain, and so the SM can work efficiently if $N_r < N_t$.

In contrast, the SM has in addition to those advantages, some disadvantages. Regarding the SE, it is sub-optimal in SM compared to the SMX, since SMX increases in order of N_r while SM increases in order of $\log_2(N_r)$ bit/symbol. In addition, if we need to increase the throughput, a fast antenna switching is needed, i.e. with small switching time, leading to a time-limited pulse shaping equal to the switching time. Finally, to detect the data, a perfect channel knowledge is needed at the receiver, and the performance of SM degrades if the wireless channels are not sufficiently decorrelated. However, orthogonal pulse shaping design could overcome this limitation.

2.4.4 Generalised spatial modulation

In the first proposed SM schemes, the number of transmit antennas used for the spatial constellation should be a power of 2 leading to an efficiency of $m = \log_2(N_t)$, meaning that during every symbol duration only one transmit antenna is active.

Increasing the number of combinations

In [62], authors proposed to overcome the condition of activating only one transmit antenna, by activating multiple transmit antennas during each symbol duration, and so the spatial symbol is mapped to a combination of multiple antenna. They called the scheme Generalised Space Shift Keying (GSSK). This method eliminates the constraint of N_t to be a power of 2, and also increase the overall SE by increasing the number of possible combinations. Let N_a be the number of active antennas from N_t transmit antennas (N_a is constant during the transmission), the number of the possible combinations is $N_c' = \binom{N_a}{N_t}$. However, the number of combinations that are considered for the transmission should be a power of 2. Therefore only $N_c = 2^{m_1}$ combinations are used, where $m_1 = \lfloor \log_2 \binom{N_a}{N_t} \rfloor$ and $\lfloor . \rfloor$ is the floor operation. For example, with 5 transmit antennas, if we choose to use N_a =2 transmit antennas each symbol duration, the total number of combinations is $\binom{2}{5} = 10$ capable to transmit 3 bits using 8 combinations. Using SSK, 8 transmit antennas are needed to transmit the 3 bits. A maximum of SE could be achieved if N_a=$N_t/2$ bit/symbol.

Furthermore, the concept of SM is applied at the generalized scheme, by sending additional M-ary symbols by the active antennas, and the scheme is called Generalised Spatial Modulation (GSM). The total number of bits conveyed by a GSM symbol is:

$$m = \lfloor \log_2 \binom{N_a}{N_t} \rfloor + \log_2(M) \text{ bit/symbol.} \tag{2.8}$$

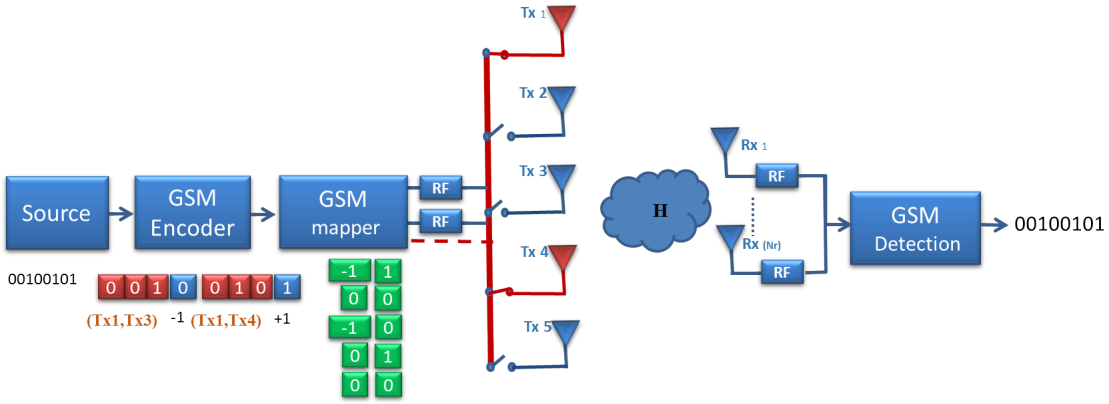

Figure 2.6 – Generalised Spatial Modulation

Spatial Mapping	000	001	010	011	100	101	110	111
Antenna Combination	(1,2)	(1,3)	(1,4)	(1,5)	(2,3)	(2,4)	(2,5)	(3,5)

Table 2.1 – GSM Mapping Table for N_t=5 and N_a=2

The BEP analysis of GSM is derived in [63], while another performance evaluation using the MRC detection is presented in [64]. In [65], Hamming code construction is used to design the constellation of the GSM. Finally, authors in [66] proposed to use the hybrid beamforming to apply the GSM in mm-Waves environment.

Block Diagram

The block diagram of GSM is illustrated in Figure 2.6. A MIMO GSM with $N_t = 5$ and $N_a = 2$, and using BPSK constellation is considered. Such system is capable to transmit 4 bits/symbol. The mapping table of the spatial symbol to the binary information is given in the table 5.1. An example of transmitting a sequence of 8 bits is illustrated in Figure 2.6, which could be sent by 2 GSM symbols: the first GSM symbol maps "0101", it is transmitted by sending the constellation "+1" through the first and fourth antenna; the second GSM symbol maps "0010", it is transmitted by sending the constellation "-1" through the first and third antenna;

At the receiver side, the GSM symbol is decoded by estimating the index of active antennas and the transmitted BPSK constellation, and then demapping the estimated symbol to the equivalent binary information using the same mapping table.

2.4.5 Extended SSK

To better exploit the spatial domain, and by taking the advantage of degree of freedom to increase the number of combinations which is translated to an increase the the SE, we proposed in [67] a new spatial scheme called ESSK. The concept of spatial mapping is that the number of active antennas N_a is not constant. With ESSK indeed, every subset

00 01 10 11	Symbol 1	Symbol 2	Symbol 3	Symbol 4
1) Segmentation	00	01	10	11
2) Spatial Mapping	(0,0)	(0,Tx2)	(Tx1,0)	(Tx1,Tx2)
Channel	 H	 H	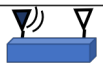 H	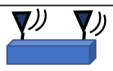 H
4) Detection	(0,0)	(0,Tx2)	(Tx1,0)	(Tx1,Tx2)
5) Demapping	00	01	10	11

Figure 2.7 – Extended SSK concept

of transmit antennas of any size could be activated to form one spatial symbol, and so the number of all possible combinations in GSSK will be summed. Consequently, the ESSK symbols are made of a number m of bits such that

$$m = \log_2 \left(\sum_{N_a=0}^{N_t} \binom{N_a}{N_t} \right) = N_t \tag{2.9}$$

Figure 2.7 provides an illustration of the ESSK scheme with $N_t = 2$. The transmitter is represented in blue with its two transmit antennas. As evident from this figure, the ESSK system allows 2 bits to be transmitted during each spatial symbol. The spatial mapping used in this example is the following:

- no antenna is activated if symbol '00' is sent,
- antenna T_2 is activated if symbol '01' is sent,
- antenna T_1 is activated if symbol '10' is sent,
- both antennas T_1 and T_2 are activated if symbol '11' is sent.

Hence, at step 3 the signal will be propagating in a fading channel. At step 4, the receiver estimates which antennas have been activated using a prior channel estimation and then deduce the transmitted spatial symbol. More details about this scheme are provided in Chapter 5.

SE increasing

Figure 2.8 illustrates the evolution of the SE of different SSK scheme with the number of transmit antennas. In SSK schemes, only spatial symbol is transmitted, so the SE is the number of transmitted bit per spatial symbol (SE=m=m_1). A linear increasing is resulted for ESSK, while for GSSK, considering the maximum number of combinations (when $N_a = N_t/2$), it still less than the SE of ESSK. The SSK provides the minimum SE that logarithmicly increases with N_t. This comparison shows the capability to reduce the architecture of the transmitter while keeping the same SE, example: for a same SE= 4 bit/symbol, 16 antennas are needed for SSK, 6 antennas for GSSK, and 4 antennas for ESSK.

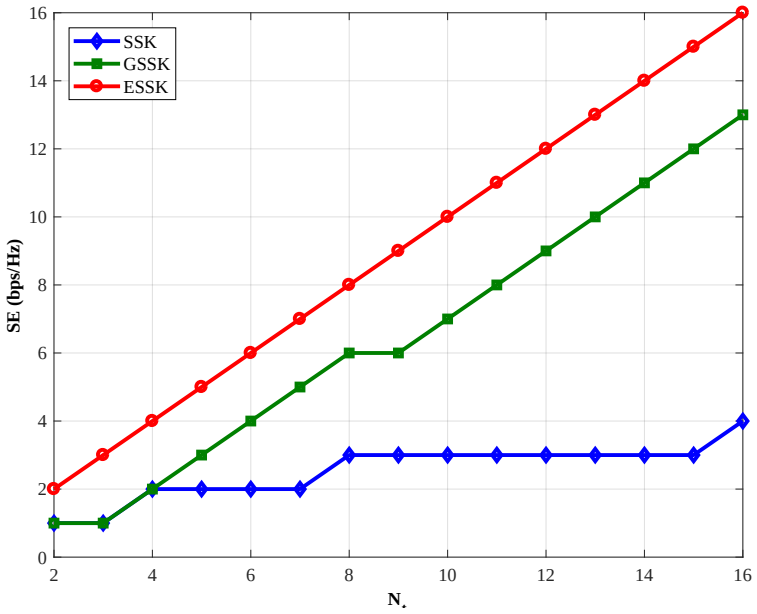

Figure 2.8 – SE of SSK, GSSK, and ESSK schemes in terms of the number of transmit antennas.

2.5 Receive Spatial Modulation (RSM)

The same concept of SM can applied for example on the receiver of a downlink, called RSM, where the index of the targeted receive antenna carries the additional spatial information. A pre-processing technique is applied at the transmitter to target a signal toward one or several receive antennas [8].

2.5.1 Principle

In RSM, the spatial symbol is allocated to the index of receive antenna, in same analogy of Transmit SM. A closed loop MIMO system is used to apply the concept of RSM. RASK transmission scheme is an RSM scheme that is analog to the SSK at the receiver, where only spatial symbols are transmitted without IQ symbols [9], [68]. A RASK transmitter forms a spatial beam which changes from one RASK symbol to another so as to target one of the N_r antennas at each symbol duration. The index of the targeted antenna is therefore associated to a predefined set of information bits. In other words, RASK uses a bit-to-antenna mapping instead of a bit-to-complex-symbol mapping used in classical digital communication schemes. Consequently, the number m of bits conveyed by a RASK symbol is:

$$m = \log_2(N_r) \tag{2.10}$$

Figure 2.9 provides an example illustrating the transmission of a sequence of 4 bits "1000" using the RASK scheme with N_r = 4 and thus m = 2 bit per spatial symbol. First, the M-ary spatial symbols are constituted from the demultiplexing of order m of the

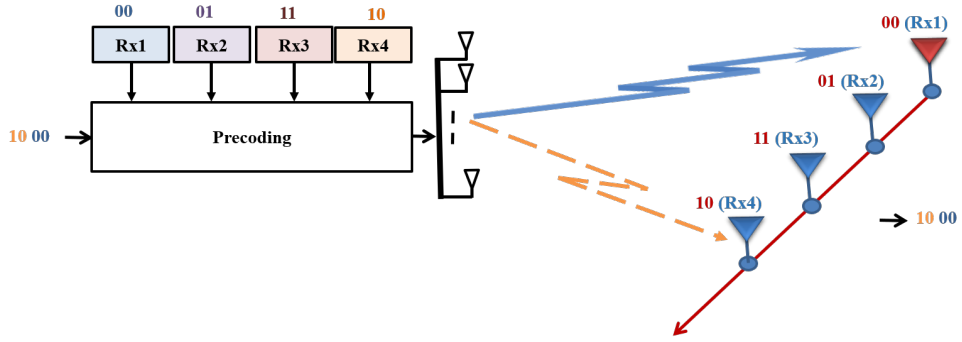

Figure 2.9 – Example of RASK System

input binary stream, with here M = 4. Afterward, the spatial symbols that determine the targeted receive antenna are related to the following spatial mapping table:

- Rx_1 is targeted if symbol '00' is sent,
- Rx_2 is targeted if symbol '01' is sent,
- Rx_3 is targeted if symbol '11' is sent,
- Rx_4 is targeted if symbol '10' is sent.

So, the transmitter will target Rx_4 in first symbol duration and Rx_1 in second symbol duration to transmit the 4 bits information. The transmitter performs a preprocessing so as to focus a signal toward the targeted antenna. Then, the receiver detects the targeted antenna among its N_r antennas, and the estimated antenna index is converted into the bit values corresponding to a predefined spatial mapping table.

As for SM, additional IQ symbol can be transmitted with the spatial symbol towards the targeted antenna, in order to send more bits per symbol.

2.5.2 System Model of RSM

The system model for RSM is quite analog to that for TSM, with the difference that a preprocessing technique is performed at the transmitter to transmit the spatial vector to the receiver. Considering an $N_t \times N_r$ MIMO trasnmission system. One of N_r receive antennas will be targeted each symbol duration depending on the binary information and the spatial mapping of the antenna index to code the spatial constellation of $m_1 = \log_2(N_r)$ bits, as a part of the information block. The other $m_2 = \log_2(M)$ bits are mapped into a constellation point in the signal domain (IQ symbol), that will be send by the activated antenna.

A block of m-bits $(m = m_1 + m_2)$ is mapped into a constellation vector $\mathbf{x}^m(i) \in \mathbb{C}^{N_t}$, i.e., $\mathbf{x}^m(i) = [x_1\ x_2\ ...\ x_{N_r}]^T$ by sending the m-th QAM symbol using the i-th antenna.

So that the signal to be emitted is

$$\mathbf{x}^m(i) = \begin{bmatrix} 0 & \dots & \underbrace{x^m}_{i-\text{th position}} & \dots & 0 \end{bmatrix}^T \tag{2.11}$$

where $x^m = 1$ for RASK modulation, and can be an IQ symbol for RSM. Spatial focusing is obtained through the pre-processing step modeled by matrix $\mathbf{W} \in \mathbb{C}^{N_t \times N_r}$ which transforms $\mathbf{x}^m(i)$ into the vector of transmitted samples $\mathbf{s}$. The received signal $\mathbf{y} \in \mathbb{C}^{N_r}$ experiences complex zero-mean additive white Gaussian noise vector $\mathbf{n}$, with a variance σ_n^2. So $\mathbf{y}$ is given by:

$$\mathbf{y} = f\mathbf{H}\mathbf{W}\mathbf{x}^m(i) + \mathbf{n}, \tag{2.12}$$

where f is a normalization factor used to guarantee that the average total transmit power $\bar{P}_t$ remains constant independently on the spatial symbol vector and the pre-processing matrix. For the sake of simplicity, the transmitted power is considered to be normalized to 1.

The block diagram of RSM is depicted in Figure 2.10. The binary information from the source is mapped to a spatial symbol that will target a subset of receive antennas, and an additional M-QAM symbol could be added to these targeted antennas. Then, the transmitter will use the information from the channel estimation to creates a pre-processing matrix in order to target the subset of receive antennas equivalent to the spatial symbol. At the receiver side, the transmitted symbol is decoded by estimating the index of the targeted antenna (could be the index of antenna that receives the maximum amount of power), and an M-QAM demodulation is further implemented to decode the other part of information.

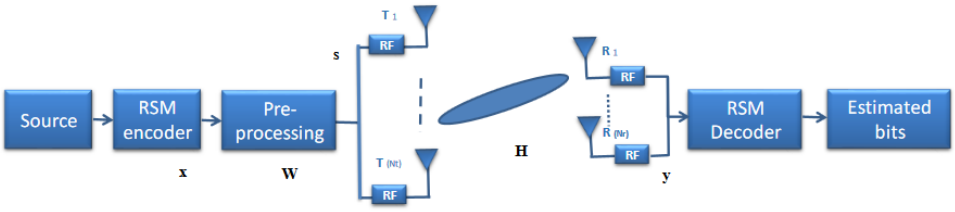

Figure 2.10 – Receive Spatial Modulation transmission system

2.5.3 Preprocessing technique

This is the part of the transmitter that is related to create a beam that will focalize an amount of energy towards the targeted receive antenna more than towards the others. It requires the knowledge of the channel impulse response at the transmitter. Generally speaking, RSM schemes assume MIMO systems with more transmit than receive antennas to allow for favorable spatial preprocessing. In this thesis, a linear pre-coding technique is considered. One first technique introduced in [9] and further experimented and studied in [69][70], where the Time Reversal (TR) is used as a precoding technique to concentrate the signal energy towards a targeted antenna. Considering a flat fading

channel and by taking the spatial dimension for the focalization, the TR precoding is implemented by the MRT precoding technique. Another solution is to implement ZF precoding at the transmitter in order to annihilate the received signals at non-targeted antennas [71].

Maximum Ratio Transmission

A preprocessing technique that enables to focus the signal in space toward a spatial dimension (targeted antenna)(Figure 3.10), where the trans-conjugate of the propagation channel matrix is used as pre-filter:

$$\mathbf{W} = \mathbf{H}^H \in \mathbb{C}^{N_t \times N_r} \tag{2.13}$$

Using this technique, it is possible to increase the spatial gain on the targeted receive antennas for the spatial modulation.

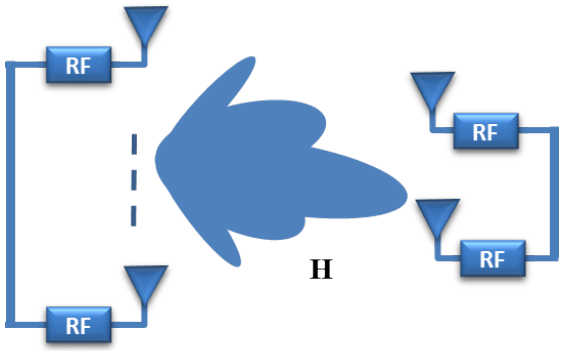

Figure 2.11 – MRT preprocessing illustration

Zero-Forcing

This technique aims to annihilate the interference on some spatial dimension, in our case those are the non-targeted antennas (Figure 2.12). We use the pseudo-inverse of the channel matrix as a pre-filter:

$$\mathbf{W} = \mathbf{H}^H(\mathbf{H}\mathbf{H}^H)^{-1} \in \mathbb{C}^{N_t \times N_r} \tag{2.14}$$

In this technique, it is required that the number of antennas satisfy $N_r \leq N_t$ so that the calculation of the pseudo inverse becomes possible.

2.5.4 History of RSM

As introduced in [8], RSM can also be referred to as Transmit Precoded SM (TPSM), since it relies on a preprocessing or spatial pre-coding operation that exploits the knowledge of the channel at the transmitter, so as to target one of the antennas of the receiver. Linear precoding are used at the transmitter such as the ZF and Minimum Mean Square Error (MMSE). A better pre-coding technique for multi-user RSM is studied in [72]. In [9], a more simple scheme equivalent to the SSK, where only the spatial information

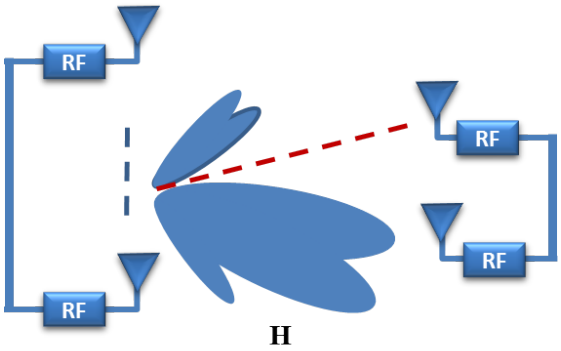

Figure 2.12 – ZF preprocessing illustration

is considered, called RASK was first described with time reversal pre-processing to concentrate the signal energy towards a targeted antenna, and a prototype was implemented in [69] [70]. Furthermore, authors in [73] studied the optimal selection of the subset of receive antennas for the better transmission. Moreover, for LOS mmWaves transmission, authors in [74] studied the capability of implementing the ZF precoding for RSM using analog beamforming under certain geometric conditions. The secrecy communications have been also motivated by the advantages of the TPSM transmission since the precoder could be optimized for different purposes. Authors in [75]–[77] studied the optimal precoding using power allocation to achieve an interesting secret transmission.

2.5.5 Multiple targeted antenna

Generalised Precoding Aided Spatial Modulation

Also, as for Transmit SM, a generalized scheme for the RSM referred to as Generalised Precoding Spatial Modulation (GPSM) was first described in [78], where the transmitter is targeting a subset of N_a antennas. Same authors studied the error probability and capacity analysis of GPSM in [79], and the performance of non-linear precoding for the same scheme in [80]. When only the spatial symbol is considered, the scheme could be called Generalised Receive Antenna Shift Keying (GRASK), where the number of bits conveyed by GRASK symbol is:

$$m = \lfloor \log_2 \binom{N_a}{N_t} \rfloor \text{ bit/symbol.} \tag{2.15}$$

Using pre-processing at the transmitter, offers a spatial multiplexing at the receiver, so unlike the GSM, not only one M-QAM is modulated at the transmitted signal, but it is possible to transmit one M-QAM symbol over each targeted antenna, i.e. N_a modulated signal. Here, m is equal to:

$$m = \lfloor \log_2 \binom{N_a}{N_t} \rfloor + N_a \log_2(M) \text{ bit/symbol} \tag{2.16}$$

In addition, authors in [81] and [82] studied the performance of GPSM in MIMO broadcast channels for multi-stream transmission. A mathematical framework for computing the accurate Average Bit Error Probability (ABEP) is calculated. Another strategy

to send the spatial symbol was proposed in [83], where two power levels were used to send it, a minimum and a maximum level, instead of having zero power for non targeted antennas. With this strategy, it is possible to combine the RSM with SMX technique, to reach a total number of bits per symbol equal to:

$$m = \lfloor \log_2 \binom{N_a}{N_t} \rfloor + N_r \log_2(M) \text{ bit/symbol.} \tag{2.17}$$

Extended Receive Antenna Shift Keying

To exploit the spatial dimension with more degrees of freedom, an extended version of the RASK is also presented in [84], where the number of targeted antenna is variable also.

The proposed ERASK scheme is also built on the SM concept at the receiver. As in ESSK, for the ERASK, N_a changes during each symbol duration with $0 \leq N_a \leq N_r$ taking all possible values, depending on the information bits, so that the number M of possible spatial symbols achieves:

$$M = \sum_{N_a=0}^{N_r} C_{N_a}^{N_r} = 2^{N_r} \tag{2.18}$$

with C_n^k the binomial coefficient giving the number of subsets of k elements of a set of n elements. Consequently, the ERASK symbols are made of m bits such that:

$$m = N_r. \tag{2.19}$$

Other studied concerning the ERASK where provided, such as the comparison of the performance when using the MRT preprocessing instead of the ZF [85], as well as the effect of channel estimation error and antenna correlation in [86]. Finally, we introduced the ERSM scheme in [87], which is based on ERASK concept, using two power level, in order to send an additional M-QAM modulated signal. Using this scheme, the total number of bits per symbol becomes:

$$m = N_r + \log_2(M) \text{ bit/symbol.} \tag{2.20}$$

2.6 Summary

In this chapter, we present an overall state of the art on different spatial modulation schemes. As figured in Figure 2.13, depending on where the knowledge of the channel is needed, the SM is divided into two categories:

- Transmit SM: the channel estimation is performed at the receiver to be used for the detection, mostly in uplink transmission.
- Receive SM: the channel estimation is performed at the transmitter to be used to create a pre-processing matrix to target the receive antennas, mostly in downlink transmission.

In addition, regarding the modulation, when only the space dimension is considered, i.e. without transmitting any IQ symbol in parallel of the spatial symbol, the scheme is called SSK for uplink and RASK for downlink. In contrast, when M-QAM modulated symbols are transmitted with the spatial symbol, the modulation is called SM for uplink and PSM for downlink.

Finally, considering the number of transmit/ receive antennas that are used to form the spatial symbol, the spatial modulation started with one active/targeted antenna per symbol duration. The "Generalized" model takes a combination of N_a antenna each symbol duration (N_a fix), and the "Extended" model takes a variable number of antenna (even zero) each symbol duration.

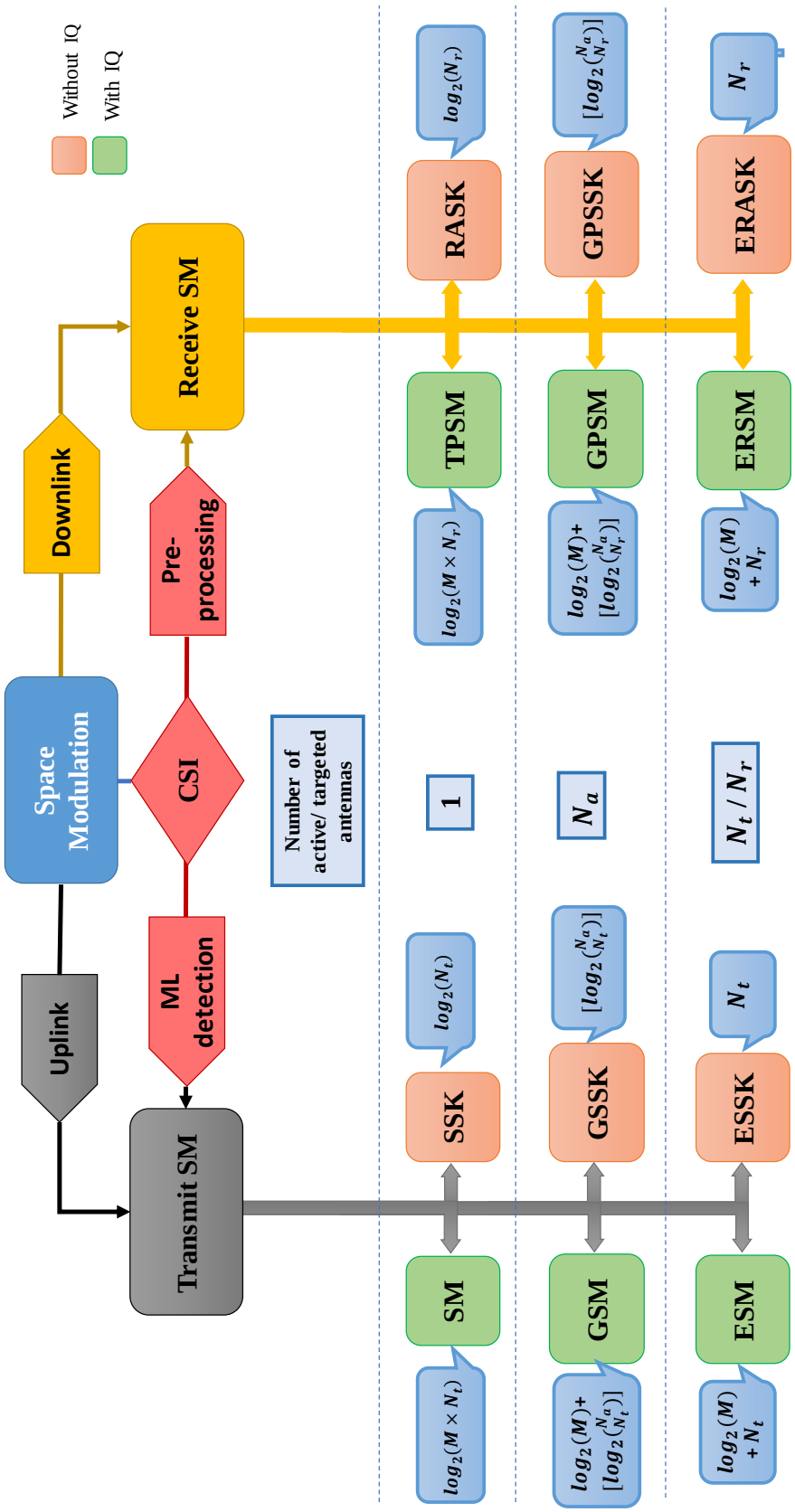

Figure 2.13 – Summary

Chapter 3

Receive Antenna Shift Keying Performance

Contents

3.1 Introduction

RASK is a MIMO transmission scheme that applies the SM concept at the receiver, where only the index of receive antenna codes the information, i.e. no additional IQ symbol is transmitted. Different precoding strategies could be used to target the corresponding receive antenna and different detection schemes with different complexity and performance. Simulation results of a RASK system combined with a Time Reversal (TR) precoding were first presented in [9]. The use of a simple Single-Tap detector was demonstrated to be efficient. A proof of concept of the RASK principle based on TR at the transmitter side was therefore straightfully implemented in [69] where a simple detector based on maximum received power level was used.

In this chapter, the theoretical performance of a RASK scheme is provided for two types of precoding, the ZF or MRT one. We lead a theoretical analysis of the transmission of spatial symbols, for coherent and noncoherent detection, and for different detection algorithms. We also proposed to use switches to reduce the number of RF chains, thus trading off some performance against complexity. Theoretical expressions of the BEP are derived for each scheme and validated through simulation results for a LOS channel. Afterward, we evaluated the RASK scheme when using MRT precoding, and we calculated the amplitude of the interference as well as the closed form of BEP. This study was validated by simulations, and by a practical implementation in a real testbed.

3.2 Concept and System Model

3.2.1 Principle of RASK

Recall from chapter 1, that the RASK scheme is one of the receive SM transmission schemes. Its principle is elaborated in details in this part. RASK applies SM at the receiver side by means of spatial focusing techniques [9]. More precisely, RASK consists of exploiting the transmit antenna array to form spatial beams and target one of the N_r receive antennas during each symbol duration. The index of the targeted antenna is associated to a predefined set of information bits, without any IQ modulation. As RASK considers one single targeted antenna at a time, the number m of bits conveyed by a RASK symbol is simply:

$$m = \log_2(N_r)\text{bits/symbol.} \tag{3.1}$$

For a convenient RASK operation, the number of useful receive antenna should, therefore, be a power of two.

00 01 11 10	Symbol 1	Symbol 2	Symbol 3	Symbol 4
1) Segmentation	00	01	11	10
2) Mapping	R1	R2	R3	R4
3) Preprocessing (focalisation)	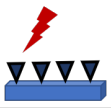			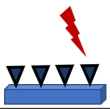
4) Detection	R1	R2	R3	R4
5) Demapping	00	01	11	10

Figure 3.1 – Example of RASK system with $N_r = 4$

Figure 3.1 provides an illustrated example for a RASK scheme with $N_r = 4$, i.e. in which $m = 2$ bits per symbol are transmitted. The corresponding spatial mapping table is given as follows:

Targeted antenna R_i	R_1	R_2	R_3	R_4
M-ary symbol	00	01	11	10

Table 3.1 – Mapping table of the spatial symbol for a 4 receive antenna RASK

3.2.2 System Model

The block diagram of a RASK transmission chain is depicted in Figure 3.2. According to the $N_t \times N_r$ MIMO system architecture previously considered, the RASK system can be modeled using the following matrix based input-output signal expression:

$$\mathbf{y} = f \cdot \mathbf{H} \underbrace{\mathbf{W}\mathbf{x}_k}_{\mathbf{s}_k} + \mathbf{n}, \tag{3.2}$$

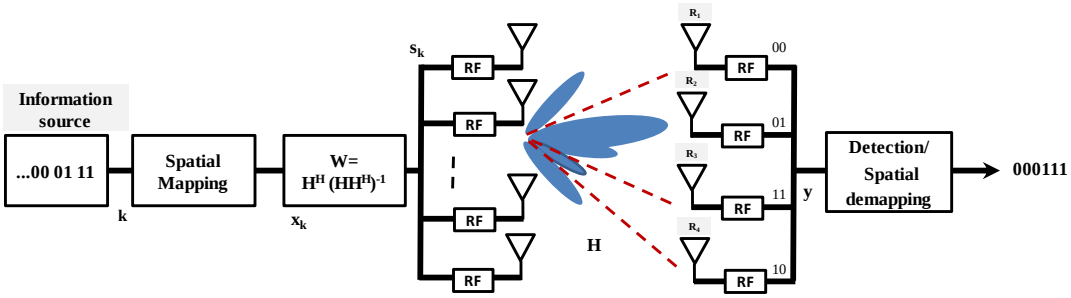

Figure 3.2 – Block diagram of a RASK transmission chain

where $\mathbf{H} \in \mathbb{C}^{N_r \times N_t}$ is the MIMO flat fading channel matrix with elements $h_{j,i}$ representing the complex channel gain between the i-th transmit antenna, denoted T_i, and the j-th receive antenna, denoted R_j. By the singular value decomposition theorem, any matrix $\mathbf{H} \in \mathbb{C}^{N_r \times N_t}$ can be written as:

$$\mathbf{H} = \mathbf{U}\mathbf{\Lambda}^{\frac{1}{2}}\mathbf{V}^H \tag{3.3}$$

where $\mathbf{U} \in \mathbb{C}^{N_r \times N_r}$ and $\mathbf{V} \in \mathbb{C}^{N_t \times N_t}$ are unitary matrices, and $\mathbf{\Lambda} \in \mathbb{R}^{N_r \times N_r}$ is a non-negative and diagonal matrix. Actually, $\mathbf{\Lambda} = \text{diag}(\lambda_1, \lambda_2, ..., \lambda_{N_r})$ is the diagonal matrix of the eigenvalues of $\mathbf{H}\mathbf{H}^H$. $\mathbf{s}_k \in \mathbb{C}^{N_t \times 1}$ is the vector of the complex samples sent through the N_t transmit antennas and intended to focus towards receive antenna R_k. $\mathbf{y} \in \mathbb{C}^{N_r \times 1}$ is the vector of the received signals on all receive antennas, where the j-th entry is y_j, and $\mathbf{n} \in \mathbb{C}^{N_r \times 1}$ is the vector of additive white Gaussian noise (AWGN) samples η_j such that $\eta_j \sim \mathcal{CN}(0, \sigma_n^2)$. Spatial focusing is obtained through the pre-processing step modeled by matrix $\mathbf{W} \in \mathbb{C}^{N_t \times N_r}$ which transforms the vector of spatial symbols $\mathbf{x}_k$ into the vector of transmitted samples $\mathbf{s}_k$. The spatial symbols $\mathbf{x}_k$ result from the spatial mapping step. They are formed such that the entries $x_k(j)$ of $\mathbf{x}_k$ verify $x_k(j) = 1$ for $j = k$ and $x_k(j) = 0$, $\forall j \neq k$, where k is the index of the antenna that should be targeted according to the spatial mapping. In other words, $\mathbf{x}_k$ can be written as

$$\mathbf{x}_k = \Big[0 \quad ... \quad \underbrace{1}_{k\text{th position}} \quad ... \quad 0\Big]^T. \tag{3.4}$$

Finally, f is a normalization factor used to guarantee that the average total transmit power $\bar{P}_t$ remains constant independently on the spatial symbol vector and the pre-processing matrix. More precisely:

$$f = \frac{1}{\sqrt{\mathbb{E}_k\{\text{Tr}(\mathbf{x}_k^H \mathbf{W}^H \mathbf{W} \mathbf{x}_k)\}}} \tag{3.5}$$

where $\text{Tr}(.)$ holds for the trace of matrix and $\mathbb{E}_k$ stands for the expectation over k. We have:

$$\text{Tr}(\mathbf{x}_k^H \mathbf{W}^H \mathbf{W} \mathbf{x}_k) = \sum_i^{N_t} \|w_{i,k}\|^2. \tag{3.6}$$

$\mathbf{x}$ takes N_r different signatures depending on the index of the targeted antenna, so the expectation is applied over k:

$$\mathbb{E}_k\{\mathrm{Tr}(\mathbf{x}_k^H\mathbf{W}^H\mathbf{W}\mathbf{x}_k)\} = \frac{1}{N_r}\mathrm{Tr}(\mathbf{W}^H\mathbf{W}) \tag{3.7}$$

Finally, equation (5.3) becomes:

$$f = \sqrt{\frac{N_r}{\mathrm{Tr}(\mathbf{W}^H\mathbf{W})}} \tag{3.8}$$

Its evaluation will be done for each precoding scheme in the following of this chapter. Note that the average transmit power is $\bar{P}_t$ =1 in this case.

As may be understood, the performance of RASK essentially relies on two main aspects which are the capability of the transmitter to accurately focus the signal towards the desired antenna, and the efficiency of the detection algorithm at the receiver side for proper decision about the targeted antennas.

3.3 ZF Precoded RASK (ZF-RASK)

The transmitter uses the pre-processing step to create a beam that will concentrate a higher amount of energy towards the targeted receive antenna than towards the other antennas. The pre-processing block requires knowledge of the channel response at the transmitter. In this section, the ZF precoding used as a pre-filter is defined as the pseudo-inverse of the channel matrix:

$$\mathbf{W} = \mathbf{H}^H(\mathbf{H}\mathbf{H}^H)^{-1} \tag{3.9}$$

In this technique, it is required that the number of antennas satisfies $N_r \leq N_t$ for the calculation of the pseudo inverse to become possible.

3.3.1 Normalization factor evaluation

The precoding matrix $\mathbf{W}$ can be also decomposed in SVD, where:

$$\mathbf{W} = \mathbf{V}\mathbf{\Lambda}^{-\frac{1}{2}}\mathbf{U}^H \tag{3.10}$$

so we have:

$$\mathbf{W}\mathbf{W}^H = \mathbf{V}\mathbf{\Lambda}^{-\frac{1}{2}}\mathbf{U}^*\mathbf{U}^H(\mathbf{\Lambda}^{-\frac{1}{2}})^*\mathbf{V}^H = \mathbf{V}(\mathbf{\Lambda}^{-1})\mathbf{V}^H, \tag{3.11}$$

where $(.)^*$ is the conjugate operator. Using equation 3.8, we have:

$$f = \sqrt{\frac{N_r}{\mathrm{Tr}(\mathbf{V}^H(\mathbf{\Lambda}^{-1})\mathbf{V})}} = \sqrt{\frac{N_r}{\mathrm{Tr}(\mathbf{\Lambda}^{-1})}} = \sqrt{\frac{N_r}{\sum_{i=1}^{N_r}\frac{1}{\lambda_i}}} \tag{3.12}$$

3.3.2 Received signal

The RASK receiver has to detect which is the targeted antenna between the N_r receive antennas in order to estimate the transmit spatial symbol. Various detection algorithms can be used for the estimation of the targeted antenna depending on the complexity which can be afforded by the receiver [9]. Using the expression of the receive signal vector in equation (3.2) detected by a Signal Detector "SD", and the expression of the pre-processing matrix in equation (3.9), it is then straightforward to obtain:

$$\mathbf{y} = f \times \mathbf{x} + \mathbf{n} \tag{3.13}$$

At the level of the receive antenna R_j, the received signal then simply writes:

$$y_j = f \times x_j + \eta_j. \tag{3.14}$$

If the receiver is able to detect the complex received signal $\mathbf{y}$, i.e. by estimating the phase in addition to the amplitude, and if the detector is based on analysing this complex signal, the detector is called "coherent detector". Otherwise, if the receiver is not performing a phase estimation, i.e. only detect the amplitude, the detector is called noncoherent detector.

In this section, two schemes of the receiver are proposed, where coherent and non-coherent detections are used and studied:

- Coherent Maximum Likelihood detector (CML), based on the application of the maximum likelihood criterion, coherent to the complex received signal
- Noncoherent Maximum Likelihood detector (NCML), a noncoherent detector that applies the ML criterion to the received signal power.

In the next part, equations of different detection schemes and algorithms are presented, with the expressions of the BEP conditioned by the channel, i.e. for a given channel realization, calculated.

3.3.3 Coherent Detection (CML)

Detector Equation

This detector needs carrier and phase synchronization per receive antenna at the receiver side, in order to detect the complex received signal. From equation (3.14), a given coherent detector has to analyze the following set of signals:

$$\forall j, \quad y_j = \begin{cases} f + \eta_j & \text{if } R_j \text{ is the targeted antenna} \\ \eta_j & \text{otherwise} \end{cases} \tag{3.15}$$

Since the ZF precoding scheme is used, no interference appears between receive antennas. The maximum likelihood receiver has been presented and studied in [78] for generalised RSM, where the equation of this detector is:

$$\hat{k} = \text{Arg}\min_j \left\{ \left\| \mathbf{y} - f\mathbf{x}_j \right\|^2 \right\} \tag{3.16}$$

since all transmit symbols are independants. The CML detector saves the signatures (the corresponding receive signals) of all possible spatial symbols transmitted (N_r signatures) in a stage of calibration, and chooses, at each symbol duration, the one that is the closest to the received signal in the Euclidean distance. Referring to [78], the Pairwise Error Probability (PEP) of the CML detector for the spatial modulation is:

$$\begin{aligned}
&\mathcal{P}(\mathbf{x}_k \to \mathbf{x}_j|\mathbf{H}) = \mathcal{P}\left(\|\mathbf{y} - f\mathbf{x}_k\|^2 > \|\mathbf{y} - f\mathbf{x}_j\|^2\right) \\
=&\mathcal{P}\left(\sum_{i=1}^{N_r} \|fx_k(i) + \eta_i - fx_k(i)\|^2 > \sum_{i=1}^{N_r} \|fx_k(i) + \eta_i - fx_j(i)\|^2\right) \\
=&\mathcal{P}\left(\sum_{i=1}^{N_r} \|\eta_i\|^2 > \sum_{i=1}^{N_r} \|\eta_i\|^2 + 2(f)^2 + 2f \times \Re\{\eta_k - \eta_j\}\right) \\
=&\mathcal{P}\left(\Re\{\eta_j - \eta_k\} > f\}\right) = \mathcal{P}\left(\Re\mathcal{N}(0, \sigma_n) > f\}\right) = Q\left(f/\sigma_n\right).
\end{aligned} \tag{3.17}$$

where Q(.) denotes the Gaussian distribution function: $Q(x) = \int_x^\infty \frac{1}{2\pi} e^{-\frac{t^2}{2}} dt$.

Efficient Implementation of the ML detector

Theorem 1. *In RASK systems with only spatial symbol transmission, if ZF pre-processing is employed, the optimal detector is reduced to a Single Tap Maximum real part comparator.*

Proof. Using ZF pre-processing, the received signal at the targeted antenna will exhibit the same phase as that of the emitted signal due to the phase compensation effect (from equation 3.14). Retaking the derivation in equation 3.17, in order to simplify the detection algorithm of ML, supposing that $\mathbf{x}_k$ is the transmitted spatial symbol:

$$\begin{aligned}
&\mathcal{P}(\mathbf{x}_k \to \mathbf{x}_j|\mathbf{H}) = \mathcal{P}\left(\Re\{\eta_j - \eta_k\} > f\}\right) \\
=&\mathcal{P}\left(\Re\{\eta_j\} > f + \Re\{\eta_k\}\right)
\end{aligned} \tag{3.18}$$

So in such receiver, if the transmitted signal is real, a valid detection is maintained if the targeted antenna detects the maximum value of the real amplitude part, and the same performance can be obtained with a simple detection algorithm. □

This algorithm avoids the receiver to carry out the channel estimation step, and thus reduces the computational complexity of the receiver.

Note that the reduced CML for ZF precoded RASK is a Single-Tap detector using $N_r - 1$ comparators. Otherwise, if we use another pre-processing technique, additional interference is added to the non targeted antennas and the CML can't be anymore reduced to the above detector. In this case, the computation complexity increases to compare all complex signatures, where $2N_r^2$ multiplications and $N_r(2N_r - 1)$ additions/subtractions are needed. More details are described in part 3.5.7.

BEP with CML detector

Theorem 2. *The expression of BEP obtained with a coherent ML receiver conditioned by the channel* $\boldsymbol{H}$ *for a ZF-RASK scheme is given by the equation:*

$$\begin{aligned}\mathcal{P}_e = \frac{N_r}{2.(N_r-1)} \int_{-\infty}^{+\infty} \frac{1}{\sqrt{\pi\sigma_n^2}} e^{\frac{-(t-f)^2}{\sigma_n^2}} \\ \times \left[1 - Q\left(\frac{t\sqrt{2}}{\sigma_n}\right)\right]^{N_r-1} dt.\end{aligned} \tag{3.19}$$

Proof. The formula that derives the analytic Average BEP $\mathcal{P}_e$ for RASK scheme is [29]:

$$\mathcal{P}_e = \frac{1}{m} \cdot \mathbb{E}\left\{\sum_{k}^{N_r}\sum_{j\neq k}^{N_r} \mathcal{P}(\mathbf{x}_k \to \mathbf{x}_j) \times d(\mathbf{x}_k, \mathbf{x}_j)\right\}, \tag{3.20}$$

where $d(\mathbf{x}_k, \mathbf{x}_j)$ is the Hamming distance between two spatial symbols $\mathbf{x}_k$ and $\mathbf{x}_j$. It is shown that the received real amplitude over all non-targeted antennas follows the same probability distribution, i.e. $\mathcal{N}(0, \sigma_n^2/2)$, so that the equation (**??**) can be expressed as:

$$\mathcal{P}_e = \frac{1}{m}\mathbb{E}\left\{\sum_{k}^{N_r}\sum_{j\neq k}^{N_r} d(\mathbf{x}_k, \mathbf{x}_j)\right\} \mathcal{P}(\mathbf{x}_k \to \mathbf{x}_{j,j\neq k}) \tag{3.21}$$

where $m = \log_2(N_r)$ bit/symbol, $\mathbb{E}\left\{\sum_k^{N_r}\sum_{j\neq k}^{N_r} d(\mathbf{x}_k, \mathbf{x}_j)\right\} = \frac{N_r \log_2(N_r)}{2(N_r-1)}$, and $\mathcal{P}\left(\mathbf{x}_k \to \mathbf{x}_{j,j\neq k}\right)$ is the Symbol Error Rate (SER). So we have:

$$\begin{aligned}\mathcal{P}_e &= \frac{1}{\log_2(N_r)} \frac{N_r \log_2(N_r)}{2(N_r-1)} \mathcal{P}(\mathbf{x}_k \to \mathbf{x}_{j,j\neq k}) \\ &= \frac{N_r}{2.(N_r-1)} \mathcal{P}\left(\mathbf{x}_k \to \mathbf{x}_{j,j\neq k}\right),\end{aligned} \tag{3.22}$$

Another way to resolve this equation consists of evaluating the complementary of the SER, i.e.:

$$\mathcal{P}\left(\mathbf{x}_k \to \mathbf{x}_{j,j\neq k}\right) = 1 - \mathcal{P}\left[\Re\{y_{j,j\in[1:N_r]}\} < \Re\{y_k\}\right], \tag{3.23}$$

where

$$\Re\{y_i\} \sim \mathcal{N}(f, \sigma_n^2/2). \tag{3.24}$$

Moreover, from appendix A, the left-hand side of the equation above can be presented by the integral:

$$\mathcal{P}\left[\Re\{y_{j,j\in[1:N_r]}\} < \Re\{y_k\}\right] = \int_{-\infty}^{+\infty} f_{y_k}(t) \prod_{j=1,j\neq k}^{N_r} F_{y_j}(t)dt, \tag{3.25}$$

where $f_{y_k}(t)$ is the probability density function of y_k:

$$f_{y_k}(t) = \frac{1}{\sqrt{\pi\sigma_n^2}} e^{\frac{-(t-f)^2}{\sigma_n^2}},$$

and $F_{y_j}(t)$ is the cumulative density function of y_j:

$$F_{y_j}(t) = 1 - Q\left(\frac{t\sqrt{2}}{\sigma_n}\right).$$

So we have:

$$\begin{aligned}
&\mathcal{P}\left[\Re\{y_{j,j\in[1:N_r]}\} < \Re\{y_k\}\right] \\
&= \int_{-\infty}^{+\infty} \frac{1}{\sqrt{\pi\sigma_n^2}} e^{\frac{-(t-f)^2}{\sigma_n^2}} \prod_{j=1,j\neq k}^{N_r} \left[1 - Q\left(\frac{t\sqrt{2}}{\sigma_n}\right)\right] dt \\
&= \int_{-\infty}^{+\infty} \frac{1}{\sqrt{\pi\sigma_n^2}} e^{\frac{-(t-f)^2}{\sigma_n^2}} \left[1 - Q\left(\frac{t\sqrt{2}}{\sigma_n}\right)\right]^{N_r-1} dt.
\end{aligned} \tag{3.26}$$

□

Lemma 3. *The BEP for the CML receiver in ZF-RASK scheme can be approximated by:*

$$\mathcal{P}_e \approx \frac{N_r}{2} Q\left(f/\sigma_n\right). \tag{3.27}$$

Proof. For high Signal to Noise Ratio (SNR) on the receiver, the value of $Q\left(\frac{t\sqrt{2}}{\sigma_n}\right)$ becomes negligible, and then the equation (3.26) can be approximated by:

$$\begin{aligned}
&\mathcal{P}\left(\Re\{y_{j,j\in[1:N_r]}\} < \Re\{y_k\}\right) \\
&\approx \int_{-\infty}^{+\infty} \frac{1}{\sqrt{\pi\sigma_n^2}} e^{\frac{-(t-f)^2}{\sigma_n^2}} \left[1 - (N_r-1)Q\left(\frac{t\sqrt{2}}{\sigma_n}\right)\right] dt \\
&= \left[1 - (N_r-1)Q\left(\frac{f}{\sigma_n}\right)\right].
\end{aligned} \tag{3.28}$$

Then equation (3.22) becomes:

$$\begin{aligned}
\mathcal{P}_e &\approx \frac{N_r}{2.(N_r-1)} \left[1 - \left(1 - (N_r-1)Q\left(\frac{f}{\sigma_n}\right)\right)\right] \\
&= \frac{N_r}{2} Q\left(f/\sigma_n\right).
\end{aligned} \tag{3.29}$$

□

3.3.4 Noncoherent Detection (NCML)

Consider now the case of noncoherent receiver that detects the received power at the antenna, without considering the phase of the signal. Let $\mathbf{r} \in \mathbb{R}^+$ be the vector of the detected power over all receive antennas, that can be calculated from $\mathbf{y}$ as:

$$\forall j, \quad r_j = \left\|y_j\right\|^2 \tag{3.30}$$

Figure 3.3 shows the block diagram of an envelope detector that can be used for the detection without the need of a down converter in the RF block, that should be used in

CML for the coherent complex demodulation of the signal. A Pass-Band filter is first used to take only the signal at the transmission carrier frequency, followed by a power converter that converts the detected power into current. A low noise amplifier is also used to increase the overall SNR before an integrator used to take the average mean detected power during the symbol duration. In this case, the detector has to analyze the square of the norm of the complex received signals:

$$\forall j, \quad r_j = \|y_j\|^2 = \begin{cases} \|f + \eta_j\|^2 & \text{if } R_j \text{ is the targeted antenna} \\ \|\eta_j\|^2 & \text{otherwise} \end{cases} \tag{3.31}$$

The receiver here estimates the spatial symbol by choosing the index of antenna that

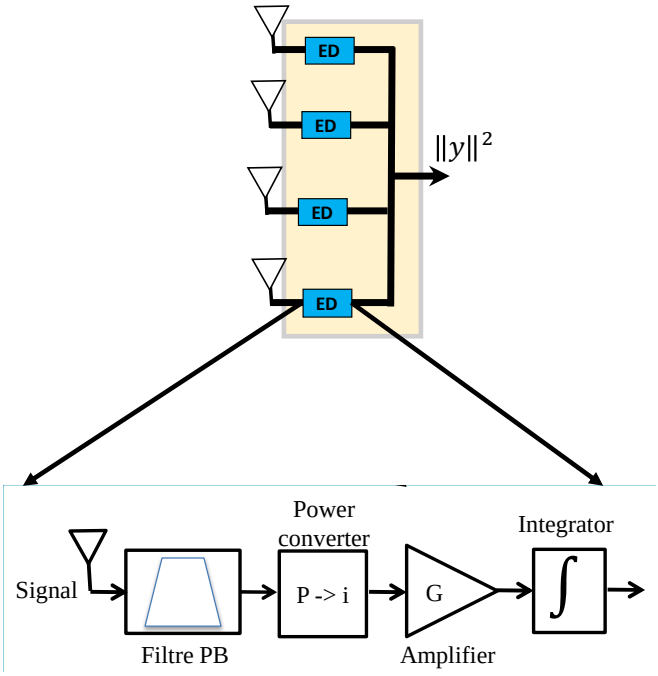

Figure 3.3 – NCML receiver with envelope detector

receives the maximum amount of power:

$$\hat{k} = \text{Arg}\max_j \|y_j\|^2 \tag{3.32}$$

also described as:

$$\forall j \in [1; N_r], \|y_j\|^2 \leq \|y_{\hat{k}}\|^2 \tag{3.33}$$

Theorem 4. *The expression of BEP of an NCML detector conditioned by the channel* $\boldsymbol{H}$ *for ZF-RASK scheme is given by the equation:*

$$\mathcal{P}_e = \frac{N_r}{2.(N_r-1)} \cdot \left[1 - \int_0^{+\infty} \frac{1}{\sqrt{2\pi}} \left(e^{-\frac{(x-m)^2}{2}} + e^{-\frac{(x+m)^2}{2}} \right) \times (1 - e^{-\frac{x^2}{2}})^{N_r - 1} dx \right]. \tag{3.34}$$

Proof. As we did for the performance analysis for the ML receiver in equation (3.22), the equation of the BEP for this detector is:

$$\mathcal{P}_e = \frac{N_r}{2.(N_r-1)} \cdot \left[1 - \mathcal{P}\left(\left\|y_{j,j\in[1:N_r]}\right\|^2 < \|y_k\|^2\right)\right]. \tag{3.35}$$

Moreover, we have:

$$\begin{aligned}\mathcal{P}(\left\|y_{j,j\in[1:N_r]}\right\|^2 < \|y_k\|^2) &= \mathcal{P}(\|\eta_{j,j\neq i}\|^2 < \|f+\eta_i\|^2) \\ &= \mathcal{P}(|\eta'_{j,j\neq i}| < |\frac{\sqrt{2}.f}{\sigma_n} + \eta'_i|),\end{aligned} \tag{3.36}$$

where:

- $|\frac{\sqrt{2}.f.A}{\sigma_n} + \eta'_i| = |m+\eta'_i| = |\mathcal{J}|$ follows a Folded-Normal distribution, i.e. $\mathcal{J} \sim \mathcal{N}(m,1)$
- $|\eta'_j| = |\frac{\sqrt{2}}{\sigma_n}\eta_j| = X \sim \mathcal{X}_2$ (Chi distribution) $\forall j \in [1:N_r], j \neq i$

so:

$$\mathcal{P}(\left\|y_{j,j\in[1:N_r]}\right\|^2 < \|y_k\|^2) = \mathcal{P}(X < |\mathcal{J}|) \tag{3.37}$$

For $x < 0$, $F_X(x) = 0$, and otherwise:

$$F_X(x) = P(1, x^2/2) = \frac{\gamma(1, x^2/2)}{\Gamma(1)} = 1 - e^{-\frac{x^2}{2}} \tag{3.38}$$

And the PDF of $|\mathcal{J}|$ is:

$$f_{|\mathcal{J}|}(x) = \frac{1}{\sqrt{2\pi}}(e^{-\frac{(x-m)^2}{2}} + e^{-\frac{(x+m)^2}{2}}) \tag{3.39}$$

Then the equation (3.36) becomes:

$$\begin{aligned}&\mathcal{P}(\left\|y_{j,j\in[1:N_r]}\right\|^2 < \|y_k\|^2) = \\ &\int_0^{+\infty} \frac{1}{\sqrt{2\pi}}(e^{-\frac{(x-m)^2}{2}} + e^{-\frac{(x+m)^2}{2}}).(1-e^{-\frac{x^2}{2}})^{N_r-1}dx.\end{aligned} \tag{3.40}$$

□

Lemma 5. *The BEP for the NCML receiver in ZF-RASK scheme can be approximated by:*

$$\mathcal{P}_e \approx \frac{N_r}{4} e^{-f^2/2\sigma_n^2}. \tag{3.41}$$

Proof. For high SNR on the receiver, the value of $e^{-\frac{x^2}{2}}$ becomes very small, and then equation (3.34) can be approximated by:

$$\mathcal{P} \approx \int_0^{+\infty} \frac{1}{\sqrt{2\pi}} \left(e^{-\frac{(x-m)^2}{2}} + e^{-\frac{(x+m)^2}{2}}\right).(1-(N_r-1)e^{-\frac{x^2}{2}})dx. \tag{3.42}$$

After some mathematical manipulations, we obtain:

$$\mathcal{P} = 1 - \frac{N_r - 1}{2} e^{-\frac{f^2}{2\sigma_n^2}}, \tag{3.43}$$

and so the equation (3.35) becomes:

$$\mathcal{P}_e \approx \frac{N_r}{4} \exp\left(-\frac{f^2}{2\sigma_n^2}\right). \tag{3.44}$$

□

3.3.5 Simulation Results

The performance of ZF-RASK system using different types of receivers is evaluated through the measurement of the Bit Error Rate (BER) versus the ratio between the symbol energy and noise spectral density, i.e. $\frac{E_S}{N_0}$. It is assumed that $\mathbf{H}$ is a MIMO flat fading channel matrix where $h_{j,i}$ are complex coefficients following an i.i.d. Rayleigh distribution. The power for each sub-channel is normalized:

$$\mathrm{E}\left[\, \left\|h_{j,i}\right\|^2 \,\right] = 1 \tag{3.45}$$

Finally, we consider that the channel response is perfectly known at the transmitter, so that perfect ZF precoding is performed. Simulations are run by implementing a sufficient number of iterations for different channel realizations and taking the mean value of the BER for each value of $\frac{E_S}{N_0}$.

Figure 3.4 gives the performance of RASK with $N_t = 16$, and $N_r = 4$ and 8, using the CML (blue curves), and respectively NCML detectors (black curves). The performance based on simulations and the analytic study for each detection method are compared. As evident from the obtained curves, for high relative SNR, where the BER becomes less than 10^{-1}, theoretical results perfectly match simulation results. Recall that increasing N_r directly translates into an increase of the spectral efficiency since the order $M = 2^m$ of the SM is such that $m = \log_2(N_r)$ with RASK. It is also observed that an increase in the order of the spatial modulation leads to a degradation of the performance. Indeed, as N_r increases, the ZF pre-processing technique has to deal with a higher number of antennas on which interference has to be canceled. Also from the figure, it seems that the CML outperforms the noncoherent one, which can be obviously concluded from the theoretical results.

3.4 Switching Effect on Performance

In NCML detector, the detection scheme is simple because requiring no down converter, and no carrier and phase synchronization are required, while all needed in the

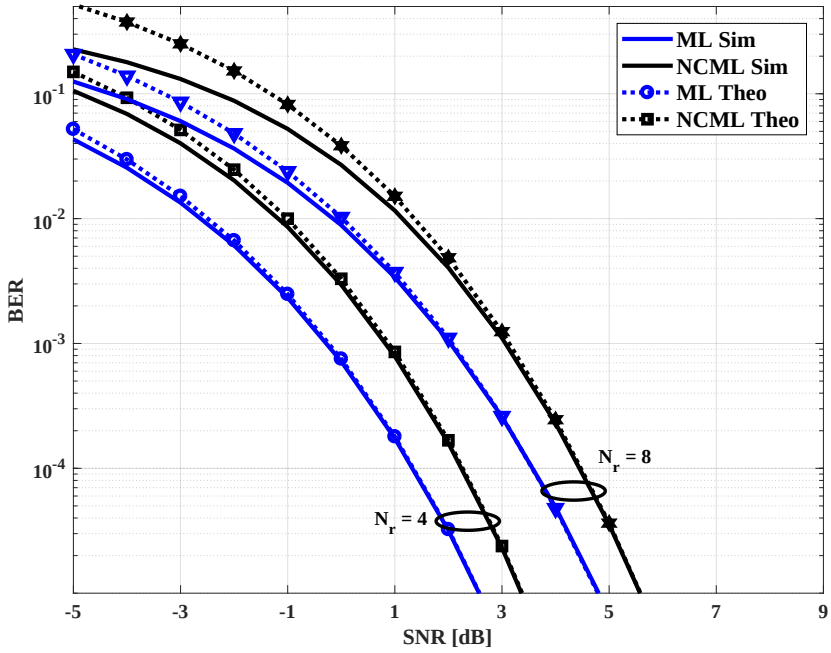

Figure 3.4 – BER performance of 16×4 and 16×8 ZF-RASK systems using CML and NCML detectors over Rayleigh channel, simulated and theoretical results

CML detector and included in the RF chain. In this section, we will propose to use switches for the CML detector, in order to reduce the number of RF chains, while keeping the NCML without switches, because of its simple detection scheme. The effect of using switches on the performance of CML will be studied and compared to the performance of NCML without switches.

3.4.1 Influence of the number of RF chains

One of the main advantages of the SM at the transmitter is the possible reduction of the number of RF chains, to reduce the overall power. For receive SM, all receive antennas should listen to the received signal during the symbol duration, and so the reduction of the number of RF chains using switches (or analog multiplexers) leads to a degradation in the effective SNR. Let N_{RF} be the number of the RF chains at the receiver, and N_S the number of switches. In a fair scenario, each switch is connected to the same number of receive antennas and $N_{RF} = N_S$ where each chain is connected to a switch as shown in Figure 3.5. We assume that all switches are identical. Let τ be the delay of switching to change the state of a switch port. Let $\bar{P}_e$ be the mean total transmitted power per symbol duration. The factor f at the transmitter is used to normalize the average transmit power to $\bar{P}_e = A^2$, and $P_b = \sigma_n^2 = N_0 B$ is the noise power. Let $\bar{P}_r$ be the mean of the received power at the targeted receive antenna. We have:

$$\bar{P}_r = \mathbb{E}_{\mathbf{x}}\{\mathrm{Tr}(\mathbf{s}_k^H \mathbf{H}^H \mathbf{H}\mathbf{s})\} = f^2 \times E_s \tag{3.46}$$

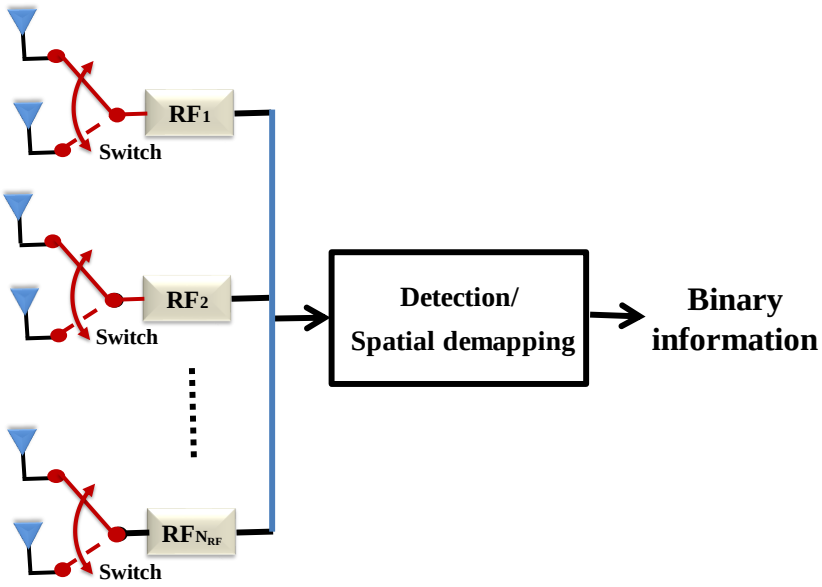

Figure 3.5 – Receiver with N_{RF} RF chain and switch

where E_s is the spatial symbol energy. Supposing that a symbol rate D_s is transmitted in a bandwidth B and that $B = D_s$, we have:

$$\text{SNR} = \frac{\bar{P}_r}{\sigma_n^2} = \frac{f^2 E_s D_s}{N_0 B} = \frac{f^2 E_s}{N_0} \tag{3.47}$$

The average time of listening over each receive antenna is $T_l = T_s N_{RF}/N_r$. Let $\bar{\tau} = \tau/T_l$. Supposing that the waveform of the received signal is rectangular, the detected energy at the received antenna E_d is equal to:

$$E_d = (1-\bar{\tau})\bar{P}_r T_l = (1-\bar{\tau}) E_s N_{RF}/N_r \tag{3.48}$$

We define ESNR as the effective SNR resulted from the detected signal when the CML detector is used. We then have:

$$\text{ESNR} = (1-\bar{\tau})\frac{f^2 E_s N_{RF}}{N_0 N_r} = \xi \text{SNR} \tag{3.49}$$

where $\xi = (1-\bar{\tau})\frac{N_{RF}}{N_r}$. For comparison purposes, we will consider the case of ideal switches, where $\bar{\tau} = 0$. In the Figure 3.6, a ZF-RASK scheme with $N_t = 32$ and $N_r = 16$ configuration is considered. The BER performance using the NCML (without switches) is drawn, as well as the BER using the CML with different numbers of RF chains and ideal switches. As evident, decreasing the number of RF chains leads to BER degradation, and for a specific number of RF chains, the NCML outperforms the CML at a predefined BER. For example, for a BER less than 5×10^{-4}, the NCML outperforms the CML for $N_{RF} \leq 14$, and for a BER more than 10^{-3} the NCML performance occurs between the CML for $N_{RF} = 13$ and $N_{RF} = 14$.

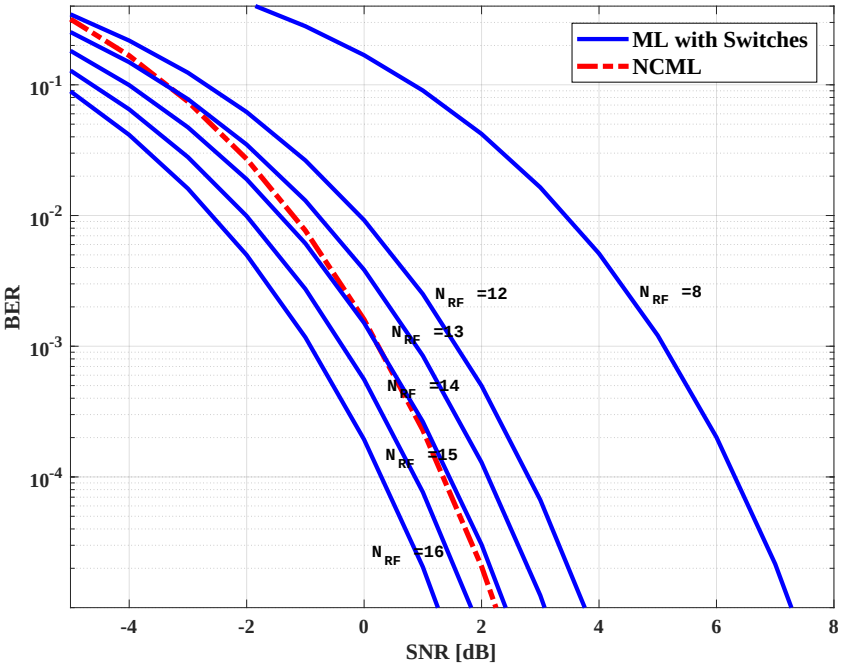

Figure 3.6 – BER of 32×16 ZF-RASK using NCML or CML detection with a variable number of RF chains using switches

3.4.2 Equivalence between Switched CML and NCML

The system performance and the receiver complexity are two parameters for choosing the better receiver. As previously shown, reducing the number of RF chains to reduce the complexity or the power consumption lead to a decrease of the performance of the system, and at some point, the noncoherent detector outperforms the coherent one. In order to fairly compare them, we can analytically calculate the equivalence of the two detection schemes. The performance of the detector is related to the detected ESNR, that is equal to ξSNR in case of CML detector, and equal to SNR in case of NCML detector. For a predefined system configuration, i.e. given N_t and N_r, and predefined targeted BEP, we calculate ξ for a coherent system to achieve the BEP with the same SNR. First, equation (3.29) and equation (3.44) that derive the performance of CML and NCML detector respectively rewrite:

$$\text{BEP} = \frac{N_r}{2} Q\left(\sqrt{\text{ESNR}}\right) = \frac{N_r}{2} Q\left(\sqrt{\xi \text{SNR}}\right). \tag{3.50}$$

and:

$$\text{BEP} = \frac{N_r}{4} \exp\left(-\text{ESNR}\right) = \frac{N_r}{4} \exp\left(-\text{SNR}\right). \tag{3.51}$$

Moreover, the SNR needed to achieve certain BEP, using the CML detector (SNR_{CML}) and NCML detector (SNR_{NCML}) are respectively:

$$\text{SNR}_{\text{CML}} = \frac{1}{\xi}\left[Q^{-1}\left(\frac{2}{N_r}\text{BEP}\right)\right]^2, \tag{3.52}$$

and:

$$\mathrm{SNR}_{\mathrm{NCML}} = -2 \times \ln(\frac{4}{N_r}\mathrm{BEP}). \tag{3.53}$$

The equivalent point of these detectors, ξ_E, is obtained when a same BEP is acheived for a same SNR, i.e. $\mathrm{SNR}_{\mathrm{CML}} = \mathrm{SNR}_{\mathrm{NCML}}$. So we have:

$$\frac{1}{\xi_E}\left[Q^{-1}\left(\frac{2}{N_r}\mathrm{BEP}\right)\right]^2 = -2 \times \ln(\frac{4}{N_r}\mathrm{BEP}). \tag{3.54}$$

And finaly we find:

$$\xi_E = -\frac{\left[Q^{-1}\left(\frac{2}{N_r}\mathrm{BEP}\right)\right]^2}{\ln(\frac{4}{N_r}\mathrm{BEP})}. \tag{3.55}$$

Note that ξ_E is independent on N_t, so the choice of the optimal receiver only depends on the receiver configuration and on the targeted BEP.

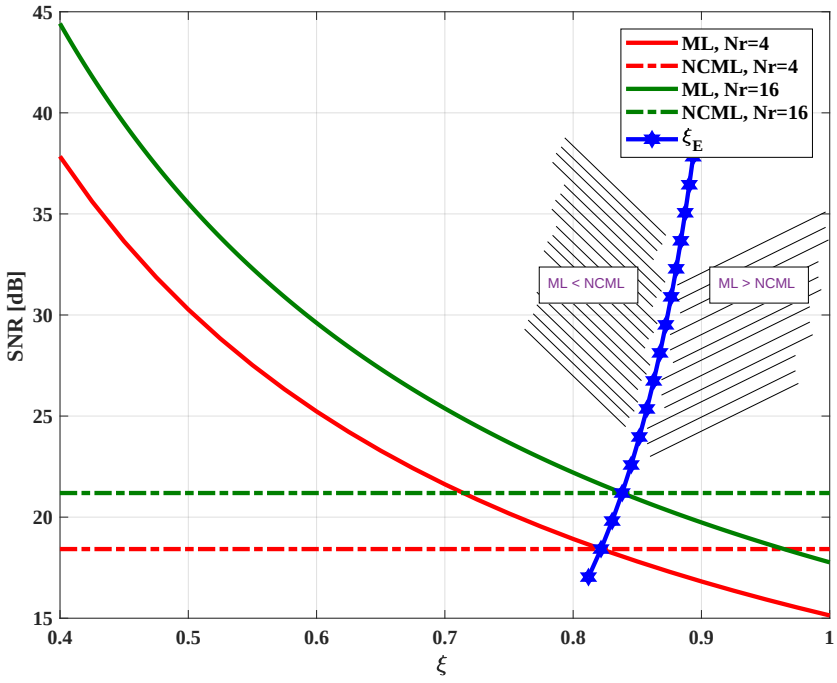

Figure 3.7 – The needed SNR to achieve a BEP=10^{-4} for a ZF-RASK system with $N_r = 4$ and $N_r = 16$ using CML and NCML detection, in terms of ξ

In Figure (3.7), the targeted BEP is fixed at 10^{-4}, and the needed SNR to achieve this BEP is evaluated as a function of ξ, i.e. the number of RF chains, for $N_r = 4$ and $N_r = 16$. Since the NCML detection is independent on the number of RF chains (in terms of complex demodulation and down-conversion, only envelopp detectors are used), the value of SNR_{NCML} is constant for each system configuration. Moreover, $\mathrm{SNR}_{\mathrm{CML}}$ decreases when the number of RF chains increases, and at ξ_E the two curves, for CML and NCML, are crisscrossing. From equation (3.55), the analytical values for ξ_E are 0.8217 for $N_r = 4$, and 0.8382 for $N_r = 16$, which can be validated by the curves.

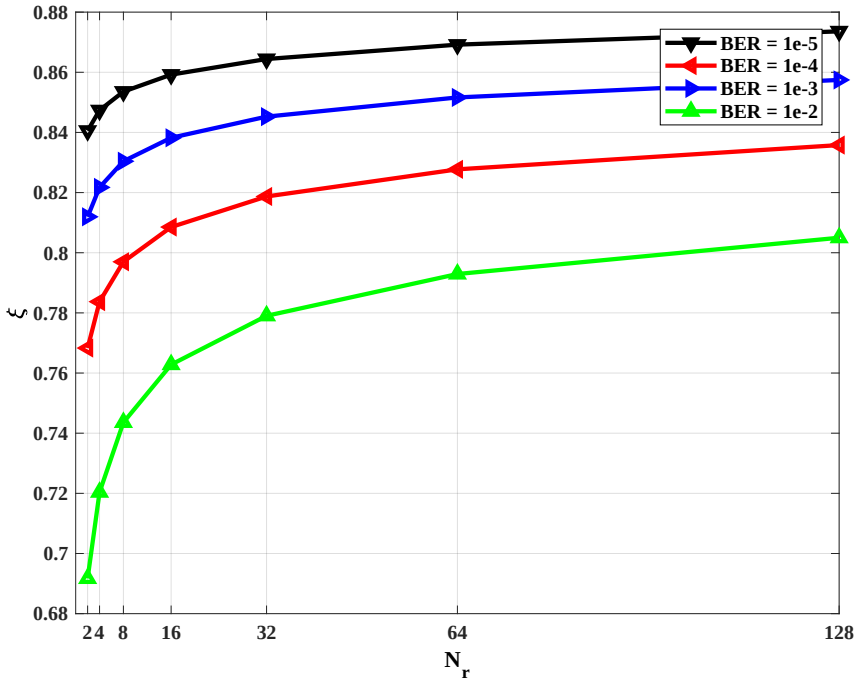

Figure 3.8 – Variation of ξ_E in terms of N_r for ZF-RASK for different targeted BEP.

The blue curve gives the set of ξ_E for different N_r. On the left side of the blue curve, the NCML detector outperforms the CML detector with switches, and on the right side, the CML outperforms the NCML. From ξ_E, we can deduce that the NCML is a better choice when $\xi < \xi_E$ in performance, in terms of complexity as well as power consumption. Asymptotically, the limit of equation (3.55) is equal to 1, since $Q(x)$ can be approximated by e^{-x^2}, and $Q^{-1}(x)$ by $-\ln(x)^2$. The Figure (3.8) shows the variation of ξ_E in terms of N_r for different targeted BER. It is shown that ξ_E increases when N_r increases and approaches 1. This means that for higher N_r, the performance of the NCML detector tends to be close to the CML detector even without switching (full of RF chains). Moreover, depending on the system and the channel coding used, for a targeted BER and for a specific system configuration, the NCML outperforms the CML under certain N_{RF} also with lower complexity and cost. Then the CML will only be a better choice if N_{RF} is more than or equal to $\lceil \xi_E \times N_r \rceil$, where $\lceil . \rceil$ is the ceil operator.

Since ξ takes real and continuous values, it is required to calculate the minimum number of RF chains to outperform the NCML detector, which depends on ξ_E and the switching time factor $\bar{\tau}$:

$$\frac{N_{RF}}{N_r} = \left\lceil \frac{\xi_E}{1-\bar{\tau}} \right\rceil . \tag{3.56}$$

Figure 3.9 shows the ratio of the number of RF chains for each receiver configuration, N_{RF}/N_r, needed to outperform the NCML in terms of N_r, for different values of $\bar{\tau}$. It is shown that for $\bar{\tau} = 0$, the ratio is higher than ξ_E because of the discretization. Thus, the higher the switching factor, the higher the number of RF chains needed to increase the ESNR. Also, for $\bar{\tau} = 0.15$, there is no RF reduction for $N_r \leq 16$, and so the switching is no longer effective. For low complexity devices, as for IoT, where the number of

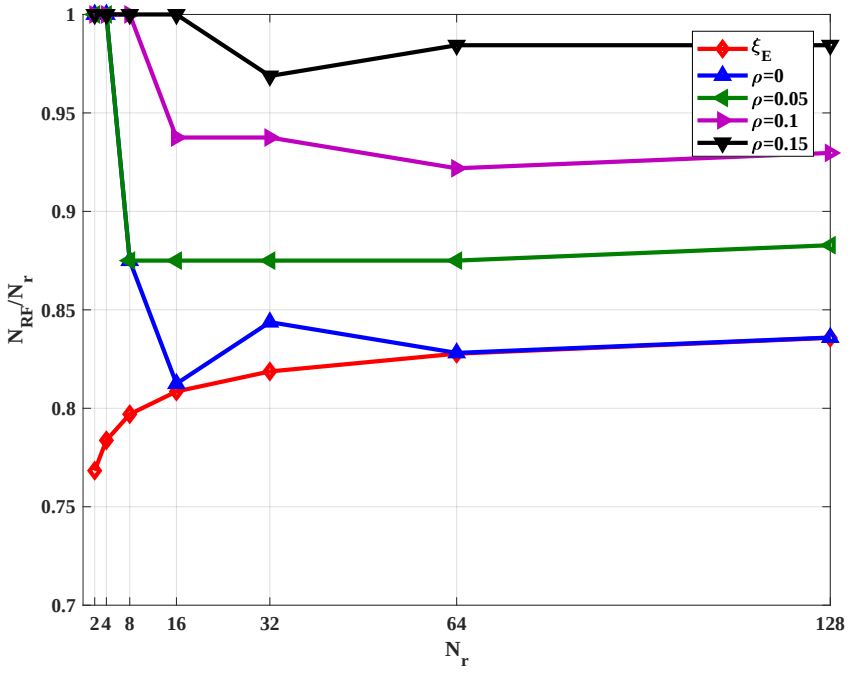

Figure 3.9 – Ratio of the number of RF chains for each receiver configuration of N_r for ZF-RASK for different switching coefficients.

antenna is limited (8 or less), it is shown that the switching with CML is no more a good choice compared to the NCML detection.

3.5 MRT Precoded RASK (MRT-RASK)

In this section, we study the performance of RASK system with MRT precoding. The also called conjugate beam-forming CBF pre-processing technique is employed, where the conjugate of the channel matrix is used as a pre-filter:

$$\mathbf{W} = \mathbf{H}^H. \tag{3.57}$$

This technique concentrates the energy on the targeted antenna and can be implemented in the time domain as Time Reversal [9], without the need of a Fourier transformation at the receiver or at the transmitter, and unlike the ZF, without any constraint on the number of transmit antennas.

3.5.1 Normalization factor evaluation

The equation of the transmitted signal is written as:

$$\mathbf{s} = f\mathbf{H}^H.\mathbf{x} \tag{3.58}$$

and the normalization factor is given by:

$$f = \frac{1}{\sqrt{\mathbb{E}_{\mathbf{x}}\{\mathrm{Tr}(\mathbf{x}_k^H.\mathbf{\Sigma}^H.\mathbf{x}_k)\}}} \tag{3.59}$$

where $\mathbf{\Sigma} = \mathbf{H}\mathbf{H}^H$. Equivalently we have:

$$f = \sqrt{\frac{N_r}{\mathrm{Tr}(\Sigma)}} = \sqrt{\frac{N_r}{\mathrm{Tr}(\mathbf{\Lambda})}} = \sqrt{\frac{N_r}{\sum_{i=1}^{N_r} \lambda_i}} \tag{3.60}$$

3.5.2 Received Signal

Using the expression of the receive signal vector in equation (3.2) and the expression of the transmitted signal in equation (3.58), it is then straightforward to obtain:

$$\mathbf{y} = f\mathbf{\Sigma}\mathbf{x} + \mathbf{n} \tag{3.61}$$

At the level of R_j, the received signal then simply writes:

$$y_j = \begin{cases} f\sum_{i=1}^{N_t} \left\|h_{j,i}\right\|^2 + \eta_j, & \text{if } j = k, \\ f\sum_{i=1}^{N_t} h_{j,i}h_{i,l}^* + \eta_j, & \text{otherwise.} \end{cases} \tag{3.62}$$

3.5.3 Coherent ML and Maximum Real Amplitude Detectors

Coherent ML Detector

The equation of the ML based detector is:

$$\hat{k} = \mathrm{Arg}\min_j \left\{ \left\|\mathbf{y} - f\mathbf{\Sigma}_j\right\|^2 \right\} \tag{3.63}$$

where $\mathbf{\Sigma}_j = \mathbf{\Sigma}\mathbf{x}_j$, and $\mathbf{\Sigma}_j(k)$ is the k-th entry of $\mathbf{\Sigma}_j$.

Because of the interference received by the non-targeted antennas, the ML detector cannot be equivalent to the maximum real part comparator as when using the ZF precoding. Consequently, the PEP conditioned on $\mathbf{H}$ is given as:

$$\begin{aligned} &\mathcal{P}(\mathbf{x}_k \to \mathbf{x}_j|\mathbf{H}) = \mathcal{P}(d_k > d_j|\mathbf{H}) \\ &= \mathcal{P}\left(\Re\{\mathbf{n}^H f(\mathbf{\Sigma}_j - \mathbf{\Sigma}_k)\} > \frac{1}{2}f^2\left\|\mathbf{\Sigma}_j - \mathbf{\Sigma}_k\right\|^2|\mathbf{H}\right) \\ &= Q\left(\frac{\left\|\mathbf{\Sigma}_j - \mathbf{\Sigma}_k\right\|}{\sqrt{2}\sigma_n/f}\right) \end{aligned} \tag{3.64}$$

where $d_j = \left\|\mathbf{y} - f\mathbf{\Sigma}_j\right\|^2$.

Maximum Real Amplitude Detector (MRA)

From equation 3.62, we can see that the targeted antenna receives a real signal. Also, in MIMO i.i.d Rayleigh fading channels, the MRT precoding will further increase the SNR for the targeted antenna [88]. This detector estimates the targeted antenna by choosing the one that receives the maximum real amplitude between all received signal (just like the CML detector used when the ZF precoding is performed). Unlike in ZF precoding, here this detector is a sub-optimal detector, that does not requires the channel knowledge and reduced to a Single Tap receiver.

$$\hat{k} = \mathrm{Arg}\max_j \Re\{y_j\} \tag{3.65}$$

This detector was used in [9] when the Time Reversal precoding was performed. For this receiver, the PEP conditioned by $\mathbf{H}$ writes:

$$\begin{aligned}\mathcal{P}(\mathbf{x}_k \to \mathbf{x}_j|\mathbf{H}) &= \mathcal{P}\left(f\Re\{\mathbf{\Sigma}_k(k) - \mathbf{\Sigma}_k(j)\} < \Re\{\eta_j - \eta_k\}|\mathbf{H}\right) \\ &= Q\left(\frac{\mathbf{\Sigma}_k(k) - \Re\{\mathbf{\Sigma}_k(j)\}}{\sqrt{2}\sigma_n/f}\right)\end{aligned} \tag{3.66}$$

3.5.4 Maximum Real Minimum Imaginary Detector (MRMI)

In order to benefit more from the information about the received signal, another simple but more efficient detector is proposed for MRT-RASK, where also no channel information is needed at the receiver. Since the targeted antenna only receives positive real amplitude signal, this detector, called Maximum Real Minimum Imaginary (MRMI) estimates the targeted antenna by choosing the antenna that has the maximum real amplitude and minimum imaginary in absolute. The equation of the detector writes:

$$\hat{k} = \text{Arg}\max_j \Re\{y_j\} - |\Im\{y_j\}| \tag{3.67}$$

where $\Im\{.\}$ is the imaginary part.

3.5.5 Noncoherent ML and Maximum Received Power Detectors

In addition to the coherent detectors described above, also the noncoherent detectors are studied when the MRT precoding is performed, and the same signal detector as these proposed in Figure 3.3 for noncoherent detector based on the received power measurement.

Noncoherent ML Detector

This detector aims to save the received power by all receive antennas corresponding to each spatial symbol, and during the transmission it will estimate the spatial symbol by detecting the signatures that have the minimum Euclidean distance with the received power signal. The equation of this receiver writes:

$$\hat{k} = \text{Arg}\min_j \left\{ \left| \|\mathbf{y}\|^2 - \|f\mathbf{\Sigma}_j\|^2 \right|^2 \right\} \tag{3.68}$$

Maximum Received Power Detector (MRP)

The MRP detector is analog to the MRA detector but based on the received power detection. So the estimated targeted antenna is the antenna that receives the maximum amount of power. The equation of the detector writes:

$$\hat{k} = \text{Arg}\max_j \|y_j\|^2 \tag{3.69}$$

The PEP conditioned by $\mathbf{H}$ is:

$$\mathcal{P}(\mathbf{x}_k \to \mathbf{x}_j|\mathbf{H}) = \mathcal{P}(\|y_k\|^2 < \|y_j\|^2) = \mathcal{P}(\|f\mathbf{\Sigma}_k(k) + \eta_k\| < \|f\mathbf{\Sigma}_j(k) + \eta_j\|). \tag{3.70}$$

As

$$\begin{aligned} &\mathcal{X}_{k,k} = \|f\mathbf{\Sigma}_k(k) + \eta_k\| \sim |\mathcal{N}(\|f\mathbf{\Sigma}_k(k)\|, \sigma_n^2)| \\ &\text{and } \mathcal{X}_{k,j} = \left\|f\mathbf{\Sigma}_j(k)\right\| + \eta_j) \sim |\mathcal{N}(\left\|f\mathbf{\Sigma}_j(k)\right\|, \sigma_n^2)|, \end{aligned} \tag{3.71}$$

we have:

$$\begin{aligned} \mathcal{P}(\mathbf{x}_k \to \mathbf{x}_j|\mathbf{H}) &= \mathcal{P}(|\mathcal{N}(\|f\mathbf{\Sigma}_k(k)\|, \sigma_n^2)| < |\mathcal{N}(\left\|f\mathbf{\Sigma}_j(k)\right\|, \sigma_n^2)|) \\ &= \int_{-\infty}^{+\infty} f_{\mathcal{X}_{k,k}}(x).(1 - F_{\mathcal{X}_{j,k}}(x))dx \end{aligned} \tag{3.72}$$

where:

$$f_{\mathcal{X}_{k,k}}(x) = \frac{1}{\sqrt{2\pi\sigma_n^2}} \left(e^{\frac{-(x-\|f\mathbf{\Sigma}_k(k)\|)^2}{2\sigma_n^2}} + e^{\frac{-(x+\|f\mathbf{\Sigma}_k(k)\|)^2}{2\sigma_n^2}} \right) \tag{3.73}$$

is the probability density function of $\mathcal{X}_{k,k}$, and

$$F_{\mathcal{X}_{j,k}}(x) = \frac{1}{2} \left[\text{erf}\left(\frac{x + \left\|f\mathbf{\Sigma}_j(k)\right\|}{\sqrt{2}\sigma_n} \right) + \text{erf}\left(\frac{x - \left\|f\mathbf{\Sigma}_j(k)\right\|}{\sqrt{2}\sigma_n} \right) \right] \tag{3.74}$$

is the cumulative density function of $\mathcal{X}_{j,k}$. After some mathematical derivation, the equation 3.72 becomes:

$$\mathcal{P}(\mathbf{x}_k \to \mathbf{x}_j|\mathbf{H}) = \frac{1}{2} \left[Q\left(\frac{\|\mathbf{\Sigma}_k(k)\| + \left\|\mathbf{\Sigma}_j(k)\right\|}{\sqrt{2}\sigma_n/f} \right) + Q\left(\frac{\|\mathbf{\Sigma}_k(k)\| - \left\|\mathbf{\Sigma}_j(k)\right\|}{\sqrt{2}\sigma_n/f} \right) \right]. \tag{3.75}$$

3.5.6 Simulation Results

In this part, the performance of MRT-RASK systems using different types of receivers is evaluated through the measurement of the BER versus $\frac{E_S}{N_0}$. As for ZF-RASK, it is assumed that $\mathbf{H}$ is a MIMO flat fading channel matrix perfectly known at the transmitter.

Figure 3.10 compares the theoretical and simulated results for the ML, MR and MP detection schemes. It gives the performance of MRT-RASK with $N_t = 16$, and $N_r = 2$, which is equal to the PEP. It is shown that theoretical results perfectly match simulation results.

In Figure 3.11, the performances of all detectors for the MRT-RASK are compared. An MRT-RASK system with $N_t = 8$ and $N_r = 4$ is considered. From the results, many conclusions could be drawn:

- The coherent detection obviously outperforms the noncoherent detection if the same algorithm is used: ML vs NCML and MR vs MP.
- The NCML can outperform the MR detector, with the cost of requiring a channel estimation at the receiver, and benefit of reducing the synchronization.
- The MRMI detector outperforms the MR and MP, to be the best detector that does not need any channel estimation at the receiver.

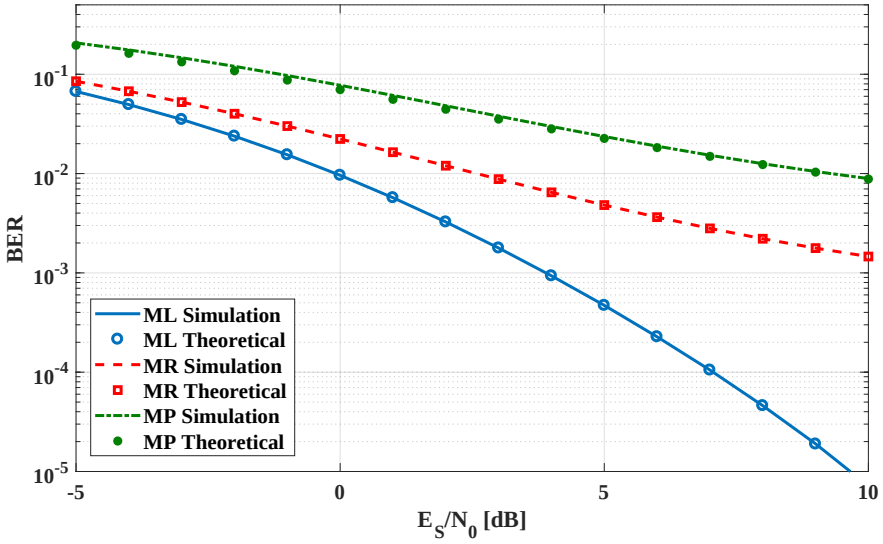

Figure 3.10 – BER performance of 16×2 MRT-RASK systems using ML, MR and MP detectors over Rayleigh channel, simulated and theoretical results

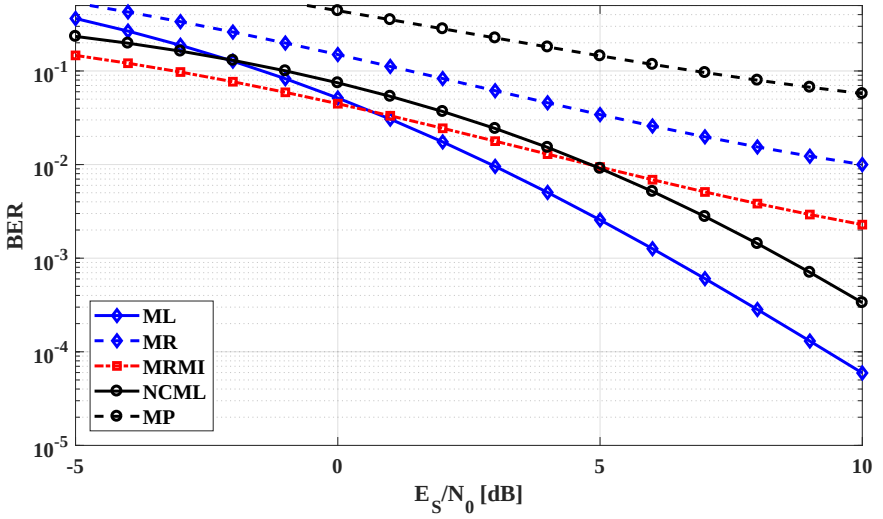

Figure 3.11 – BER performance of 8×4 MRT-RASK systems using all detectors over Rayleigh channel

3.5.7 Computational Complexity Analysis

In this part, we compare the computational complexity of different receivers presented for ZF-RASK and MRT-RASK.

Table 5.1 summarizes the complexity of the transmitter and different receivers for ZF-RASK on the base-band processing. The ZF-precoding applied at the transmitter requires $N_r^3 + N_t N_r$ multiplications to involve the channel matrix inversion that will be saved in a $N_t N_r$ memory size. While for MRT-precoding, an only conjugate operation of

	Multipl.	Add./Sub.	Comparison	Memory
Transmitter:				
ZF/ MRT processing	N_tN_r	N_tN_r	0	$2N_tN_r$
Receiver:				
ML detection	$2N_r^2$	$N_r(3N_r-1)$	N_r-1	$2N_r$
MRA detection	0	0	N_r-1	0
MRMI detection	0	N_r	N_r-1	0
NCML detection	N_r^2	$N_r(2N_r-1)$	N_r-1	N_r
MRP detection	0	0	N_r-1	0

Table 3.2 – Complexity of the transmitter and different receivers for RASK with ZF and MRT precoding

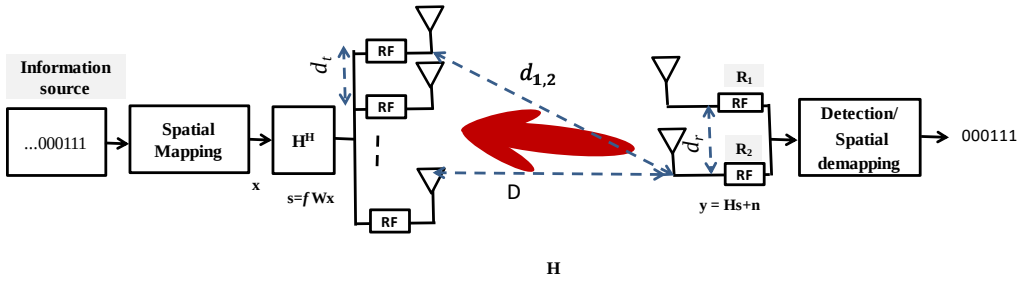

Figure 3.12 – Block diagram of RASK

all channel matrix is required. During the precoding (ZF or MRT), N_tN_r multiplications and N_tN_r additions are used for the multiplication of the precoding matrix with the spatial symbol. At the receiver, the coherent ML detectors require a memory of size $2N_r$ to save all signatures $f\mathbf{x}$, and they compute the amount of $\|\mathbf{y}-f\mathbf{x}\|^2$ using $2N_r$ subtractions, $2N_r$ multiplications, and N_r-1 additions, for each signature. After that, N_r-1 comparison operations are performed to find the minimum. When noncoherent detection is employed, the received signal is a real positive value, so the complexity will be reduced to N_r subtractions, N_r multiplications, N_r-1 additions for each signature, and N_r-1 comparison operations and an allocation of N_r numbers in memory. For the MP and MR detectors, only N_r-1 comparisons are needed to find the spatial index of the targeted antenna, where the MR detector needs a perfect synchronization to be implemented, unlike the MP detector which only measures the power at each antenna. Finally, the MRMI needs N_r substractions before the N_r-1 comparisons.

3.6 LoS Deterministic Scenario

In Line-of-sight (LoS) scenario, the reflections and the scattering of the signal are less, and the channel could be considered as deterministic. In this part, the performance of RASK is evaluated in LoS scenario.

3.6.1 Channel Model

Assuming a deterministic MIMO LOS channel taking into account the free space propagation effect on the signal, $\mathbf{H} = (h_{i,j})_{1\leq i\leq N_t,\, 1\leq j\leq N_r}$, let:

$$\tilde{h}_{j,i} = \left(\frac{\lambda}{2\pi d_{i,j}}\right)^2 e^{j\theta} \tag{3.76}$$

with $\theta = 2\pi d_{i,j}/\lambda$. λ is the wavelength of the wave used, and let $d_{i,j}$ the euclidean distance between T_i and R_j, be the complex non normalized channel coefficient. Also let:

$$\beta = \left(\frac{\lambda}{2\pi D}\right)^2 e^{j\theta_0} \tag{3.77}$$

where $\theta_0 = 2\pi D/\lambda$, and D the distance between the transmitter and the receiver, be the normalization factor. The normalized MIMO-LOS coefficients are then given by $h_{j,i} = \tilde{h}_{j,i}/\beta$.

3.6.2 System Model and Received Signal

The block diagram of the RASK system in LOS scenario is depicted in Figure 3.12. The MRT pre-processing is employed at the transmitter to form the spatial symbol. The receiver is equipped with 2 receive antennas to allow for a transmission of 1 spatial bit per symbol.

Using equation 3.62 of received signal at the level of R_j , for $j = k$, we have:

$$\begin{aligned} y_k &= f \times \sum_{i=1}^{N_t} h_{k,i}^2 + \eta_k \\ &\approx f \times N_t + \eta_k \end{aligned} \tag{3.78}$$

For the non targeted antennas, the received amplitude is the interference amplitude which can be given after mathematical derivation by:

$$y_{j,j\neq k} \approx f\left(\frac{\sin(\pi N_t G)}{\sin(\pi G)}\right)x + \eta_j \text{ where } G = \frac{d_t d_r}{D\lambda}. \tag{3.79}$$

Let $A_S = f.N_t$ and $A_I = f\left(\frac{\sin(\pi N_t G)}{\sin(\pi G)}\right)$, and define SIR the signal to interference ratio, which is the ratio of the useful received power on the targeted antenna and the interference received power on the non-targeted antenna. We have:

$$\text{SIR} = \left(\frac{A_S}{A_I}\right)^2 = \left(\frac{\sin(\pi G) \times N_t}{\sin(\pi N_t G)}\right)^2. \tag{3.80}$$

3.6.3 Analytical Study

In this scenario, assume that the MRP detector is used. The BEP of MRT-RASK scheme with $N_r = 2$ is given by:

$$\mathcal{P}_e = \frac{1}{2}(\mathcal{P}(\mathbf{x}_1 \to \mathbf{x}_2) + \mathcal{P}(\mathbf{x}_2 \to \mathbf{x}_1)) \tag{3.81}$$

which is equal to the PEP. Moreover, since the channel is assumed to be deterministic, the average BEP is equal to the BEP conditioned by **H**. Consequently, the closed form of the BEP is:

$$\mathcal{P}_e = \left[Q\left(\frac{A_S + A_I}{\sigma_n} \right) + Q\left(\frac{A_S - A_I}{\sigma_n} \right) \right]. \tag{3.82}$$

Figure 3.13 shows the BER performance of the MRT-RASK versus the ratio between the

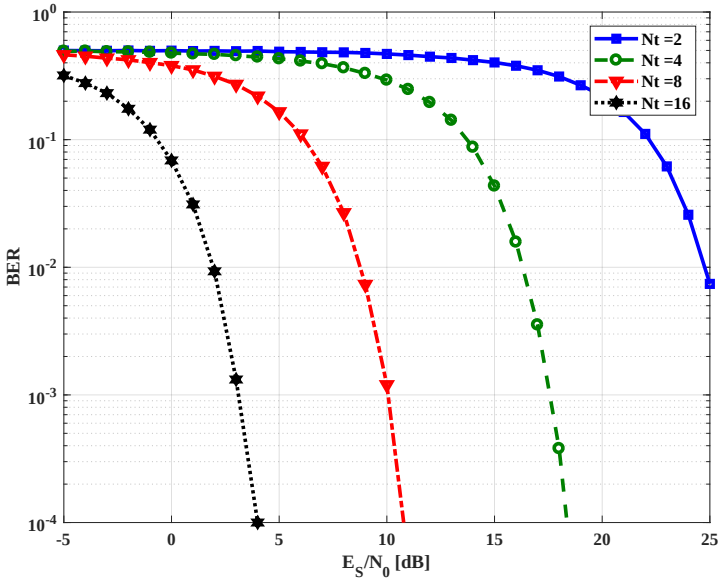

Figure 3.13 – BER performance of a MIMO LoS MRT-RASK transmission system, for $d_r = \lambda$, $d_t = \lambda/2$ and $D = 15\lambda$

average symbol energy level and noise level, when the MRP detector is used. MIMO MRT-RASK systems with $N_r = 2$ and $N_t = 2$, 4, 8 or 16 antennas are considered. The channel is assumed to be LOS, with no fading, and with $D = 15\lambda$, $d_t = \lambda/2$ and $d_r = \lambda$. As evident from the obtained curves, increasing the number of the transmit antennas leads to improvement of the performance, because of the increase in the focusing gain. The improvement is approximately 6 dB for each time we double the number of transmit antennas, which is mean that it is referred to the gain of the antenna array beamforming. In Figure 3.14, we measured the received power on the non-targeted antenna while targeting the other one, for different distances d_r between the two antennas. It is shown that the form of the beam change in the distance having local maximum and minimum, and that increasing the number of transmit antennas leads to more directive beam, which explains the improvement of the performance in Figure 3.13. Note that because of the normalization of the transmission channel, the amplitude of the interference for $N_t = 16$ is higher than the others near the targeted antenna. The received amplitude at the targeted antenna is also the highest, and the beam is more directive.

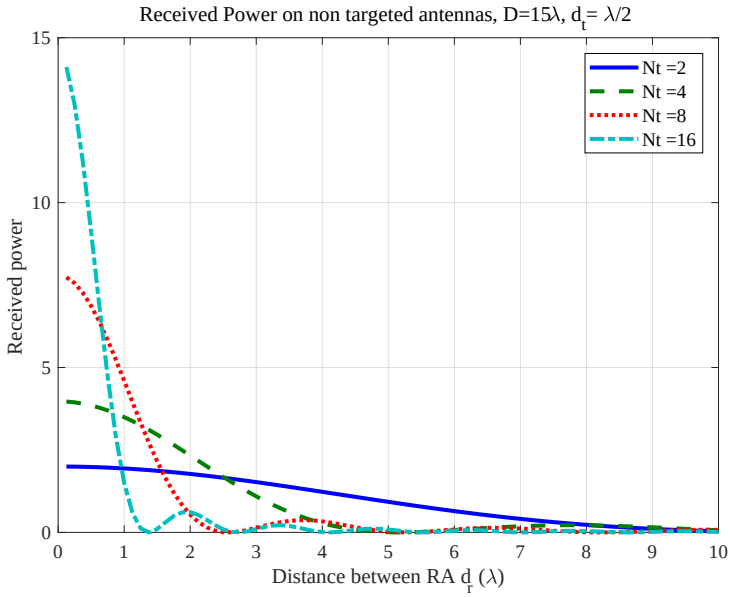

Figure 3.14 – Received power on the non-targeted antenna in terms of the distance between receive antennas

3.7 Practical Testbed

A RASK Time-Division Duplexing (TDD) MIMO transmission system between a transmitter featuring $N_t = 4$ antennas and a receiver with $N_r = 2$ antennas is considered. The system is implemented using two FPGA-based motherboards (WARP v3), with additional radio board (FMC-RF-2X45) and clock board (CM-MMCX) for each, configured with the WARPLab Reference Design, as described in [69].

A 125 kbps RASK transmission at $\nu = 2.4$ GHz is considered in MIMO LOS configuration with $D = 15\lambda$, $d_r = \lambda/4$ and $d_t = \lambda/2$. A Time Reversal pre-processing technique is used to target the RA. Figure 3.15 shows the detected power at the two receive antennas, the blue color for R_1 and the green for Rx_2, when targeting Rx_1 (left figure), and R_2 (right figure). Table 5.1 shows the measurement results and their associated theoretical results for the considered environment. A BER equal to 0.2549 is obtained with the testbed, which is close to the BEP obtained with theoretical approach equal to 0.2028. Moreover, for the SIR measurement, it is shown that theoretically, a same SIR on the two receive antennas equal to 0.0343 dB is obtained, because of the geometry of the system. But with testbed measurement, we calculate the mean of the received power on each antenna during the transmission. R_1 gives a result equal to 0.0380 dB that is close to the theoretical one, while Rx_2 provides a higher SIR equal to 0.6811 dB, that is caused by some reflections in the environment that will improve the focusing toward this RA.

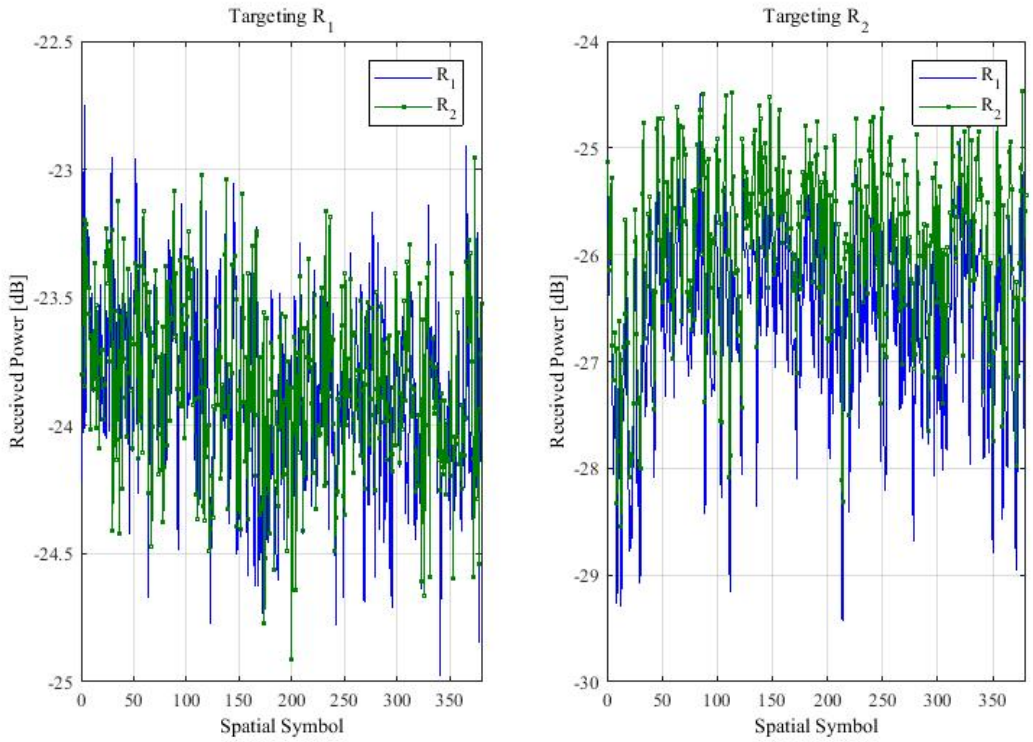

Figure 3.15 – Received power on each antenna targeting R_1 (Left) and R_2 (right)

3.8 Summary

In this chapter, the RASK scheme was studied using ZF and MRT precoding. We demonstrated that when ZF precoding is used, the ML detection is reduced to a single tap receiver, because of interference cancellation. Otherwise, for MRT precoding, the interference between antennas leads to a difference in performance between the ML detector, and the single tap detector used for ZF-RASK. The computational complexity was also studied to classify different detectors. To reduce the complexity of RF chains at the receiver, two strategies where proposed: one is to use noncoherent detection by envelope detectors, and another to use switches. It is shown that at some point the

	Theoretical Result	Testbed Result
SIR -Targeting Rx1	0.0343 [dB]	0.0380 [dB]
SIR -Targeting Rx2	0.0343 [dB]	0.6811 [dB]
BER	0.2028	0.2549

Table 3.3 – Testbed and theoretical SIR and BER results of a 4x2 MIMO LOS channel with $\nu = 2.4$ GHz, $D = 15\lambda$, $d_r = \lambda/4$ and $d_t = \lambda/2$.

noncoherent detection is proofed to be better. For MRT RASK, the ML detector remains more complex and needs channel estimation. We proposed different detectors for MRT-RASK that doesn't need channel estimation. The computation complexity was studied and compared, and analytical derivations the theoretical BEP for some detectors was provided and validated through simulations. Finally, the performance of MRT-RASK was analytically studied under LOS channel scenario and validated through simulations and practical implementation. In a future work, the analytical BEP for the ML and MRMI detectors for MRT-RASK will be derived.

Chapter 4

Extended Receive Antenna Shift Keying

Contents

4.1 Introduction

A classical RASK scheme with N_r receive antennas allows for the transmission of $\log_2(N_r)$ spatial bits per symbol duration. In this chapter, we propose a novel spatial scheme referred to as Extended RASK (ERASK) to improve the SE, that is equal to the number of bit per spatial symbol, of SM at the receiver side by allowing a transmission towards variable number of receive antennas simultaneously, where N_a can change every spatial symbol duration depending on the data information to transmit, contrary to GPSM [78] where N_a is the same whatever the spatial symbol. We demonstrate how ERASK provides N_r spatial bits instead of $\log_2 N_r$ for RASK and $\lfloor \log_2 \binom{N_a}{N_r} \rfloor$ for GPSM. We also present several detectors that can be carried out at the receiver side as well as their expected theoretical performance when the ZF precoding is used. A performance comparison is then made with the classical RASK scheme on the basis of simulation results. Afterward, the effect of channel estimation error and antenna correlation is studied and evaluated in this chapter, with the analytical performance. In comparison, the ERASK with MRT precoding is presented, with an analytical study, to be also compared to the ZF-RASK. Finally, the ERSM scheme, that allows the transmission of ERASK and IQ symbols simultaneously, is presented and studied, where the optimal ratio of power levels was calculated, as well as the analytical performance.

4.2 Extended Receive Antenna Shift Keying

4.2.1 Principle

00 01 10	Symbol 1	Symbol 2	Symbol 3	Symbol 4
1) Segmentation	00	01	10	11
2) Mapping	(0,0)	(0,R2)	(R1,0)	(R1,R2)
3) Preprocessing and transmission	X			
4) Detection	(0,0)	(0,R2)	(R1,0)	(R1,R2)
5) Demapping	00	01	10	11

Figure 4.1 – Example of the Extended-RASK system with $N_r = 2$

As the RASK scheme, the ERASK scheme that is an extension of the RASK one is a receive spatial modulation without the parallel transmission of IQ symbols. Unlike RASK and GPSM where the number of targeted antennas N_a is constant, for the ERASK, N_a changes each T_s with $0 \leq N_a \leq N_r$ taking all possible values, depending on the information bits, so that the number M of possible spatial symbols achieves:

$$M = \sum_{N_a=0}^{N_r} C_{N_r}^{N_a} = 2^{N_r} \tag{4.1}$$

with C_n^k the binomial coefficient giving the number of subsets of k elements of a set of n elements. Consequently, the ERASK symbols are made of a number m of bits such that:

$$m = N_r. \tag{4.2}$$

Figure 4.1 provides an illustration of the ERASK scheme with $N_r = 2$. As evident from the figure, steps 1 and 2 allow for forming M-ary spatial symbols with $M = 4$ and transmitting 2 bits during each T_s. The spatial mapping used in this example is the following:

- no antenna is targeted ($N_a = 0$) if symbol '00' is sent,
- antenna R_2 is targeted ($N_a = 1$) if symbol '01' is sent,
- antenna R_1 is targeted ($N_a = 1$) if symbol '10' is sent,
- both antennas R_1 and R_2 are targeted ($N_a = 2$) if symbol '11' is sent.

Hence, at step 3, the pre-processing is performed at the transmitter so as to create a beam to concentrate the transmitted energy towards the N_a targeted antennas. At step 4, the receiver estimates which antenna or antennas have been focused on by analyzing the amount of received energy at each antenna, and then deduces the transmitted spatial symbol. Specific detectors have thus to be designed, as proposed in the sequel.

4.2.2 System model for ZF-RASK

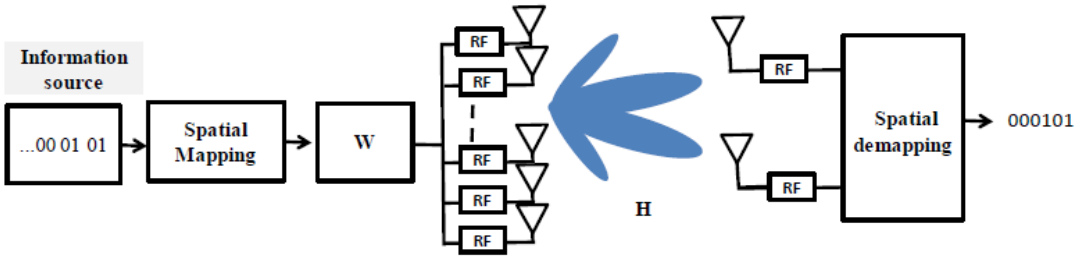

Figure 4.2 – Block diagram of Extended-RASK

In this part, we first set up the model for a communication system making use of the ERASK scheme. Then, we introduce the pre-processing scheme carried out to form the spatial symbols and the equation of the received signals on each antenna.

System Model

A MIMO system with N_t transmit antennas and N_r receive antennas is considered. Assuming a flat fading channel between the transmitter and the receiver, the receive signal vector can be written as

$$\mathbf{y} = \mathbf{H}\mathbf{s} + \mathbf{n} \tag{4.3}$$

where $\mathbf{H} \in \mathbb{C}^{N_r \times N_t}$ is the MIMO channel matrix with elements $h_{j,i}$ representing the complex channel coefficient between the i-th transmit antenna, denoted by T_i, and the

j-th receive antenna, denoted by R_j. $\mathbf{y} \in \mathbb{C}^{N_r \times 1}$ is the vector of the received signals on all receive antennas, $\mathbf{s} \in \mathbb{C}^{N_t \times 1}$ is the vector of the transmitted signals by all emitting antennas, and $\mathbf{n} \in \mathbb{C}^{N_r \times 1}$ is the vector of AWGN samples η_j at the receive antenna R_j such that $\eta_j \sim \mathcal{CN}(0, \sigma_n^2)$. The block diagram of the ZF-ERASK system is depicted in Figure 4.2. A group of $m = N_r$ bits is mapped to a spatial symbol $\mathbf{x} \in \mathbb{C}^{N_r \times 1}$ which is written as

$$\mathbf{x} = \begin{bmatrix} x_1 & x_2 & \dots & x_{N_r} \end{bmatrix}^T \text{ where } x_j \in \{0, A\}.$$

The value taken by each x_j entry determines the set of targeted receive antennas such that:

$$x_j = \begin{cases} 0, & \text{if } R_j \text{ is not targeted,} \\ A, & \text{if } R_j \text{ is targeted.} \end{cases} \tag{4.4}$$

We can remarque that A can also be an IQ symbol to carry additional information, but in ERASK we concentrate on schemes with low complexity detection. So, we only consider spatial information by assuming that A is constant.

Then, the pre-processing block transforms the vector of spatial symbols $\mathbf{x}$ into the vector of transmitted signals $\mathbf{s}$ using the pre-processing matrix $\mathbf{W} \in \mathbb{C}^{N_t \times N_r}$. Consequently, the transmitted signal is written as:

$$\mathbf{s} = f\mathbf{W}\mathbf{x} \tag{4.5}$$

where f is a normalization factor used to guarantee that the average total transmit power $\bar{P}_t$ is equal to 1. More precisely, we have:

$$f = \frac{1}{\sqrt{\sigma_x^2 \mathrm{Tr}(\mathbf{W}.\mathbf{W}^H)}} \tag{4.6}$$

Since $\mathbf{x}$ has i.i.d. entries, the variance $\sigma_x^2 = \mathbb{E}_x \left[x_j x_j^* \right]$ does not depend on j and comes in factor of the trace computation. Then, each entry of $\mathbf{x}$ is of amplitude A with a probability that can be easily verified to be $\frac{1}{2}$, leading to $\sigma_x^2 = \frac{A^2}{2}$.

Received Signal

In case of ZF precoding, the pseudo-inverse of the channel matrix is used as a pre-filter:

$$\mathbf{W} = \mathbf{H}^H (\mathbf{H}\mathbf{H}^H)^{-1}. \tag{4.7}$$

It is then straightforward to obtain the expression of the receive signals:

$$\mathbf{y} = f\mathbf{x} + \mathbf{n}. \tag{4.8}$$

At the level of the receive antenna R_j, the received signal then simply writes:

$$y_j = f \times x_j + \eta_j. \tag{4.9}$$

4.2.3 Detection Schemes

To estimate the spatial symbol, the receiver should detect for each receive antenna whether it has been targeted by the transmitter or not. This detection can be carried out with different types of receivers, leading to different performance and complexity.

From equation (4.50), a given detector has to analyze the following set of signals:

$$\forall j, \quad y_j = \begin{cases} f \times A + \eta_j & \text{if } R_j \text{ is targeted} \\ \eta_j & \text{otherwise.} \end{cases} \tag{4.10}$$

Since the ZF precoding scheme is used, no interference appears between receive antennas. In addition, since all combinations of the targeted antenna are possible with the ERASK scheme, no correlation exists between the receive antenna signals. Consequently, the demodulation process can be led through an independent and parallel signal analysis per antenna.

Maximum Likelihood Detector (Real Amplitude Threshold)

Let us first derive the performance of the ML detector. The ML detector should exhaustively search among all the possible receive signal which one is the closest to transmit one. Let us denote by $\mathbf{x}_k$ the k-th out of $K = 2^{N_r}$ possible transmitted signal vectors with a given combination of it entries $x_k(k)$ equal to A, and the rest being zeroed. The equation of the ML receiver can then be written as:

$$\hat{\mathbf{x}}_k = \text{Arg}\min_k \sum_{j=1}^{N_r} \left\| y_j - f x_j(k) \right\|^2. \tag{4.11}$$

Owing to the parallel detection process discussed above, the ML detector can be rewritten as:

$$\forall j, \quad \hat{x}_j = \text{Arg}\min_{x_j=\{A,0\}} \left\| y_j - f x_j \right\|^2 \tag{4.12}$$

meaning that $\hat{x}_j$ is estimated separately at each antenna and is simply obtained by choosing whether A or 0 has been transmitted. Hence, the ML detector at each receive antenna can be carried out by means of a simple threshold detector. Suppose that the channel estimation at the transmitter for the pre-processing is perfect, the received signal at the targeted antenna will then exhibit the same phase as the emitted signal due to the phase compensation effect of the ZF precoder. Considering that the target signal $x_j = A$ is of known phase ϕ_A at the receiver, the receiver can compensate the phase of the received signal and compare the real part obtained to a predefined amplitude threshold ν:

$$\hat{x}_j = \begin{cases} 0, & \text{if } \Re\{y_j \times e^{-\phi_A}\} \leq \nu, \\ A, & \text{if } \Re\{y_j \times e^{-\phi_A}\} \geq \nu, \end{cases} \tag{4.13}$$

where the optimal threshold is easily deduced from:

$$\nu = \mathbb{E}\left\{ \frac{\Re\{y_{j0} e^{-\phi_A}\} + \Re\{y_{j1} e^{-\phi_A}\}}{2} \right\} = \frac{fA}{2}, \tag{4.14}$$

with y_{j0} (resp. y_{j1}) the receive signal on antenna R_j if this antenna is not targeted (resp. targeted). Note that such a threshold can in practice be estimated during a calibration phase using dedicated pilot symbols.

Using such a threshold detector, the derivation of the theoretical binary error probability $\mathcal{P}_e$ can be led as follows. First, understanding that $\mathcal{P}_e$ for ERASK is independent of the receive antenna R_j, while remembering that the probability $\mathcal{P}(y_{j1})$ that one particular antenna R_j is targeted is of $\frac{1}{2}$, we have:

$$\mathcal{P}_e = \frac{1}{2} \cdot \mathcal{P}(y_{j0} \rightarrow y_{j1}) + \frac{1}{2} \cdot \mathcal{P}(y_{j1} \rightarrow y_{j0}). \tag{4.15}$$

Then, applying the threshold detection, we obtain:

$$\mathcal{P}_e = \frac{1}{2} \times \left[\mathcal{P}\left(\nu \leq \Re\{\eta_j\}\right) + \mathcal{P}\left(\Re\{f.A + \eta_j\} \leq \nu\right) \right]. \tag{4.16}$$

Since noise samples are centered circularly Gaussian of variance σ_n^2, we finally get:

$$\begin{aligned} \mathcal{P}_e =& \mathcal{P}\left(\mathcal{N}\left(0, \frac{\sigma_n^2}{2}\right) \geq \frac{f.A}{2}\right) \\ =& \frac{1}{2} Q\left(\frac{f.A}{\sqrt{2}\sigma_n}\right). \end{aligned} \tag{4.17}$$

Such a result indicates that the system performance is driven by f which directly depends on the MIMO channel characteristics.

Power Threshold (PT) Detector

The ML detector studied above needs the carrier synchronization to be led at the receiver side. Let us now consider the case of a non-coherent receiver that detects the received power at the antenna, and compares it to a pre-defined threshold. Hence, the detection process is such that:

$$x_j = \begin{cases} 0, & \text{if } |y_j|^2 \leq \nu, \\ A, & \text{if } |y_j|^2 \geq \nu. \end{cases} \tag{4.18}$$

The optimal decision is then obtained choosing the following threshold:

$$\nu = \mathbb{E}\left\{\frac{|y_{j0}|^2 + |y_{j1}|^2}{2}\right\} = \frac{(f.A)^2}{2} + \sigma_n^2. \tag{4.19}$$

As in the ML detector case, the decision is made at each receive antenna in parallel, yielding:

$$\mathcal{P}_e = \frac{1}{2} \times \left(\mathcal{P}(\nu \leq \left\|\eta_j\right\|^2) + \mathcal{P}(\left\|f.A + \eta_j\right\|^2 \leq \nu)\right). \tag{4.20}$$

After some mathematical manipulations detailed in the proof below, we obtain:

$$\mathcal{P}_e = \frac{1}{2} e^{-\frac{\nu}{\sigma_n^2}} + \frac{1}{4}\left[Q\left(\frac{f.A - \sqrt{\nu}}{\sigma_n/\sqrt{2}}\right) - Q\left(\frac{f.A + \sqrt{\nu}}{\sigma_n/\sqrt{2}}\right)\right], \tag{4.21}$$

which can be further simplified at low noise level as,

$$\mathcal{P}_e \approx \frac{1}{4}\left[Q\left(\frac{f.A-\sqrt{\nu}}{\sigma_n/\sqrt{2}}\right) - Q\left(\frac{f.A+\sqrt{\nu}}{\sigma_n/\sqrt{2}}\right)\right]. \tag{4.22}$$

As for the ML detector, the performance is impacted by f.

Proof: First, letting $\|\eta_j\|^2 = \frac{\sigma^2}{2}\left\|\eta'_j\right\|^2$ where $\left\|\eta'_j\right\|^2 \sim \mathcal{X}_2^2$ (Chi squared distribution with 2 degrees of freedom), we have

$$\mathcal{P}(\nu \leq \|\eta_j\|^2) = \mathcal{P}\left(\frac{2.\nu}{\sigma^2} \leq \left\|\eta'_j\right\|^2\right) = e^{-\frac{\nu}{\sigma^2}}. \tag{4.23}$$

On the other hand, at high SNR, i.e. if $f.A \gg \sigma$, $\|f.A+\eta_j\|^2$ can be approximated by $\|f.A+\Re\{\eta_j\}\|^2$, hence:

$$\begin{aligned}\mathcal{P}(\|f.A+\eta_j\|^2 \leq \nu) &\approx \mathcal{P}(\|f.A+\Re\{\eta_j\}\|^2 \leq \nu)\\ &= \mathcal{P}(|f.A+\Re\{\eta_j\}| \leq \sqrt{\nu})\end{aligned} \tag{4.24}$$

where $|f.A+\Re\{\eta_j\}| = |\mathcal{J}|$ following a Folded-Normal distribution, i.e. $\mathcal{J} \sim \mathcal{N}(f.A, \sigma^2/2)$. Then, it comes to:

$$\mathcal{P}(|f.A+\Re\{\eta_j\}| \leq \sqrt{\nu}) = \frac{1}{2}\left[Q\left(\frac{f.A-\sqrt{\nu}}{\sigma_n/\sqrt{2}}\right) - Q\left(\frac{f.A+\sqrt{\nu}}{\sigma_n/\sqrt{2}}\right)\right] \tag{4.25}$$

which finally leads to the result of equation (4.21). ■

4.2.4 Simulation results

The performance of the proposed ZF-ERASK system using the 2 receivers is evaluated through the measurement of the BER versus the ratio between the average transmit power level and noise level, i.e. $\frac{\bar{P}_t}{\sigma_n^2}$. It is assumed that $\mathbf{H}$ is a MIMO flat fading channel matrix perfectly estimated at the transmitter, where $h_{j,i}$ are complex coefficients following i.i.d. Rayleigh distribution. The power for each sub-channel is normalized:

$$E\left[\,\|h_{j,i}\|^2\,\right] = 1.$$

Simulations are run by implementing a sufficient number of iterations for different channel realizations and taking the mean value of the BER for each value of $\frac{\bar{P}_t}{\sigma^2}$.

Figure 4.3 gives the performance of ZF-ERASK with $N_r = 2$ or 4 and $N_t = 8$ using the ML and PT receivers. The performance based on simulations and analytic study are compared. As evident from the obtained curves, theoretical results perfectly match simulation results for each receiver. It is also observed that the ML receiver obviously outperforms the PT receiver, which is easily understood since the latter detector is non-coherent and does not take advantage of the received signal phase knowledge. In Figure 4.4, we provide the simulation results considering an ERASK system with $N_t = 36$ and $N_r = 2$, 3, 4 or 5, leading to a SE equal to 2, 3, 4 and 5 respectively (the SE is calculated as the number of bits that could be transmitted by one symbol, here it is equal

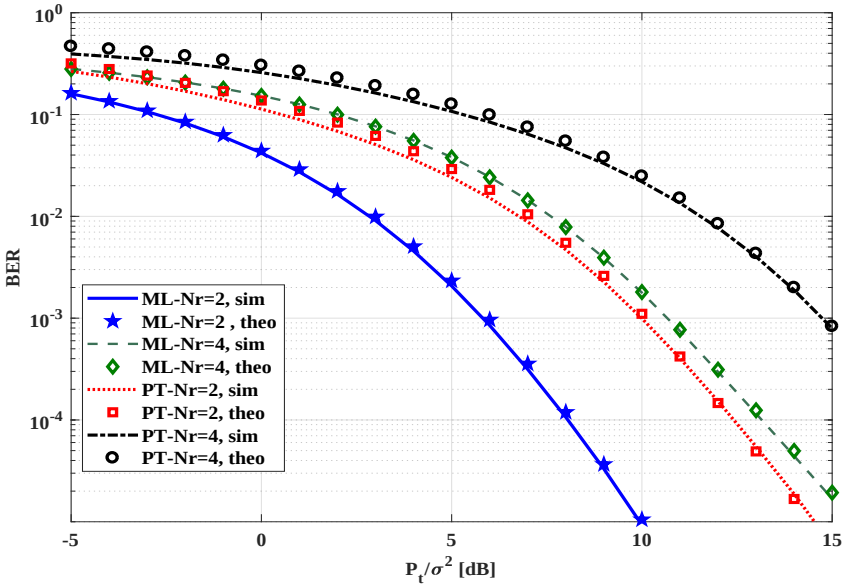

Figure 4.3 – ERASK performance using ML and PT detectors with $N_t = 8$ - Comparison of theoretical performance and simulation results

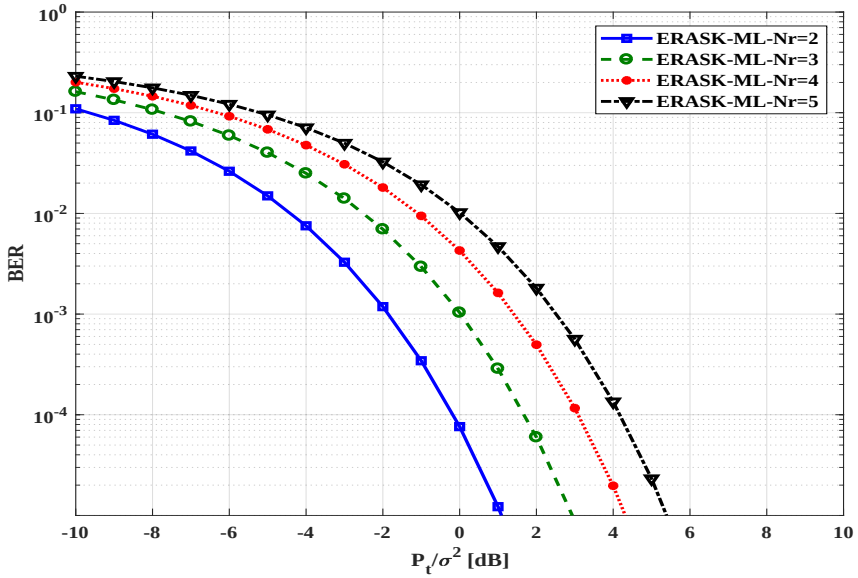

Figure 4.4 – Performance of ERASK with ML receiver - N_t=36.

to the order of modulation). The performance is evaluated using the ML coherent detector. The results show that as expected, the higher the modulation order the greater the performance degradation. As N_r increases, the ZF pre-processing technique has to deal with a higher number of antennas on which interference has to be canceled, thus degrading the power gain of the overall system. However, it is noticed that the degradation of the performance remains reasonable between different orders of modulation.

For instance, doubling the SE from $N_r = 2$ to $N_r = 4$ leads to a degradation of roughly 3 dB only.

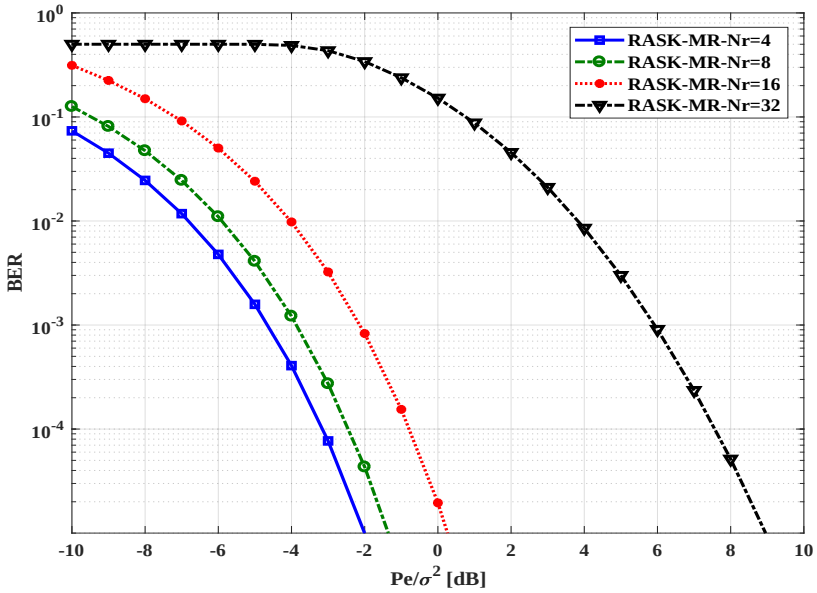

Figure 4.5 – Performance of conventional RASK with ML receiver - N_t=36.

For comparison purpose, the performance of the conventional RASK system with $N_t = 36$, and $N_r = 4$, 8, 16, and 32 to provide an SE of 2, 3, 4 and 5 respectively, are given in Figure 4.5.

Hence, the number of receive antennas is adapted so as to reach the same orders of modulation as with ERASK: Simulations are run using a coherent detector as pro-

SE	2	3	4	5
N_r for RASK	4	8	16	32
N_r for ERASK	2	3	4	5

Table 4.1 – The number of receive antenna needed for RASK and ERASK systems to acheive certain SE

posed in [9]. The obtained curves show that the RASK system outperforms the ERASK one when the order of modulation is low (for SE less or equal to 4). However, the performance dramatically decreases when M increases since the number of antennas at the receiver side increases exponentially. In such a situation, e.g. for $N_r = 32$ and N_t =36, the channel matrix becomes harder to invert, which makes the interference cancellation on the non-targeted antennas harder to accomplish. We can then conclude by comparing with Figure 4.4 that the ERASK is less immune than the RASK for low $\frac{p_t}{\sigma^2}$. Meanwhile, the latter needs a higher number of receive antennas to achieve the same SE ($N_r = 2^m$ for RASK instead of $N_r = m$ for ERASK).

4.3 Imperfect Channel Estimation and Antenna Correlation

As any RSM system, ERASK relies on precoding techniques meaning that a channel estimation at the transmitter is needed. In actual cases, supplying the transmitter with accurate channel estimation is a difficult task. The negative effects of channel estimation errors on the performance of SM at the transmitter when operating over flat Rayleigh fading channels is investigated in [89], and authors in [71] addressed the problem of imperfect or partial channel estimation at the transmitter on the transmit precoding for RSM. In this part, we evaluate the effect of imperfect channel estimation at the transmitter on the ERASK scheme assuming ZF preprocessing and using a real amplitude threshold. In addition, we study the impact of antenna correlation which may also have a strong impact on the performance of SM systems.

4.3.1 Imperfect Channel Estimation at the Transmitter

A perfect channel knowledge at any side of the transmission system is impossible in practical situations. In this chapter, the transmitter is assumed to be capable of accurately tracking the long term average channel estimation at the transmitter. This can be for instance plausible in TDD mode, where the reciprocity of the channel can apply. However, we consider in the sequel that an instantaneous channel estimation error is added to the long term channel estimation, such that we have:

$$\mathbf{H} = \bar{\mathbf{H}} + \tilde{\mathbf{H}} \tag{4.26}$$

where $\bar{\mathbf{H}}$ represents the average long term channel estimation that is accurately estimated at the transmitter, and $\tilde{\mathbf{H}}$ denotes the instantaneous channel estimation deviation matrix where all entries obey the complex Gaussian distribution $\tilde{h}_{j,i} \sim \mathcal{CN}(0, \sigma_H^2)$. Since $\bar{\mathbf{H}}$ is estimated at the transmitter, then the pseudo-inverse of $\bar{\mathbf{H}}$ is used as a prefilter:

$$\mathbf{W} = \bar{\mathbf{H}}^H (\bar{\mathbf{H}}\, \bar{\mathbf{H}}^H)^{-1}. \tag{4.27}$$

4.3.2 Transmit and Receive Spatial Correlation

Performance of SM schemes is often evaluated over an independent Rayleigh fading per antenna link. In this part, the correlation between transmit antenna, and between receive antennas is taken into account to evaluate the robustness of the system ERASK. Employing the Kronecker correlation model [90] for that purpose, the MIMO channel can be rewritten as:

$$\mathbf{H} = \mathbf{R}_r^{1/2} \mathbf{H}_I (\mathbf{R}_t^{1/2})^T \tag{4.28}$$

where $\mathbf{H}_I \sim \mathcal{CN}(\mathbf{0}, \mathbf{I})$ is the channel matrix with independent entries, and $\mathbf{R}_r$ and $\mathbf{R}_t$ represent the receive and transmit spatial correlation matrices at the receive and transmit arrays, respectively. The correlation matrices are generated using the exponential model, such that $\mathbf{R}_r(i,j) = \rho_r^{|i-j|}$ and $\mathbf{R}_t(i,j) = \rho_t^{|i-j|}$, where $0 \leq \rho_r, \rho_t \leq 1$. Then combining the correlation model with the imperfect channel estimation model, we may write the MIMO channel as:

$$\mathbf{H} = \underbrace{\mathbf{R}_r^{1/2} \bar{\mathbf{H}}_I (\mathbf{R}_t^{1/2})^T}_{\bar{\mathbf{H}}} + \underbrace{\mathbf{R}_r^{1/2} \tilde{\mathbf{H}}_I (\mathbf{R}_t^{1/2})^T}_{\tilde{\mathbf{H}}} \tag{4.29}$$

where matrix $\bar{\mathbf{H}}$ represents the full known part of the channel and matrix $\tilde{\mathbf{H}}$ represents the unknown part of the channel, both integrating correlation effects.

4.3.3 Received Signal and Detection Algorithm

From the above model, in which the estimation of the channel includes errors, the equation of the received signal becomes:

$$\mathbf{y} = f\mathbf{x} + f\tilde{\mathbf{H}}\mathbf{W}\mathbf{x} + \mathbf{n} \tag{4.30}$$

which can be re-expressed at each received antenna as:

$$y_j = f \times x_j + f \times \sum_{k=1}^{N_r} \sum_{i=1}^{N_t} \tilde{h}_{j,i} w_{i,k} x_k + \eta_j, \tag{4.31}$$

where $w_{i,k}$ is the entry of $\mathbf{W}$ at the i-th row and j-th column. As expected from the erroneous channel knowledge, ZF precoding fails in properly isolating the entries of the spatial symbol vector which gives rise to a residual interference term in the latter two expressions.

4.3.4 Performance Analysis

Based on the obtained receive signal in equation (4.31), we provide the analytical derivation for the theoretical BEP performance of the ZF-ERASK system under imperfect channel estimation. The generic expression of the BEP $\mathcal{P}_e$ can be written as:

$$\mathcal{P}_e = \frac{1}{m} \cdot \mathbb{E}\left\{ \sum_{k=1}^{N_r} \sum_{j=1, j\neq k}^{N_r} \mathcal{P}(\mathbf{x}_k \rightarrow \mathbf{x}_j) \cdot d(\mathbf{x}_k, \mathbf{x}_j) \right\} \tag{4.32}$$

where $d(\mathbf{x}_k, \mathbf{x}_j)$ is the Hamming distance between two spatial symbols $\mathbf{x}_k$ and $\mathbf{x}_j$, and $\mathcal{P}(\mathbf{x}_k \rightarrow \mathbf{x}_j)$ is the PEP. All spatial signatures are possible and equally likely in the ERASK scheme, so that for each receive antenna, the probability of being targeted or not is independent of the fact that any other receive antenna is also targeted. Consequently, evaluating the global BEP of the ERASK system amounts to getting the BEP on each receive antenna. Let us define $\mathcal{P}(y_{j1})$ (resp. $\mathcal{P}(y_{j0})$) as the probability that one particular antenna R_j is targeted (resp. not targeted), and $\mathcal{P}(y_{j0} \rightarrow y_{j1})$ (resp. $\mathcal{P}(y_{j1} \rightarrow y_{j0})$) the conditional probability that one particular antenna R_j is detected as being targeted (resp. not targeted) knowing that it was not (resp. it was). We then have,

$$\mathcal{P}_e = \mathcal{P}(y_{j0}) \cdot \mathcal{P}(y_{j0} \rightarrow y_{j1}) + \mathcal{P}(y_{j1}) \cdot \mathcal{P}(y_{j1} \rightarrow y_{j0}). \tag{4.33}$$

Since $x_k \in \{0, A\}$ with a probability of $\frac{1}{2}$, we have $\mathcal{P}(y_{j0}) = \mathcal{P}(y_{j1}) = \frac{1}{2}$. In addition, following the threshold criteria introduced in subsection 4.2.3, we can then simply restate the BEP expression as,

$$\mathcal{P}_e = \frac{1}{2} \cdot \mathcal{P}\left(y_{j0} > \frac{f \cdot A}{2}\right) + \frac{1}{2} \cdot \mathcal{P}\left(y_{j1} < \frac{f \cdot A}{2}\right). \tag{4.34}$$

The probabilities of false detection in equation (4.34) have to be analyzed from the expression of the received signal at antenna R_j given in equation (4.50). It is important to keep in mind that the interference term embedded in equation (4.50) depends on the other targeted antennas. It can be statistically represented as:

$$f \times \sum_{k=1}^{N_r} \sum_{i=1}^{N_t} \tilde{h}_{j,i} w_{i,k} x_k \sim \mathcal{CN}(0, \sigma_l^2). \tag{4.35}$$

$$\text{where } \sigma_l^2 = \sum_{k=1}^{N_r} x_k^2 \sum_{i=1}^{N_t} f^2 \left\| w_{i,k} \right\|^2 \sigma_H^2. \tag{4.36}$$

Now expressing the normalization factor f as:

$$f^2 = 2/(A^2 \times \sum_{i=1}^{N_t} \sum_{j=1}^{N_r} \left\| w_{i,j} \right\|^2), \tag{4.37}$$

the expression of the interference variance in (4.36) becomes:

$$\sigma_l^2 = \sum_{k=1}^{N_r} x_k^2 \frac{2}{A^2 \times N_r} \sigma_H^2 \tag{4.38}$$

on average over all possible spatial symbols. We can then decompose all possible spatial signals to determine the distribution of the interference and the additive white noise depending on the number N_a of targeted antennas as:

$$\sigma_l^2 = 2\sigma_H^2 \times N_a / N_r, \tag{4.39}$$

where $0 \leq N_a \leq N_r$. Then, defining $\mathcal{P}(N_a)$ as the probability of error detection if N_a antennas are targeted, we have from equation (4.34):

$$\begin{aligned} \mathcal{P}(N_a) &= \frac{1}{2} \cdot \mathcal{P}\left(\Re\{f.A + \mathcal{CN}(0, \sigma_l^2 + \sigma_n^2)\} < \frac{f.A}{2} \right) \\ &\quad + \frac{1}{2} \cdot \mathcal{P}\left(\Re\{\mathcal{CN}(0, \sigma_l^2 + \sigma_n^2)\} > \frac{f.A}{2} \right) \\ &= Q\left(f.A/2\sqrt{\sigma_n^2 + \sigma_l^2} \right). \end{aligned} \tag{4.40}$$

As a result, the general equation of the BEP taking every subset of targeted antennas is given as:

$$\mathcal{P}_e = \frac{1}{2^{N_r}} \sum_{N_a=0}^{N_r} C_{N_r}^{N_a} Q\left(f.A/2\sqrt{\sigma_n^2 + 2\sigma_H^2 \times N_a/N_r} \right). \tag{4.41}$$

Finally, introducing the ratio between the average transmit power level to the interference and noise level as:

$$\text{SNR} = \frac{\bar{P}_t}{\sigma_n^2 + \sigma_l^2} = \frac{1}{\sigma_n^2 + \sigma_l^2}, \tag{4.42}$$

the equation of the BEP performance given in equation (4.53) becomes:

$$\mathcal{P}_e = \frac{1}{2^{N_r}} \sum_{N_a=0}^{N_r} C_{N_r}^{N_a} Q\left(\frac{f.A}{2}\sqrt{\text{SNR}}\right). \tag{4.43}$$

Such a result indicates that the system performance is driven by f, which directly depends on the MIMO channel characteristics, the number of receive antennas and the deviation of the channel estimation error (embedded in the SNR). Hence, it can already be anticipated that the BEP will degrade as:

- f decreases. This will occur as the antenna correlation increases, since f becomes weak when the channel matrix is badly conditioned.
- N_r increases. This translates the fact that a higher amount of antenna interference has to be canceled with large receive antenna arrays.
- σ_I^2 increases. This is a direct consequence of the channel estimation impairments.

4.3.5 Simulation results

The performance of the ZF-ERASK system based on a parallel threshold detection and under imperfect channel estimation is evaluated through the measurement of the BER versus SNR. More precisely, in the following curves, the variance of the channel estimation deviation is set to a constant value and the level of the Gaussian noise at the receiver changes to illustrate the BER in terms of the SNR. It is assumed that $\bar{\mathbf{H}}$ is a MIMO flat fading channel matrix where $\bar{h}_{j,i}$ are complex coefficients following an i.i.d. Rayleigh distribution and the entries of the matrix of instantaneous channel estimation deviations are complex coefficients following the complex Gaussian distribution with a variance σ_H^2. The power for each sub-channel is normalized as:

$$E\left[\left\|\bar{h}_{j,i}\right\|^2\right] + \sigma_H^2 = 1,$$

and the correlated model described in equation (4.29) is used for various values of ρ. Simulations are carried out by implementing a sufficient number of iterations for different channel realizations.

In Figure 4.6, we first compare the simulated (markers) and theoretical (dashed lines) BER values for an ERASK system with $N_t = 8$, and $N_r = 2$ and 4. For each N_r, results are given for two different channel estimation accuracies, namely σ_H = 0.4 and 0.5. No antenna correlation is used in this figure. As evident from the obtained curves, theoretical results perfectly match simulation results for any configuration. Then, as expected from the analysis of equation (4.53), it is observed that increasing the order of the spatial modulation (i.e. increasing N_r), or degrading the channel estimation at the transmitter quality leads to strong performance degradation. In both cases indeed, the sum of added interference increases which translates into the form of error floors at high SNR.

The effect of the correlation at the transmitter and the receiver of the system, combined with the impact of channel estimation errors, is shown in Figure 4.7. The considered ERASK system is set with $N_t = 8$ and $N_r = 2$. Two configurations are compared.

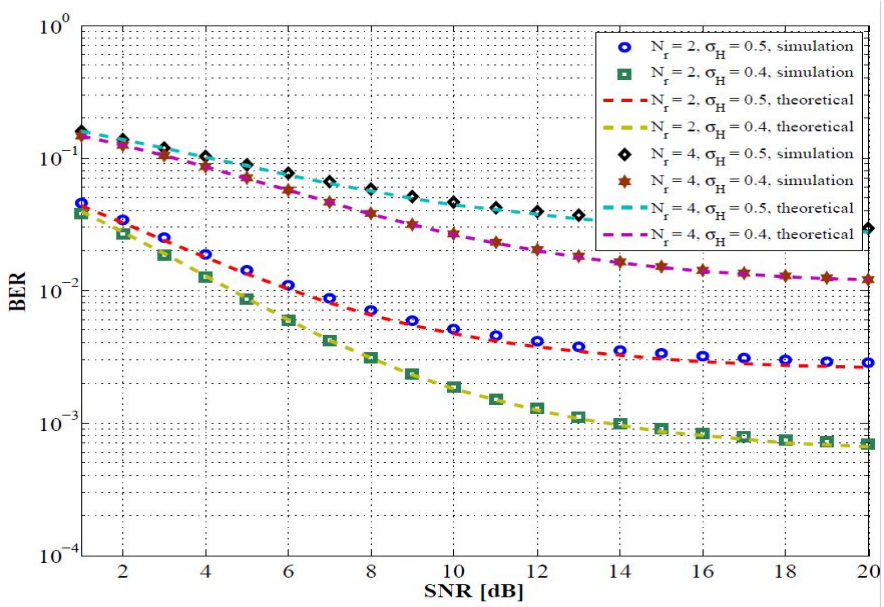

Figure 4.6 – Theoretical and simulation results comparison of BER vs SNR performance of ERASK over uncorrelated Rayleigh fading channels. $N_t = 8$, $N_r = 2$ and 4, σ_H=0 and 0.2

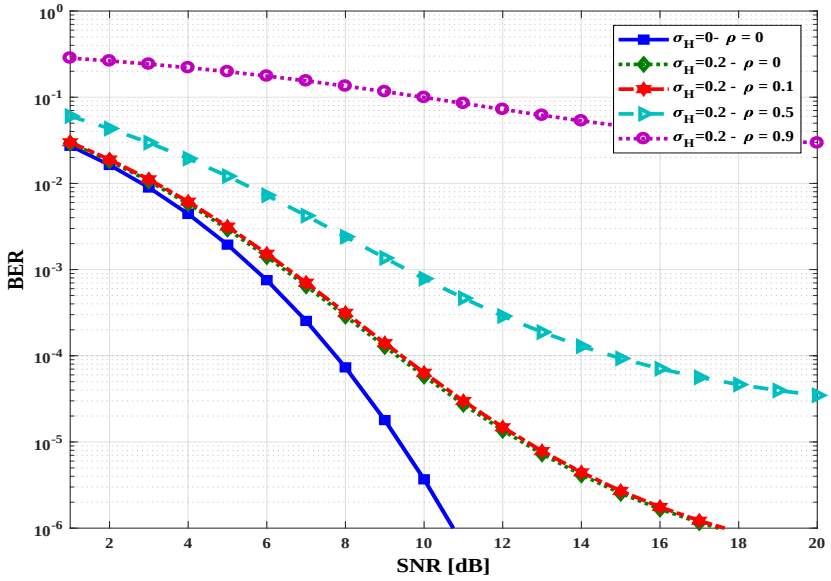

Figure 4.7 – BER vs SNR performance of ERASK with $N_t = 8$ and $N_r = 2$ over Rayleigh fading channels for perfect channel estimation and no correlation, and for σ_H= 0.2 with correlation factor $\rho = 0$, 0.1, 0.5 and 0.9

The first one, used as a reference, assumes perfect channel estimation at the transmitter and no correlation. The second one considers a deviation of the estimation error of $\sigma_H = 0.2$ and different correlation factor levels ($\rho = 0$, 0.1, 0.5 and 0.9). The ERASK

performance obviously degrades when the correlation factor increases (lower f), and when channel estimation error is added (higher σ_l^2). Nevertheless, the degradation remains still acceptable for $\rho \leq 0.5$ with a performance degradation of less than 4 dB at a 10^{-3} BER compared to the perfect conditions, and less than 3 dB when only the channel estimation error is included ($\sigma_H = 0.2$, $\rho = 0$). Interestingly, the curves obtained without correlation and with $\rho = 0.1$ are almost undistinguished, which indicates that under a given quality of the channel estimation, the antenna correlation has no impact on the performance.

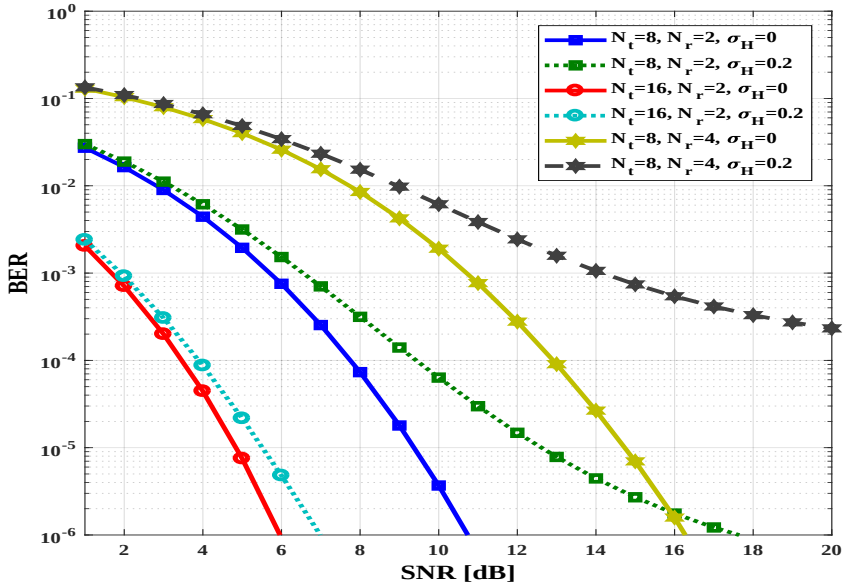

Figure 4.8 – BER vs SNR performance of ERASK over Rayleigh fading channels with antenna correlation factor $\rho = 0.1$, $N_t = 8$ and 16, $N_r = 2$ and 4, σ_H= 0 and 0.2

In Figure 4.8, various ERASK system settings (i.e. various $N_t \times N_r$) are compared with and without channel estimation inaccuracies, and with fixed correlation factor $\rho = 0.1$. First comparing the curves with $N_t = 8$, it is verified that the larger the receive antenna array, the stronger the degradation of the performance. Indeed, as the number of receive antennas increases, the amount of inter-antenna interference becomes higher at the receiver side and the defect of interference cancellation of the ZF scheme due the channel estimation errors becomes more significant. This fact corroborates the analysis made on equation (4.43). Reversely, analyzing the curves with $N_r = 2$ but changing N_t leads to the conclusion that the ZF precoding is less sensitive to poor channel estimation at the transmitter when a larger number of transmit antenna, is used. This indicates that using large transmit arrays, and thus exploiting higher spatial focusing gains, is favorable to channel estimation inaccuracies.

4.4 MRT-RASK

In this section, the MRT is employed for the pre-processing step, where, in the flat fading channel, the trans-conjugate of the channel matrix is used as a pre-filter:

$$\mathbf{W} = \mathbf{H}^H. \tag{4.44}$$

The transmitted signal is written as:

$$\mathbf{s} = f\,\mathbf{W}\mathbf{x} = f\,\mathbf{H}^H\mathbf{x} \tag{4.45}$$

where

$$f = \sqrt{\frac{2}{A^2\mathrm{Tr}(\mathbf{H}^H\,\mathbf{H})}} \tag{4.46}$$

is a normalization factor used to guarantee that the average total transmit power $\bar{P}_t$ is equal to 1.

However, unlike the ZF preprocessing used in [84] where the required number of antennas should satisfy the constraint $N_r \leq N_t$ so that the matrix inversion remains possible, for MRT processing, it is straightforward to obtain the expression of the receive signals:

$$\mathbf{y} = f\,\mathbf{H}\,\mathbf{H}^H\,\mathbf{x} + \mathbf{n} \tag{4.47}$$

without any pseudo inverse channel matrix computation.

At the level of R_j, the received signal then writes:

$$\begin{aligned} & y_j(k) = \\ & f\left(\sum_{i=1}^{N_t}\left\|h_{j,i}\right\|^2 \times x_j(k) + \sum_{i=1}^{N_t}\sum_{l=1,l\neq j}^{N_r} h_{j,i}h_{i,l}^{*}x_l(k)\right) + \eta_j \\ =& \beta_j \times x_j(k) + I_j(k) + \eta_j \end{aligned} \tag{4.48}$$

where

$$\beta_j = f\sum_{i=1}^{N_t}\left\|h_{j,i}\right\|^2$$

is the amplitude of the receive signal toward antenna R_j, and

$$I_j(k) = f\sum_{i=1}^{N_t}\sum_{l=1,l\neq j}^{N_r} h_{j,i}h_{i,l}^{*}x_l(k)$$

is the additional interference to the antenna R_j when sending the spatial symbol $\mathbf{x}_k$. It is shown that the focused signal $x_j(k)$ is multiplied by a real amplitude, while a complex interference is added to the received signal depending on the spatial symbol, which is caused by inter-antennas interference.

4.4.1 Detection

The *Real Amplitude Threshold* detector used in ZF-ERASK as ML detector, will be used in this section also for MRT-ERASK. Notice that this detector is not equivalent to the ML detector as for ZF-RASK systems because of interference at the non-targeted antennas. Detecting if antenna R_j is targeted will therefore be obtained by:

$$\hat{x}_j(k) = \begin{cases} 0, & \text{if } \Re\{y_j\} \leq \nu_j, \\ 1, & \text{if } \Re\{y_j\} \geq \nu_j, \end{cases} \tag{4.49}$$

where ν_j is a predefined amplitude threshold at the antenna R_j. From equation (4.48), a given detector has to analyze the following set of signals:

$$\forall j, \quad y_j(k) = \begin{cases} \beta_j + I_j(k) + \eta_j & \text{if } R_j \text{ is targeted} \\ I_j(k) + \eta_j & \text{otherwise.} \end{cases} \tag{4.50}$$

The interference factor $I_j(K)$ changes between different values; depending on the spatial symbol, between a minimum value when all other antennas are not targeted, and a maximum value when all other antennas are targeted:

$$\min_K(I_j) = 0$$

$$\max_K(I_j) = f \sum_{i=1}^{N_t} \sum_{l=1, l\neq j}^{N_r} h_{j,i} h_{i,l}^*.$$

From equation (4.50), we can define ν_j as:

$$\nu_j = \frac{\beta_j + \max_k(\Re\{I_j\})}{2}. \tag{4.51}$$

4.4.2 Analytical Performance

In this part, we derive the analytical approach for the BEP performance of the ERASK system employing MRT preprocessing.

Let $\mathcal{P}_e(k)$ be the probability of error when sending the spatial symbol $\mathbf{x}_k$. We obtain:

$$\begin{aligned} \mathcal{P}_e(k) = & \frac{1}{2} \times \left[\mathcal{P}\left(\nu_j \leq \Re\{I_j(K) + \eta_j\}\right) + \mathcal{P}\left(\Re\{\beta_j + I_j(K) + \eta_j\} \leq \nu_j\right) \right] \\ & \mathcal{P}\left(\mathcal{N}(0, \frac{\sigma_n^2}{2}) \geq \nu_j - \Re\{I_j(K)\}\right) \\ = & Q\left(\frac{\nu_j - \Re\{I_j(K)\}}{\sigma_n/\sqrt{2}}\right). \end{aligned} \tag{4.52}$$

As a result, the general equation of the BEP is given as:

$$\mathcal{P}_e = \frac{1}{N_r 2^{N_r}} \sum_{j=1}^{N_r} \sum_{K=1}^{2^{N_r}} Q\left(\frac{\beta_j + \Re\{\max_k(I_j)\} - 2\Re\{I_j(K)\}}{\sigma_n \sqrt{2}}\right). \tag{4.53}$$

4.4.3 Simulation results

In this part, BER performance is provided versus the ratio between the average of the symbol energy and the noise spectral density of the ERASK system: $\frac{E_S}{N_0}$. The channel is considered to be normalized, so we have:

$$\frac{E_S}{N_0} = \frac{1}{\sigma_n^2}.$$

It is assumed that $\mathbf{H}$ is a MIMO flat fading channel matrix where $h_{j,i}$ are complex coefficients following an i.i.d. Rayleigh distribution. The power for each sub-channel is normalized:

$$E\left[\left\|h_{j,i}\right\|^2\right] = 1.$$

Finally, we consider that the channel response is perfectly known at the transmitter.

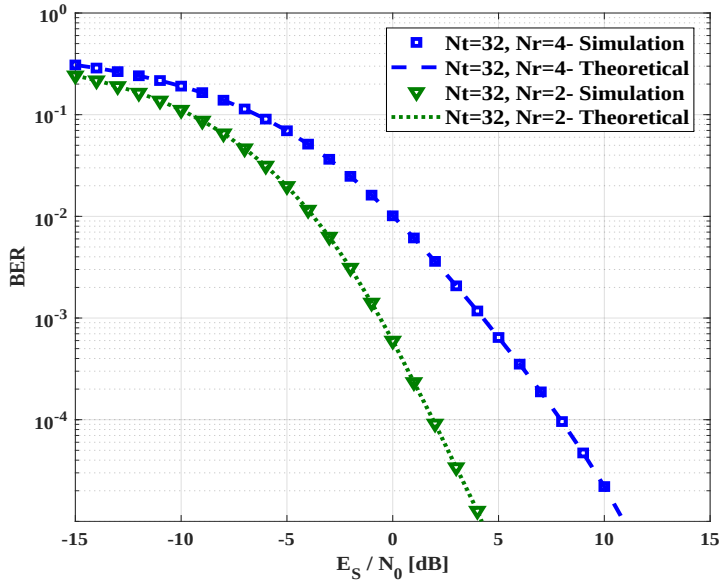

Figure 4.9 – BER performance of two MRT-ERASK over Rayleigh fading channel, N_t= 32, N_r=2 and 4, simulation and theoretical results

Simulations are run by implementing a sufficient number of iterations for different channel realizations, and taking the mean value of the BEP for each value of $\frac{E_S}{N_0}$. In all simulations, the receiver uses the Real Amplitude Threshold (RAT) detection to estimate the spatial symbol.

In Figure 4.9, we compare the simulation results with the theoretical results provided by the derivation of the theoretical analysis of the BEP . Two MRT-ERASK with $N_t = 32$ transmit antenna, and with $N_r = 2$ and 4 are provided. Results obviously show that the simulation results perfectly match with the theoretical derivation.

In Figure 4.10, simulation results are presented considering an ERASK system with $N_t = 8$, 16, 32 and 64, and with $N_r = 2$ and 4. The results first show that for a given number of receive antennas, the higher the number of transmit antenna, the better the performance due to a better focusing gain and a lower interference level towards

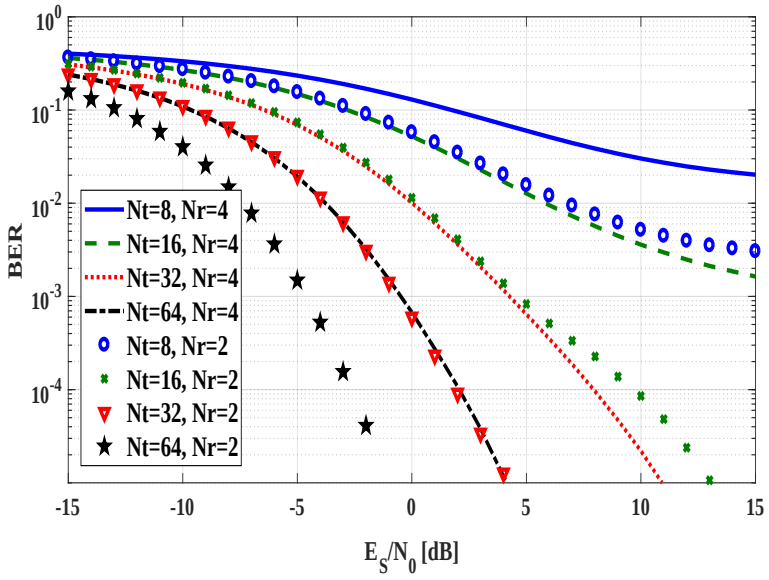

Figure 4.10 – Comparison of the BER performance of two MRT-ERASK over a Rayleigh fading channel, N_r=2 and 4

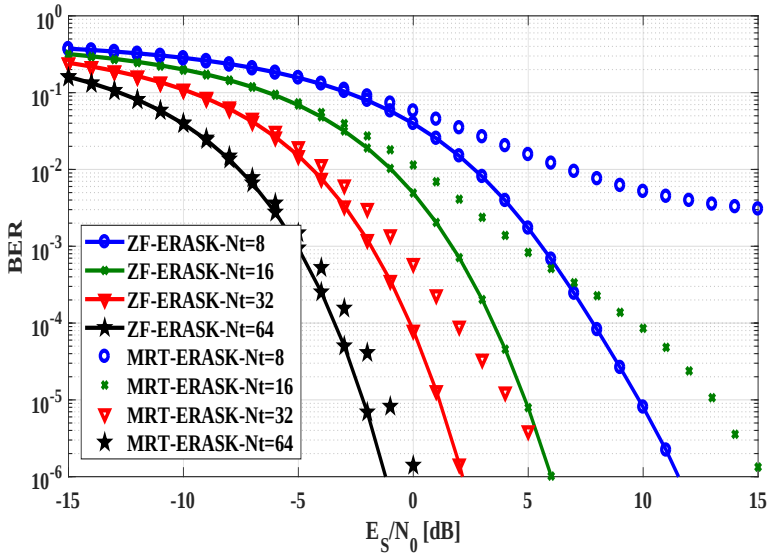

Figure 4.11 – Comparison of the BER performance of MRT-ERASK and ZF-ERASK over a Rayleigh fading channel, N_r=2

the non-targeted antennas as concluded in [91]. As also evident from this figure, the higher the order of the spatial modulation, i.e. the number of receive antennas N_r, the greater the performance degradation. Indeed, as N_r increases, the trace $\mathbf{H}^H\mathbf{H}$ that is proportional to N_r also increases, and so the normalization factor f that controls the signal amplitude of the received signal in equation (4.48) decreases.

In Figure 4.11, we consider ERASK systems with $N_r = 2$, and with $N_t = 8, 16, 32$ and 64. The ZF and the MRT preprocessing are employed and compared for all system configurations. As evident from the obtained curves, the higher N_t is, the better the performance of the two systems. Also, for all system configurations, the ZF-ERASK outperforms the MRT-ERASK, because of the interference cancellation. Nevertheless, the difference in performance decreases when increasing the number of transmit antennas, which makes the MRT-ERASK more suitable because of the lower implementation complexity compared to the Zero-Forcing system that requires a matrix inversion.

4.5 Extended Receive Spatial Modulation

4.5.1 ERSM Principles

The idea behind the proposed Extended RSM (ERSM) introduced in chapter 2 consists of merging conventional IQ modulation based on Phase Shift Keying (PSK) and the Extended RASK concept previously presented. Hence, with conventional ERASK, one of the possible combinations of spatial symbols consists of not targeting any receive antenna, i.e. zero power transmission, and then it is impossible to send any additional information as IQ mapping. To overcome this limitation, a non-zero power level can also be used to be allocated for non targeted antennas. More precisely, at each symbol duration, each receive antenna is targeted with one among two power levels $\{P_1, P_2\}$ and receives the same IQ symbol. In this scheme, the number M_1 of possible spatial symbols is equal to 2^{N_r}, providing a transmission of $m_s = N_r$ spatial bits. Consequently, the total SE of ERSM is:

$$m = m_s + m_M \tag{4.54}$$

where $m_M = \log_2(M)$, and M is the order of an M-order modulation. For ERSM, an M-PSK modulation is considered in order to have the same power level for all IQ symbols when the same spatial bit is transmitted.

000 101 100 111	**Symbol 1**	**Symbol 2**	**Symbol 3**	**Symbol 4**
1) Segmentation	**00 0**	**10 1**	**10 0**	**11 1**
2) Spatial & PSK mapping	$(-\sqrt{P_1}, -\sqrt{P_1})$	$(\sqrt{P_1}, \sqrt{P_2})$	$(-\sqrt{P_2}, -\sqrt{P_1})$	$(\sqrt{P_2}, \sqrt{P_2})$
3) Preprocessing (focalisation)				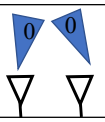
4) Detection	$(-\sqrt{P_1}, -\sqrt{P_1})$	$(\sqrt{P_1}, \sqrt{P_2})$	$(-\sqrt{P_2}, -\sqrt{P_1})$	$(\sqrt{P_2}, \sqrt{P_2})$
5) Demapping	**00 0**	**10 1**	**10 0**	**11 1**

Figure 4.12 – Illustration of ERSM concept

Figure 4.12 provides an illustration of the ERSM scheme principle with $N_r = 2$ and a BPSK modulation, resulting in an SE of $m = 3$ bits/s/Hz. The signal with power P_1 (resp. P_2) is represented in yellow (resp. blue). The BPSK symbols are represented by their phase: 0 or π. Steps 1 and 2 allow for forming a super symbol transmitting

3 bits during each symbol duration. The spatial mapping used in this example is the following:

- P_1 is allocated to targeted antenna to transmit '0',
- P_2 is allocated to targeted antenna to transmit '1'.

The two power levels must be carefully selected to minimize the total error probability, so let us define:

$$\gamma = \frac{P_2}{P_1} \tag{4.55}$$

with $P_1 < P_2$ (i.e. $\gamma > 1$). In order to have an average total transmit power equal to 1, we have:

$$P_1 = \frac{2}{(1+\gamma)N_r} \tag{4.56}$$

and

$$P_2 = \frac{2\gamma}{(1+\gamma)N_r}. \tag{4.57}$$

In the following, an optimal value for γ is calculated. The transmitted signal also depends on an additional bit related to a BPSK modulation. Hence, at step 3, the preprocessing is performed at the transmitter so as to create a beam to concentrate the allocated energy towards the targeted antennas. At step 4, the receiver estimates the phase of the sum of all signals in order to demodulate the BPSK bit, and then it estimates which power level was allocated by analyzing the amount of received signal amplitude at each antenna to deduce the transmitted spatial symbol.

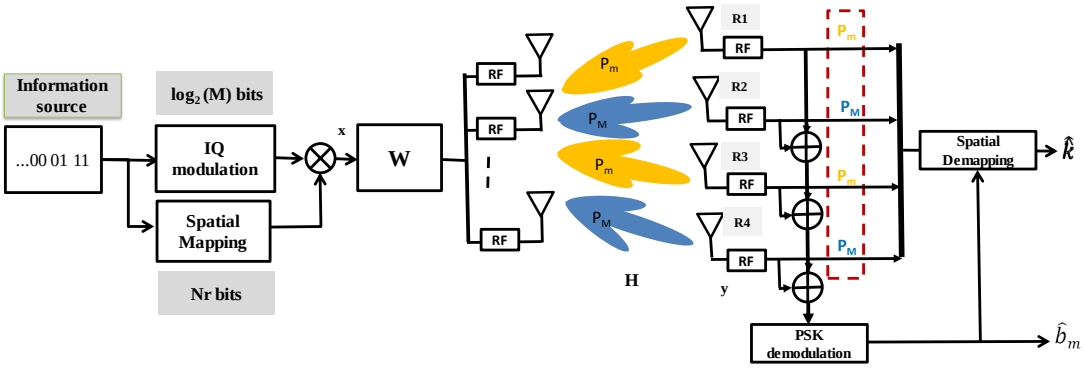

Figure 4.13 – Block diagram of ERSM system

4.5.2 Block Diagram of ERSM

The block diagram of the ERSM system is depicted in Figure 4.13. A group of m bits is mapped onto a super-symbol vector $\mathbf{x} \in \mathbb{C}^{N_r \times 1}$:

$$\mathbf{x} = \left[x_k^b\right]^T = \left[x_1^b \quad x_2^b \quad \ldots \quad x_{N_r}^b\right]^T \tag{4.58}$$

where $b \in 1, ..., M$ is a symbol taken from an M order modulation and k denotes the spatial symbol. The mapping is made of two stages, one for the IQ symbol and another for the spatial symbol. An M-PSK modulation symbol in the form of $x^b = e^{i\theta_b}$ is first constructed, depending on the bit stream to transmit. Then, the spatial symbol is mapped by allocating different power levels to the targeted receive antennas in applying the power allocation vector $\mathbf{P}_k$:

$$x_k^b = \mathbf{P}_k x^b \tag{4.59}$$

with

$$\mathbf{P}_k = \begin{bmatrix} \sqrt{p_{1,k}} & \sqrt{p_{2,k}} & \dots & \sqrt{p_{N_r,k}} \end{bmatrix}^T \tag{4.60}$$

where $p_{i,k}, i \in [1, N_r]$ are taken from the set $\{P_1, P_2\}$ according to the spatial symbol k.

Then, the pre-processing block transforms the vector of spatial symbols $\mathbf{x}$ into a vector of transmitted signals denoted by $\mathbf{s} \in \mathbb{C}^{N_t \times 1}$ using the ZF pre-processing matrix:

$$\mathbf{s} = f\mathbf{W}\mathbf{x} \tag{4.61}$$

where

$$f = \frac{1}{\sqrt{\sigma_x^2 \mathrm{Tr}(\mathbf{W}.\mathbf{W}^H)}} \tag{4.62}$$

is a normalization factor used to guarantee that the average total transmit power $\bar{P}_t$ is equal to 1. Since $\mathbf{x}$ has i.i.d. entries, the variance $\sigma_x^2 = \mathbb{E}_x \left[x_j x_j^* \right]$ is independent of j and comes in factor of the trace computation. Then, each entry of $\mathbf{x}$ is of amplitude $\sqrt{P_1}$ or $\sqrt{P_2}$ with a probability that can be easily verified to be $\frac{1}{2}$, leading to $\sigma_x^2 = \frac{P_1+P_2}{2}$.

At the receiver, the expression of the receive signals is straightforwardly obtained:

$$\mathbf{y} = f\mathbf{x} + \mathbf{n}. \tag{4.63}$$

At the level of the receive antenna R_j, the received signal then simply writes:

$$\begin{aligned} y_{j,k} =& f \times x_j^b + \eta_j \\ =& f\sqrt{p_{j,k}} \times x^b + \eta_j. \end{aligned} \tag{4.64}$$

An M-PSK demodulation is operated to detect the IQ symbol transmitted and a spatial detection based on the level of the received amplitude at each receive antenna is used to complete the whole transmit symbol detection. First, all received signals are summed up, and an M-PSK demodulation is performed to estimate the transmitted IQ symbol. We define z_k, the sum of the received signals when sending the spatial symbol k:

$$z_k = \sum_{j=1}^{N_r} y_{j,k} = \left(\sum_{j=1}^{N_r} \sqrt{p_{j,k}} \right) f x^b + \sum_{j=1}^{N_r} \eta_j. \tag{4.65}$$

The estimated IQ symbol $\tilde{x}_b$ from the demodulation of z_k is used to compensate the phase of all received signals in order to detect the spatial symbol. Accordingly, the receiver at R_j compares the compensated received signal to a predefined threshold ν:

$$p_{j,k} = \begin{cases} P_1, & \text{if } \Re\{y_j / \tilde{x}^b\} \leq \nu, \\ P_2, & \text{if } \Re\{y_j / \tilde{x}^b\} \geq \nu. \end{cases} \tag{4.66}$$

The optimal threshold is easily deduced from:

$$\nu = \mathbb{E}\left\{\frac{\Re\{y_{j,1}/\tilde{x}^b\} + \Re\{y_{j,2}/\tilde{x}^b\}}{2}\right\} = \frac{f(\sqrt{P_1}+\sqrt{P_2})}{2}, \tag{4.67}$$

with y_{j1} (resp. y_{j2}) the receive signal on antenna R_j if this antenna is targeted with the power level P_1 (resp. targeted by the power level P_2). Note that such a threshold can in practice be estimated during a calibration phase using dedicated pilot symbols.

4.5.3 ERSM Performance and Optimum Power Ratio

Binary Error Probability performance

In this part, we provide the performance analysis of the ERSM scheme by deriving the BEP defined by $\mathcal{P}_e$. A perfect channel estimation at the transmitter and synchronization between antennas are supposed. Let $\mathcal{P}_{SS}$ be the probability of error for the spatial symbol, and $\mathcal{P}_{PSK}$ be the average BEP of the M-PSK modulation. Each receive antenna has an equal probability of being targeted by P_1 or P_2, so the total BEP becomes:

$$\mathcal{P}_e = \frac{(m_s\mathcal{P}_{SS} + m_M\mathcal{P}_{PSK})}{m}. \tag{4.68}$$

Let $\mathcal{P}_{PSK_k}$ be the BEP of the M-PSK modulation when sending the spatial symbol k. $\mathcal{P}_{PSK_k}$ can be approximated at high SNR and Gray mapping by [29]:

$$\begin{aligned}\mathcal{P}_{PSK_k} \approx & \frac{1}{m_M} Q\left(\sqrt{\frac{E_s}{N_0}}\sin(\pi/M)\right) \\ = & \frac{1}{m_M} Q\left(\frac{\sum_{j=1}^{N_r}\sqrt{p_{j,k}} f \sin(\pi/M)}{\sqrt{N_r}\sigma_n}\right).\end{aligned} \tag{4.69}$$

Let N_k be the number of receive antennas that are targeted with power level P_2, i.e. the associated spatial bit is "1". We have:

$$\mathcal{P}_{PSK_k} = \frac{1}{m_M} Q\left(\frac{\left(N_r\sqrt{P_1} + N_k(\sqrt{P_2}-\sqrt{P_1})\right) f \sin(\frac{\pi}{M})}{\sqrt{N_r}\sigma_n}\right). \tag{4.70}$$

All spatial symbols are equally likely to be sent, so the average BEP of the M-PSK symbol is:

$$\mathcal{P}_{PSK} = \frac{1}{2^{N_r}} \sum_{N_k=0}^{N_r} C_{N_r}^{N_k} \mathcal{P}_{PSK_k}. \tag{4.71}$$

On the other hand, the probability of error in the spatial bit $\mathcal{P}_{Sb}$ is:

$$\begin{aligned}\mathcal{P}_{Sb} = & \frac{1}{2}\mathcal{P}\left(\sqrt{P_1}x_{b_j} \to \sqrt{P_2}x_{b_j}\right) \\ & + \mathcal{P}\left(\sqrt{P_2}x_{b_j} \to \sqrt{P_1}x_{b_j}\right),\end{aligned} \tag{4.72}$$

where $\mathcal{P}\left(x \to y\right)$ is the probability to send x and detect y.

Then, after applying the threshold detection, and supposing that the PSK symbol is well estimated, we obtain:

$$\begin{aligned}\mathcal{P}_{Sb} =& \frac{1}{2} \times \left[\mathcal{P}\left(\nu \leq \Re\{f\sqrt{p_1}x_{b_j} + \eta_j\}\right) \right. \\ & \left. + \mathcal{P}\left(\Re\{f\sqrt{p_2}x_{b_j} + \eta_j\} \leq \nu\right) \right]\end{aligned} \tag{4.73}$$

and after mathematical derivations, we get:

$$\mathcal{P}_{Sb} = Q\left(\frac{f.(\sqrt{P_2} - \sqrt{P_1})}{2\sigma_n}\right). \tag{4.74}$$

In fact, since the compensation of the phase is needed before the spatial detection, it seems that the PSK demodulation affects the spatial detection. But for high SNR, the effect is negligible, and it is evident to take the approximation of the performance supposing that the phase is well estimated. The BEP of the whole spatial symbol is given as:

$$\mathcal{P}_{SS} = \frac{1}{N_r}\sum_{j=1}^{N_r}\mathcal{P}_{Sb}. \tag{4.75}$$

We can notice that, assuming a perfect channel estimation at the transmitter for the pre-processing, as well as the same signal to noise ratio for each receive antenna and decorrelation between these receive antenna, we can straightforwardly get:

$$\mathcal{P}_{SS} = \mathcal{P}_{Sb} \tag{4.76}$$

Optimal Power Ratio γ

The optimal value of γ has to deal with the difference between two power levels to minimize the error in the spatial detection, and should satisfy a sufficient signal-to-noise ratio for the symbol transmitted with the lower power level summation, i.e. when all receive antennas are targeted with P_1, in order to minimize the error in the M-PSK demodulation.

Define f_S as:

$$f_S(\gamma) = \frac{f}{2\sigma_n}(\sqrt{P_2} - \sqrt{P_1}) = \frac{f}{2\sigma_n}\frac{\sqrt{\gamma} - 1}{\sqrt{1+\gamma}} \tag{4.77}$$

and f_M as:

$$f_M(\gamma) = \frac{\sqrt{N_r}f}{\sigma_n}\sqrt{P_1}\sin(\pi/M) = \frac{f}{\sigma_n}\frac{\sqrt{N_r}\sin(\pi/M)}{\sqrt{1+\gamma}} \tag{4.78}$$

as the functions that are taken from the error probability of equations (4.74) and (4.69) respectively. So we have:

$$\gamma_{opt} = \arg\max_{\gamma}\Big\{\min\{f_S(\gamma), f_M(\gamma)\}\Big\} \tag{4.79}$$

that becomes:

$$\gamma_{opt} = \arg\max_{\gamma}\Big\{\min\Big\{\frac{f}{2\sigma_n}\frac{\sqrt{\gamma} - 1}{\sqrt{1+\gamma}}, \frac{f}{\sigma_n}\frac{\sqrt{N_r}\sin(\pi/M)}{\sqrt{1+\gamma}}\Big\}\Big\}. \tag{4.80}$$

This optimization equation is equivalent to finding the value of γ that makes the two terms equal, which gives:

$$\gamma_{opt} = (1 + 2\sqrt{N_r}\sin(\pi/M))^2. \tag{4.81}$$

4.5.4 Simulation Results

The performance of the proposed ERSM scheme is evaluated through the measurement of the BER versus the ratio between the average transmit power level and noise level, i.e. $\frac{\bar{P}_t}{\sigma_n^2}$, defined as the transmitted SNR. It is assumed that $\mathbf{H}$ is a MIMO flat fading channel matrix where $h_{j,i}$ are complex coefficients following an i.i.d. Rayleigh distribution. The power for each sub-channel is normalized:

$$E\left[\, \|h_{j,i}\|^2 \,\right] = 1$$

. Finally, we consider that the channel response is perfectly known at the transmitter, so that perfect ZF pre-processing is performed.

Simulations are run by implementing a sufficient number of iterations for different channel realizations and taking the mean value of the BER for each SNR value.

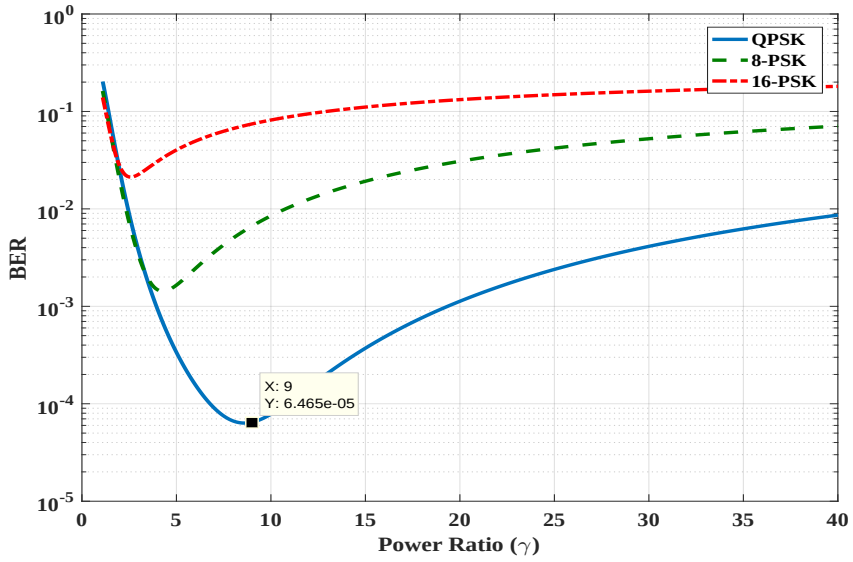

Figure 4.14 – BER vs power ratio γ for a 8×2 MIMO with ERSM QPSK, 8-PSK and 16-PSK

In Figure 4.14, the performance of the ERSM system with $N_r = 2$ and $N_t = 8$ is provided as function of the power ratio γ. A minimum BER is reached at the point of the optimal value of γ that was analytically calculated in the previous part. In later simulations, the optimal value of γ is taken to choose the power levels.

In Figure 4.15, we compare the simulation results with the theoretical results provided by the derivation of the theoretical analysis of the BER. Three ERSM with $N_t = 8$ transmit antenna, and with different configurations regarding N_r and the order of IQ

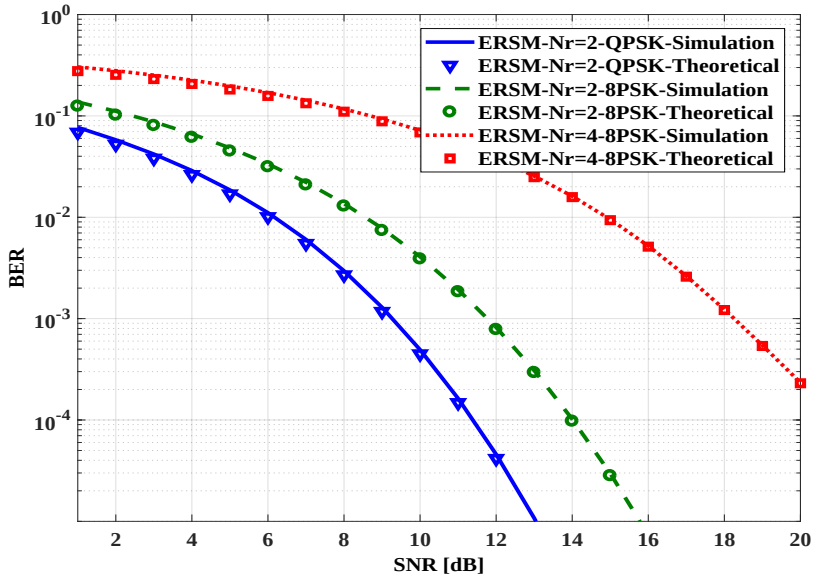

Figure 4.15 – Theoretical and Simulation BER results for 8×2 and 8×4 ERSM with QPSK and 8-PSK, with Rayleigh fading.

modulation are provided: ERSM-QPSK with $N_r = 2$, ERSM-8PSK with $N_r = 2$, and ERSM-8PSK with $N_r = 4$. Results obviously show that the simulation results perfectly match with the theoretical derivation for high SNR, and with a negligible difference for low SNR.

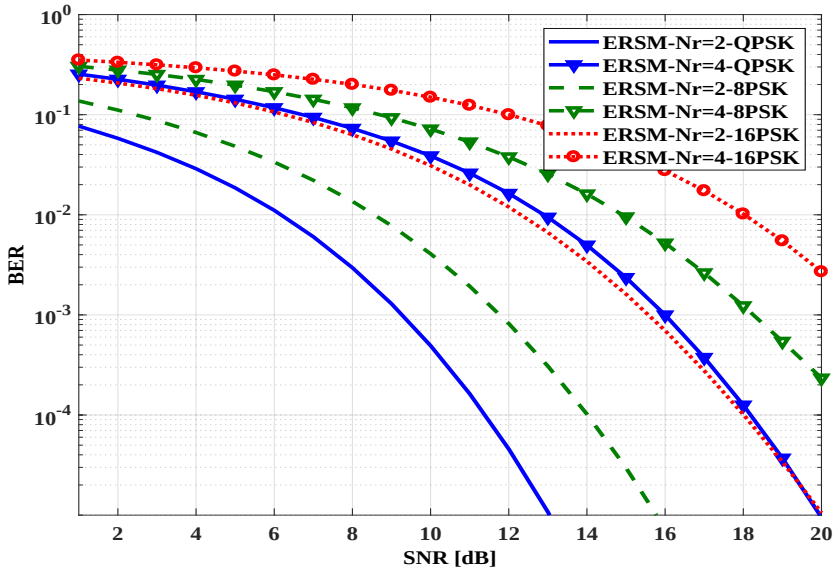

Figure 4.16 – BER vs SNR for a 8×2 and 8×4 MIMO ERSM, for QPSK, 8-PSK, and 16-PSK with Rayleigh fading

In Figure 4.16, the performance of the ERSM system when increasing the SE by

increasing the order of spatial modulation, i.e. N_r, or by increasing the order of IQ modulation is presented. Recall that the SE of the system is $N_r + \log_2(M)$. We provide different ERSM systems with N_t= 8, N_r = 2 or 4, and with M=4, 8 and 16 for each configuration. Results obviously show that increasing the SE, whether by increasing N_r or M, leads to a degradation in performance. But when focusing on the same SE but with different system configurations, i.e. for N_r= 2 with 16-PSK, and N_r= 4 with QPSK modulation, (the SE=5 bit/s/Hz for each) it is shown that the performance is approximately the same, especially when increasing the SNR. This result is because the optimal solution is chosen since for the higher SNR, the dominant error in the IQ symbols results from the symbol with the lower power (i.e. when the spatial symbol is all zeros). We demonstrate in the analytical part that the optimal ratio results if the error in the spatial modulation is equal to the error resulting from the IQ symbol with the minimum power.

4.6 Summary

In this chapter, the ERASK that was proposed to improve the spectral efficiency of spatial modulation at the receiver side to N_r, by allowing a transmission towards a variable number of receive antennas simultaneously, was presented. We presented several detectors for that can be carried out at the receiver side as well as their expected theoretical performance, and we demonstrate that when the ZF precoding is used, the ML detection is reduced to a simple amplitude threshold. Coherent and non-coherent detection were presented and compared, and results showed that the coherent detector obviously always outperforms the non-coherent one, nevertheless the proposed non-coherent ones offer a very reduced complexity. Also, the error in channel estimation and the effect of correlation between antenna where studied, and results show that ERASK with ZF precoding remains robust under some limitations. In addition, the ERASK with MRT precoding was presented and compared to the ZF-RASK. ZF-RASK outperforms the MRT-RASK but with the cost of computational complexity. But, the more the number of transmit antenna increases, more the performance of the two precodings becomes the same, and then the criteria of choosing the precoder is based on the implementation complexity. Finally, the ERSM scheme, that allows the transmission of ERASK and IQ symbols simultaneously, was studied, and the optimal ratio of power levels was calculated, to give the better performance. It was shown that when the optimal ratio is used, increasing the spectral efficiency by the spatial dimension, or increasing the order of IQ modulation, gives the same performance.

Chapter 5

Extended Space Shift Keying

Contents

5.1 Introduction

In this chapter, we first propose a novel scheme referred to as Extended SSK (ESSK) for the uplink transmission of a device connected to a Base Station. In order to improve the SSK of transmit spatial modulations, we propose to simultaneously activate a variable number of transmit antennas. This number of active antennas changes at each spatial symbol duration depending on the set of bits to transmit and according to a spatial mapping function. We demonstrate how ESSK symbol is made of N_t bits. We also study the Maximum Likelihood detector that can be carried out at the receiver side as well as the expected theoretical performance. Also, we study the performance of the system when ZF equalization is performed at the receiver before the detection. At the end of this chapter, we proposed a complete Uplink and Downlink transmission system between a base station and a connected device based on the extended SM.

5.2 Scheme Principle

The ESSK scheme is built on the SSK concept at the transmitter where the number of active antennas N_a is variable during each time symbol T_s ($0 \leq N_a \leq N_t$). As for ERASK [84], N_a can take all possible values between 0 and N_r depending on the useful information to transmit so that the number of possible spatial symbols is $M = 2^{N_t}$ providing the transmission of N_t bits per spatial symbol.

00 01 10 11	**Symbol 1**	**Symbol 2**	**Symbol 3**	**Symbol 4**
Segmentation	**00**	**01**	**10**	**11**
Spatial Mapping	**(0,0)**	**(0,T2)**	**(T_1,0)**	**(T_1, T2)**
Channel	 **H**	 **H**	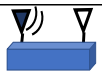 **H**	 **H**
Detection	**(0,0)**	**(0, T2)**	**(T_1,0)**	**(T_1, T2)**
Demapping	**00**	**01**	**10**	**11**

Figure 5.1 – Example of the Extended-SSK system with $N_t = 2$ for uplink transmission

Figure 5.1 provides an illustration of the ESSK scheme with $N_t = 2$. The connected device is represented in blue with its two transmit antennas. As evident from this figure, the ESSK system allows 2 bits to be transmitted during each spatial symbol. The spatial mapping used in this example is the following:

- no antenna is activated if symbol '00' is sent,
- antenna T_2 is activated if symbol '01' is sent,
- antenna T_1 is activated if symbol '10' is sent,
- both antennas T_1 and T_2 are activated if symbol '11' is sent.

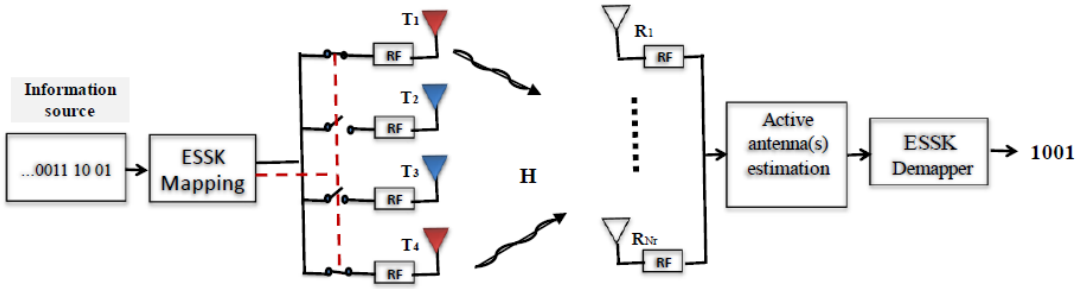

Figure 5.2 – Block Diagram for Extended-SSK

Hence, at step 3 of the system description, the receiver (the base station) estimates which antennas have been activated by analyzing the received signal and then deduces the transmitted spatial symbol.

5.3 System model and Block Diagram

In this part, we first set up the model for a communication system making use of the ESSK scheme. Then, we introduce the detection methods used for symbol estimation.

5.3.1 System Model

MIMO system with N_t transmit antennas and N_r receive antennas is considered. Assuming a flat fading channel between the transmitter and the receiver, the receive signal vector can be written as:

$$\mathbf{y} = \mathbf{H}.\mathbf{s} + \mathbf{n} \tag{5.1}$$

where $\mathbf{H} \in \mathbb{C}^{N_r \times N_t}$ is the MIMO channel matrix with element $h_{j,i}$ representing the complex channel coefficient between the i-th transmission antenna, denoted by T_i, and the j-th receiving antenna, denoted by R_j. $\mathbf{y} \in \mathbb{C}^{N_r \times 1}$ is the vector of the received signals at all the receive antennas, $\mathbf{s} \in \mathbb{C}^{N_t \times 1}$ is the vector of the transmitted signals by all the transmit antennas, and $\mathbf{n} \in \mathbb{C}^{N_r \times 1}$ is the vector of additive white Gaussian noise (AWGN) samples η_j such that $\eta_j \sim \mathcal{CN}(0, \sigma_n^2)$.

5.3.2 Block Diagram

The block diagram of the ESSK system is depicted in Figure 5.2. A group of $m = N_t$ bits is mapped to a spatial symbol $\mathbf{x} \in \mathbb{C}^{N_t \times 1}$ which is written as:

$$\mathbf{x} = \begin{bmatrix} x_1 & x_2 & \dots & x_{N_t} \end{bmatrix}^T \text{ where } x_i \in \{0, 1\}.$$

The value taken by each x_i entry determines the set of active transmit antennas such that:

$$x_i = \begin{cases} 0, & \text{if } T_i \text{ is not active,} \\ 1, & \text{if } T_i \text{ is active.} \end{cases} \tag{5.2}$$

The spatial symbol vector is normalized by a factor f before being emitted, used to guarantee that the average total transmit power $\bar{P}_t$ is equal to 1:

$$f = \frac{1}{\sqrt{\sigma_x^2 N_t}}. \tag{5.3}$$

If we consider that each entry of $\mathbf{x}$ is of amplitude 1 with a probability that can be easily verified to be $\frac{1}{2}$, we have that $\sigma_x^2 = \frac{1}{2}$, which finally yields:

$$f = \sqrt{\frac{2}{N_t}}. \tag{5.4}$$

Consequently, the transmitted signal is written as:

$$\mathbf{s} = f\mathbf{x}. \tag{5.5}$$

5.4 Detection strategies

5.4.1 Maximum Likelihood (ML)

ML detection equation

At the receiver, a number N_r of receive antennas detect the signal. From equation (5.1) and equation (5.5), if we are sending the spatial symbol k, the received signal vector writes:

$$\mathbf{y}_k = f \sum_{i=1}^{N_t} \mathbf{h}_i x_i(k) + \mathbf{n} = f\mathbf{h}_k^{eq} + \mathbf{n} \tag{5.6}$$

where $\mathbf{h}_k^{eq}$ is the equivalent channel vector received when sending the spatial symbol k. The detector has to estimate the index of antenna(s) that have been activated. The equation of the ML is:

$$k = \text{argmin}_j \left\| \mathbf{y} - f\mathbf{h}_j^{eq} \right\|^2 \tag{5.7}$$

Performance analysis

The BER performance of the ESSK is given by the union bound equation:

$$\mathcal{P}_e = \sum_j \sum_k \frac{\mathbf{d}(\mathbf{x}_j, \mathbf{x}_k)}{M} \mathcal{P}(\mathbf{x}_j \to \mathbf{x}_k) \tag{5.8}$$

where $\mathcal{P}(\mathbf{x}_k \to \mathbf{x}_j)$ is the PEP and $d(\mathbf{x}_k, \mathbf{x}_j)$ is the hamming distance between two spatial symbols $\mathbf{x}_k$ and $\mathbf{x}_j$. Using Equation (5.7), the PEP conditioned on $\mathbf{H}$ is given as:

$$\begin{aligned} &\mathcal{P}(\mathbf{x}_k \to \mathbf{x}_j|\mathbf{H}) = \mathcal{P}(d_k > d_j|\mathbf{H}) \\ &= \mathcal{P}\left(\Re\{\mathbf{n}^H(\mathbf{h}_j^{eq} - \mathbf{h}_k^{eq})\} > \frac{1}{2} \left\| \mathbf{h}_j^{eq} - \mathbf{h}_k^{eq} \right\|^2 |\mathbf{H} \right) \\ &= Q(\sqrt{\kappa}) \end{aligned} \tag{5.9}$$

where $d_j = \left\| \mathbf{y} - f\mathbf{h}_j^{eq} \right\|^2$ and $Q(x)$ is the Gaussian distribution function: $Q(x) = \int_x^\infty \frac{1}{2\pi} e^{-\frac{t^2}{2}} dt$. We have also:

$$\kappa = \frac{\left\| \mathbf{h}_j^{eq} - \mathbf{h}_k^{eq} \right\|^2}{2\sigma_n^2} = \frac{\sum_{i=1}^{2N_r} \alpha_i^2}{2\sigma_n^2} \tag{5.10}$$

where $\alpha_i \sim \mathcal{N}(0, \sigma_\alpha^2)$ with $\sigma_\alpha^2 = \frac{f^2 \mathbf{d}(\mathbf{x}_j, \mathbf{x}_k)}{4}$. The Average PEP for different channel realization is given by:

$$\mathcal{P}(\mathbf{x}_k \to \mathbf{x}_j) = \mathbb{E}_{\mathbf{H}}[\mathcal{P}(\mathbf{x}_k \to \mathbf{x}_j)] = \int_0^\infty Q(\sqrt{u}) p_\kappa(u) du, \tag{5.11}$$

where p_κ is the PDF of κ. The random variable κ is chi-squared distributed with c=$2N_r$ degrees of freedom, so we have:

$$p_\kappa(u) = \frac{u^{\frac{c}{2}-1} \exp\left(-\frac{u}{2\sigma_\alpha^2}\right)}{(2\sigma_\alpha^2)^{\frac{c}{2}} \Gamma(\frac{c}{2})}, \tag{5.12}$$

which has a closed form expression given in [92]:

$$\mathcal{P}(\mathbf{x}_k \to \mathbf{x}_j) = \gamma_\alpha^{N_r} \sum_{k=1}^{N_r - 1} C_k^{N_r - 1 + k} (1 - \gamma_\alpha)^k \tag{5.13}$$

where $\gamma_\alpha = \frac{1}{2}\left(1 - \sqrt{\frac{\sigma_\alpha^2}{1+\sigma_\alpha^2}}\right)$.

5.4.2 Equalization

In the ERASK scheme, the channel estimation is used to create the precoding matrix used to transmit the spatial symbol. The same matrix can be used in uplink for the equalization, which is why it is interesting to evaluate the performance of the ESSK when using equalization.

Equalized Signal

The received signal $\mathbf{y}$ given in equation (5.1) is further equalized. Assuming perfect channel estimation at the receiver side, the equation of spatially equalized signals is:

$$\mathbf{z} = f\mathbf{W}\mathbf{H}\mathbf{x} + \mathbf{W}\mathbf{n} \tag{5.14}$$

where $\mathbf{W} \in \mathbb{C}^{N_t \times N_r}$ is the equalization matrix. As a final step, a detector is used to estimate the spatial symbols from the equalized signal and demappes it to deliver the bit sequence corresponding to the mapping rule described above. The receiver uses the spatial equalization step to reconstruct the spatial symbol vector. The ZF equalization is employed, so:

$$\mathbf{W} = (\mathbf{H}^H \mathbf{H})^{-1} \mathbf{H}^H. \tag{5.15}$$

Since the channel matrix is expected to be converted into an identity matrix after ZF equalization, any inter-antenna interference is removed at this step. To make it possible, the required number of antennas should however satisfy the constraint $N_t \leq N_r$ so that the matrix inversion remains possible. Assuming such a constraint is fulfilled, it is then straightforward to obtain the expression of the equalized signals:

$$\mathbf{z} = f\mathbf{x} + \boldsymbol{\mu} \tag{5.16}$$

where $\boldsymbol{\mu} = \mathbf{Wn}$. Let μ_i be the i-th component of the vector $\boldsymbol{\mu} \in \mathbb{C}^{N_t \times 1}$, and $w_{i,j}$ be the complex coefficient of matrix $\mathbf{W}$ in the i-th row and j-th column:

$$\mu_i = \sum_{j=1}^{N_r} w_{i,j}\eta_j. \tag{5.17}$$

To estimate the spatial symbols, the receiver should detect whether each transmit antenna is activated or not. From equation (5.16), the detector has to analyze the following set of signals:

$$\forall i, \quad z_i = \begin{cases} f + \mu_i & \text{if } T_i \text{ is activated} \\ \mu_i & \text{otherwise.} \end{cases} \tag{5.18}$$

Since the ZF spatial equalization scheme is used, no interference appears between signal samples impinging at each receive antenna. In addition, since all activated antenna combinations are possible with the ESSK scheme, no correlation exists between the receive equalized signals. Consequently, the demodulation process can be led through an independent and parallel signal analysis per symbol, thereby simplifying the application of the maximum likelihood decision criterion. This is a strong asset of ESSK compared to conventional SM or GSM.

Equalized ML detection

The Equalized ML (EQ-ML) detector should exhaustively search among all the possible equalized receive signatures for the one that gives the closest signal to the received one. Let us denote by $\mathbf{x}_k$ the kth out of $K = 2^{N_t}$ possible transmitted signal vectors with a given combination of its entries $x_i(k)$ equal to 1 and the rest being zeroed. The equation of the ML receiver can then be written as:

$$\hat{\mathbf{x}}_k = \text{Arg}\min_{\mathbf{x}_k} \sum_{i=1}^{N_t} \|z_i - f x_i(k)\|^2 \tag{5.19}$$

where $\|.\|^2$ denotes the euclidean norm. Owing to the parallel detection process discussed above, the EQ-ML detector can be rewritten as:

$$\forall i, \quad \hat{x}_i = \text{Arg}\min_{x_i=\{1,0\}} \|z_i - f x_i\|^2 \tag{5.20}$$

meaning that $\hat{x}_i$ is estimated separately at each element of vector $\mathbf{z}$ and is simply obtained choosing whether 1 or not has been transmitted. Hence, the EQ-ML detector at each element can be carried out by means of a simple threshold detector. Suppose that

the channel estimation for the ZF is perfect at the receiver. The equalized signal will then exhibit the same phase of the emitted signal due to the phase compensation effect of the ZF equalizer. Since the transmit symbol is real, the receiver can compare the real part obtained to a predefined amplitude threshold ν:

$$x_i = \begin{cases} 0, & \text{if } \Re\{z_i\} \leq \nu, \\ 1, & \text{if } \Re\{z_i\} \geq \nu, \end{cases} \tag{5.21}$$

where the optimal threshold is easily deduced from:

$$\nu = \mathbb{E}\left\{ \frac{\Re\{z_{i0}\} + \Re\{z_{i1}\}}{2} \right\} = \frac{f}{2} \tag{5.22}$$

with z_{i0} (resp. z_{i1}) the i-th element of equalized receive signal vector if the antenna T_i wasn't active (resp. active). Note that such a threshold can in practice be estimated during a calibration phase using dedicated pilot symbols.

Performance Analysis

Using such a threshold detector, the derivation of the theoretical BER can be led as follows. Recalling that the probability $\mathcal{P}(z_{i1})$ (resp. $\mathcal{P}(z_{i0})$) that one particular antenna T_i is active (resp. inactive) is $\frac{1}{2}$, we have:

$$\mathcal{P}_e(z_i) = \frac{1}{2}\mathcal{P}(z_{i0} \to z_{i1}) + \frac{1}{2}\mathcal{P}(z_{i1} \to z_{i0}). \tag{5.23}$$

Then, applying the threshold detection, we obtain:

$$\mathcal{P}_e(z_i) = \frac{1}{2} \times \left[\mathcal{P}\left(\nu \leq \Re\{\mu_i\}\right) + \mathcal{P}\left(\Re\{f + \mu_i\} \leq \nu\right) \right]. \tag{5.24}$$

Noise samples are centered circularly Gaussian of variance σ_n^2. After the equalization, the new equalized noise in equation (5.17) is still centered circularly Gaussian:

$$\mu_i \sim \mathcal{CN}(0, \|w_i\|^2 \sigma_n^2)$$

where w_i is the i-th row of th equalization matrix $\mathbf{W}$. We get:

$$\begin{aligned} \mathcal{P}_e(z_i) =& \mathcal{P}\left(\mathcal{N}\left(0, \sum_{j=1}^{N_r} w_{i,j}^2 \frac{\sigma_n^2}{2}\right) \geq \frac{f}{2} \right) \\ =& Q\left(\frac{f}{\sqrt{2}\,\|w_i\|\,\sigma_n} \right) \\ =& Q\left(\sqrt{\frac{1}{N_t\,\|w_i\|^2\,\sigma_n^2}} \right). \end{aligned} \tag{5.25}$$

Since all transmit antennas have the same probability of being activated or not, the expression of the BER is:

$$\mathcal{P}_e = \frac{1}{N_t} \sum_{i=1}^{N_t} Q\left(\sqrt{\frac{1}{N_t\,\|w_i\|^2\,\sigma_n^2}} \right). \tag{5.26}$$

5.5 Simulation Results

5.5.1 Simulation descriptions

The performance of the proposed system is evaluated through the measurement of the BER versus the SNR that is equal to the ratio between the average transmit power level and noise level, i.e. SNR=$\frac{\bar{P}_t}{\sigma_n^2}$. It is assumed that $\mathbf{H}$ is a MIMO flat fading channel matrix where $h_{j,i}$ are complex coefficients following an i.i.d. Rayleigh distribution. The power for each sub-channel is normalized:

$$E\left[\left\|h_{j,i}\right\|^2\right] = 1$$

Finally, we consider that the channel response is perfectly known at the receiver, so that perfect ZF equalization is performed. Simulations are run by implementing a sufficient number of iterations for different channel realizations, and taking the mean value of the BER for each value of SNR.

5.5.2 Theoretical Result Validation

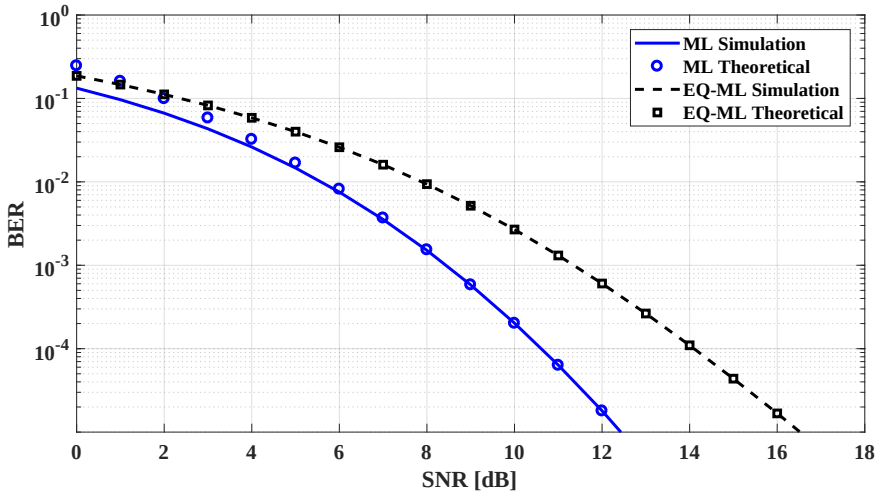

Figure 5.3 – BER performance of 4x8 ESSK system, using ML and EQ-ML detection, theoretical and simulation comparison

Analytical derivations of the BER are compared to the simulation results in Figure 5.3. An ESSK system with $N_r = 8$ receive antennas at the base station and $N_t = 4$ transmit antennas is considered. The performance is evaluated using the ML and EQ-ML detection. As evident from the obtained curves, theoretical results perfectly match simulation results. Also, it is seen that the ML without equalization outperforms the ML after equalization (EQ-ML).

5.5.3 ML vs EQ-ML performance

In Figure 5.4, we compare the performance of ML and EQ-ML detection considering different configurations for N_r, and for the same N_t=4. ESSK systems with N_r= 4, 8, 16

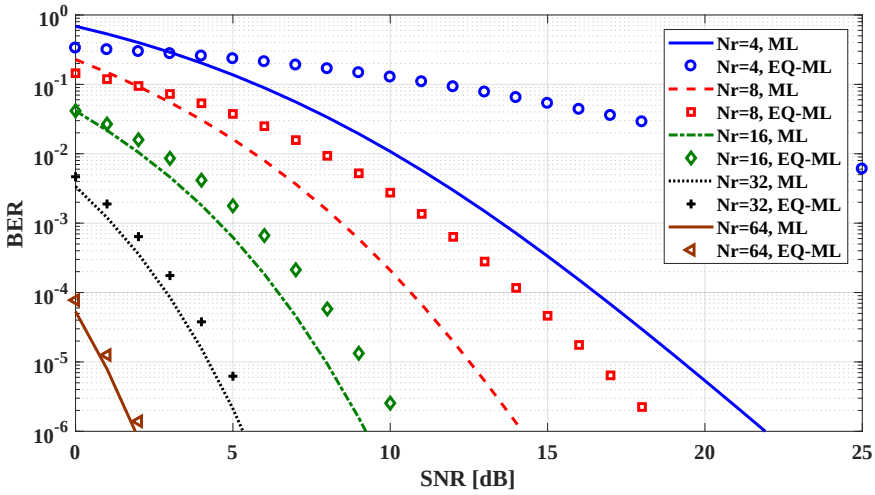

Figure 5.4 – BER performance of 2x8 ESSK system, using ML and EQ-ML detection, theoretical and simulation comparison

and 32 are simulated using the two detection methods. It is shown that ML detection outperforms the EQ-ML detection, but the more N_r increases, the more the difference in performance decreases, and they become approximately the same for $N_r = 32$.

5.5.4 Duality ESSK ERASK

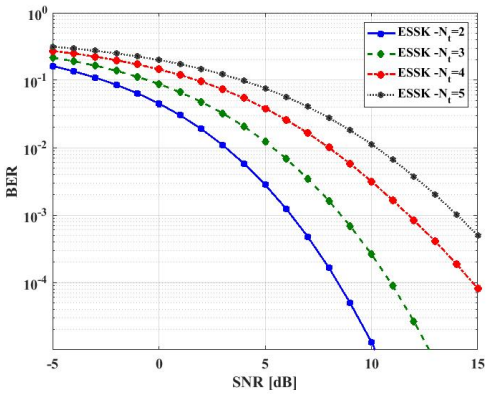

(a) ESSK performance using EQ-ML detection with $N_r = 8$ - Theoretical and simulation comparison

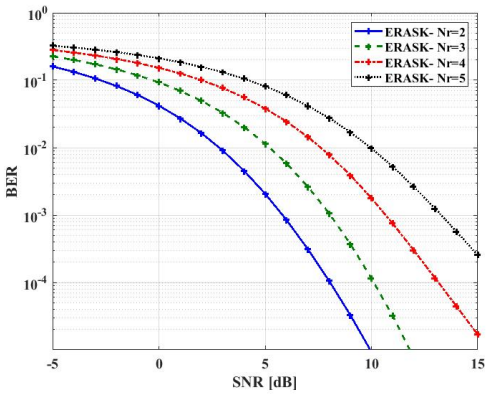

(b) ERASK performance using ML detection with $N_t = 8$ - Theoretical and simulation comparison

The uplink/ downlink duality in the MIMO wireless systems has been studied for different precoding- postcoding strategies [93]–[95]. Since the SM is a special kind of MIMO system, then a duality can be deduced between the transmit and receive SM.

In Figure 5.5a, we provide the simulation results considering an ESSK system with $N_r = 8$ receive antennas at the base station and 4 different transmit antenna array dimensions, namely $N_t = 2$, 3, 4 and 5 at the device. On the other hand, in Figure 5.5b,

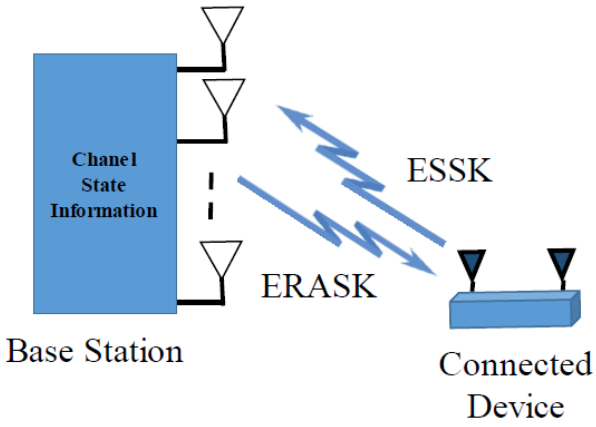

Figure 5.6 – Visualization of the transmission between Base Station and Connected Device

the simulation results considering an ERASK system with $N_t = 8$ transmit antennas at the base station and 4 different receive antenna array dimensions, namely $N_r = 2, 3, 4$ and 5 at the device. The two configurations seem to be the uplink and downlink transmission between the base station and a connected device. Note that for both scenarios, we are measuring the BER versus the SNR at the connected device. The performance is evaluated using the EQ-ML detection for ESSK and ML for ERASK. For both configurations, increasing the order of modulation, i.e. N_t for ESSK or N_r for ERASK, leads to a degradation in performance. Also, for the same order of modulation, we have approximately the same performance in the two transmissions, which proves the duality of transmission between ERASK and ESSK.

5.6 Uplink and Downlink Transmission System

	ERASK (Downlink)	ESSK (Uplink)
Base Station	ZF preprocessing (need CSI)	ZF equalization (need CSI)
Connected Device	Threshold detector	ON-OFF Keying

Table 5.1 – Operations needed at the base station and the connected device for Up-link and Down-link

Considering a transmission system between a base station and a connected device as shown in Fig. 5.6. The combination of the ERASK scheme for a Down-link transmission and the ESSK scheme for Up-link transmission provides a complete system that provides a low complexity processing at the connected device side, and a quite higher complexity at the base station side. Table 5.1 shows the main operations needed for the

Up-link and Down-link transmissions at the base station and connected device sides. It is shown that a Channel State Information (CSI) is needed at the base station for the ZF preprocessing and equalization, while a simple threshold detection and ON-OFF Keying emission is needed at the connected device. Moreover, the base station can be implemented with a high number of antennas so it can creates a good focalization beam for the downlink, and to better detect the received signal at the uplink transmission. Note that the preprocessing matrix and the equalization matrix could be deduced from the same estimation, as demonstrated in [67].

5.7 Summary

In this Chapter, the ESSK transmission scheme was presented and studied as an analog to the ERASK for the uplink transmission of a device connected to a Base Station. The concept of ESSK was presented, and we demonstrated how ESSK provides transmission of $m = N_t$ bits per spatial symbol duration, which is the number of receive antennas in downlink when ERASK is implemented. We also studied the ML detector, as well as the expected theoretical performance, and then the performance of the system when ZF equalization is performed. The ML detector outperforms the based equalizer detector, but results showed that the more the number of transmit antennas increases, the smaller the difference in performance is. Thus, we demonstrated the duality in performance between ERASK, and ESSK such that the based equalizer detector is implemented. Finally, an Uplink and Downlink transmission system between a base station and a connected device based on the extended SM has been proposed, and we showed how the computational complexity is reduced at the connected device.

Chapter 6

Hybrid Beamforming for Receive Antenna Shift Keying in mmWaves

Contents

6.1 Introduction

In this chapter, we present a novel framework considering the RASK technique with hybrid beamforming in a mmWave propagation environment. We describe the channel model, followed by the beamforming strategies, where a combination of analog beamforming and digital precoding is performed. The achievable SE is analytically and numerically studied. The BER performance of the framework is analytically and numerically studied with a maximum likelihood detector. All the theoretical and numerical analyses are done for the pure LoS channel environment and sparse multi-path channels in order to fully characterize high-frequency environments such as mmWave systems. The work in this chapter has been done in collaboration with my colleague Dr. Mohammad Shehata.

6.2 Background

In order to support the tremendous number of devices and sensors that will become connected to the internet, a framework needs to be established that can achieve low complexity, high EE and SE, and large Band Width for extended coverage. Massive MIMO [96] can be a good candidate to provides a transmission with high SE [97] through SDMA enabled by digital precoding algorithms. However, scaling up massive MIMO with digital precoding suffers from hardware problems. The large array size, the power consumption and the hardware complexity required (one RF chain is needed per antenna element) are the main limiting factors [98].

In order to unleash the massive MIMO gains and cope with the limitations, the mmWave systems [99]–[101] evolved as a key enabler. In mmWave systems, the massive MIMO arrays can be deployed with acceptable form factors due to the small wavelength. Moreover, hybrid beamforming [102] is also an important enabler for practical implementation of massive MIMO at mmWave systems. In order to achieve the SE gains of massive MIMO systems a dedicated RF chain and a mixed analog-digital device are needed per antenna, which is practically unfeasible at mmWave systems due to hardware and power consumption limitations [98]. Moreover, hybrid beamforming enables practical implementation of massive MIMO at mmWave systems by allowing to employ less RF chains and mixed analog-digital devices compared to the number of antennas, thus allowing for a trade-off between the hardware complexity and the achievable SE [103]. Moreover, it is shown that hybrid beamforming can achieve close SE performance compared to the more complex fully digital precoding system in mmWave systems given the fact that the mmWave channel is sparse. Thus, hybrid beamforming can fully capture the limited dimension of the channel using a small number of RF chains, while achieving the massive transmit antenna array gains [104].

Thus, due to all the aforementioned characteristics of RASK, it can be understood that combining RASK with hybrid beamforming in mmWave systems can reveal to be a win-win approach. Given the fact that mmWave systems suffer from high power consumption, high hardware cost and sensitivity to complex computations, RASK is crucial for mmWave mobile receivers in the downlink scenario in order to achieve high SE with low BER and low energy consumption/hardware complexity. Henceforth, providing a solution for practical mmWave based Mobile Terminals (MTs) at low cost

and low power consumption is provided.

Recently, a lot of work started to consider a framework combining both SM and mmWaves for the aforementioned reasons [105]–[113]. The work in [106] is considered a valuable baseline in which the performance of the SM in mmWave scenario was studied in a special deployment scenario in which no interference exists between the spatial streams targeting different receive antennas. Thus, only analog beamforming is utilized. These results are considered impractical and incomplete, since, in realistic deployments, this interference nulling assumption is not valid. In this chapter, we extend the work presented in [106] to be more complete and cover all possible deployment scenarios, and we extend the analog beamforming to be a hybrid one, in order to consider a possible mitigation of the interference between the spatial streams in practical deployments.

6.3 System and Channel Model

In this part, we first set up the model for a communication system utilizing the RASK scheme in a flat fading channel. Then, we introduce the pre-processing scheme carried out to form the spatial focusing symbols, together with introducing the channel model and the beamforming architectures used within our framework.

6.3.1 System Model Description for mmWaves RASK

In our framework, we consider the same system model presented in chapter 3, but this time the transmitter have an additional analog beamformer to be used in the hybrid beamforming. The input-output signal expression is:

$$\mathbf{y} = \mathbf{H} \underbrace{f\mathbf{P}\mathbf{x}}_{\mathbf{s}} + \mathbf{n}, \tag{6.1}$$

where $\mathbf{P} \in \mathbb{C}^{N_t \times N_r}$ is the hybrid beamformer (instead of the digital beamformer $\mathbf{W}$) used for the spatial focusing.

The block diagram of the RASK system with hybrid beamforming is depicted in Figure 6.1. The transmission principle and the spatial mapping presented in chapter 3 remain the same. The only difference is that the transmitter now is occupied with analog and digital part to form a beamformer that is based on hybrid beamforming architecture. The hybrid beamformer is represented as: $\mathbf{P} = \mathbf{F}_{RF}\mathbf{W}$, where $\mathbf{W} \in \mathbb{C}^{L_t \times N_r}$ represents the digital precoder and $\mathbf{F}_{RF} \in \mathbb{C}^{N_t \times L_t}$ denotes the analog beamformer, given that L_t represents the number of available RF chains at the transmitter, and the number of the spatial streams to be supported equals N_r. Thus, the expression of the normalization factor used to maintain the average transmit power at one, which is also ensured for the average transmit power for fairness of detection for RASK, writes:

$$f = \frac{1}{\sqrt{\mathbb{E}_x \left\{ \mathrm{Tr}\left((\mathbf{P}\mathbf{x})^H \mathbf{P}\mathbf{x} \right) \right\}}}. \tag{6.2}$$

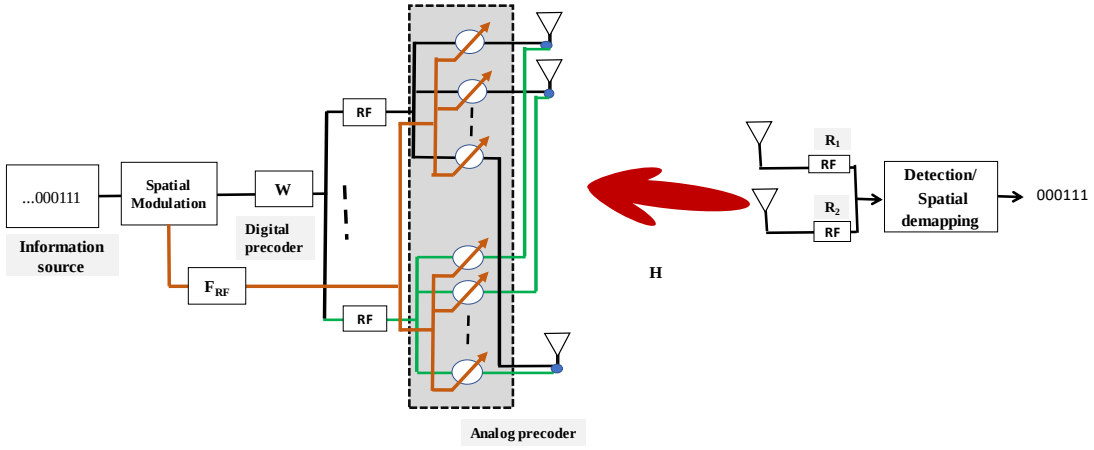

Figure 6.1 – Block diagram of RASK with mmWave hybrid beamforming architecture

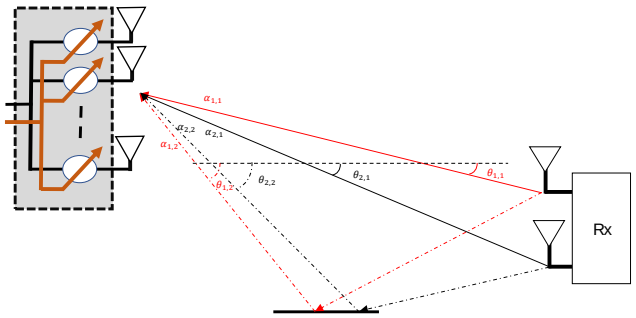

Figure 6.2 – Channel illustration based on geometric model

6.3.2 Channel Model

In order to accurately describe the channel model used throughout our work, we provide two cases, between which the realistic mmWave channel scenario is bounded. These two bounds are: the pure LoS propagation scenario [114] and the sparse multipath scattering scenario [115]. It is well known that in mmWave bands, the signal suffers from severe pathloss, limited scattering [116], limited diffraction effects [117] and high blockage probability [118] because of the small wavelengths at such frequencies. Henceforth, the mmWave channel is known to be sparse [119], [120]. Thus, the geometric channel model adopted in this chapter for the RASK scheme is illustrated in Figure 6.2 can be generically expressed as:

$$\mathbf{h}_k = \sqrt{\frac{N_t}{I_k}} \sum_{p=1}^{I_k} \alpha_{k,p} \mathbf{a}_t^H(\theta_{k,p}) \tag{6.3}$$

where $\alpha_{k,p}$ is the complex amplitude of propagation path p which is one of the received I_k paths by receive antenna R_k with the path loss effect, such that $\mathbb{E}[|\alpha_{k,p}|^2] = \hat{\alpha}$ in case of sparse multi-path scenario. Otherwise, in the pure LoS scenario, $I_k = 1$ and $\alpha_{k,p}$ is normalized ($\alpha_{k,p} = 1$). $\theta_{k,p}$ represents the Angle of Departure (AoD) for path p of R_k, such that $\theta_{k,p} \in [0, 2\pi]$. Moreover, $\mathbf{a}_t(\theta_{k,p})$ denotes the transmit array steering vector which depends on the array geometry. Throughout the chapter, we utilize the Uniform Linear Array (ULA) transmit array. Thus, $\mathbf{a}_t(\theta_{k,p})$ is expressed as:

$$\mathbf{a}_t(\theta_{k,p}) = \frac{1}{\sqrt{N_t}}[1, e^{j\frac{2\pi}{\lambda^w} d_t \cos(\theta_{k,p})}, ..., e^{j(N_t-1)\frac{2\pi}{\lambda^w} d_t \cos(\theta_{k,p})}]^T \tag{6.4}$$

where λ^w is the wavelength of the signal and d_t is the inter-element antenna spacing at the transmitter. Thus, the MIMO channel $\mathbf{H} \in \mathbb{C}^{N_r \times N_t}$ can be expressed as

$$\mathbf{H} = [\mathbf{h}_1^T, \mathbf{h}_2^T, ..., \mathbf{h}_{N_r}^T]^T. \tag{6.5}$$

6.4 Beamforming Strategies

In this section, the hybrid beamforming strategy adopted in the chapter is explained in details. Two analog beamformers are proposed for the two-channel environments proposed (pure LoS / sparse multi-path). These analog beamformers will be augmented with ZF digital precoder for the RASK implementation.

6.4.1 Analog LoS path Beamsteering

This approach is the most classic analog beamforming, specifically for LoS dominant environments such as mmWave environments [120]. In this approach the analog beam is steered towards the channel path with the highest power (LoS path or the best non LoS path in case no LoS path exists). The LoS beamsteering represents the solution of the SNR maximum eigenvalue maximization problem given the phased array constant amplitude constraint:

$$\begin{aligned} \mathbf{f}_{LoS} = \underset{\mathbf{f}}{\operatorname{argmax}}\, \lambda_{max} & \left\{ \sum_{p=1}^{P} |\alpha_p|^2 \mathbf{a}_t(\theta_p)^H \mathbf{f}\mathbf{f}^H \mathbf{a}_t(\theta_p) \right\} \\ \text{s.t. } & \|\mathbf{f}\| = 1. \end{aligned} \tag{6.6}$$

Thus, the maximum eigenvalue λ_{max} is allocated to the dominant path, which is considered as the LoS path. So, to maximize the SNR of the maximum eigenvalue, the beamformer apply the conjugate beamforming concept only to the LoS path. In result, only the knowledge of the LoS AoD $\theta_{k,p_{LoS}}$ is required for calculating the LoS beamformer as follows:

$$\mathbf{f}_{LoS} = \mathbf{a}_t(\theta_{p_{LoS}}). \tag{6.7}$$

Since the beamformer is normalized, it is sufficient to steer the transmit signal toward the angle of the LoS path to apply the LoS beamsteering.

6.4.2 Analog Equal Gain Transmission

In case the mmWave channel is a multi-path one and not pure LoS, utilizing LoS beamsteering is inefficient. This is due to the fact that it fails to capture the energy gains offered by the multiple paths of the channel. Thus, in this case EGT [121] [122] is a more efficient analog beamforming technique. In EGT the analog beamforming problem is formulated as:

$$\begin{aligned} \mathbf{f}_{EGT} = \underset{\mathbf{f}}{\text{argmax}} \sum_{p=1}^{P} |\alpha_p|^2 \mathbf{a}_t(\theta_p)^H \mathbf{f}\mathbf{f}^H \mathbf{a}_t(\theta_p) \\ \text{s.t. } \|\mathbf{f}\| = 1. \end{aligned} \tag{6.8}$$

Henceforth, the SNR maximization problem is not limited to the maximum eigenvalue only as in LoS beamsteering. The solution to this problem is the traditional MRT precoder. However, the constant gain constraint is taken into account in equation (6.8) to consider realistic hardware limitations forced by the analog phased array RF networks. Thus, in this case, the closed form solution is the EGT technique [121], and the EGT beamformer is calculated as follows:

$$\mathbf{f}_{EGT} = \frac{e^{j\angle \mathbf{h}^H}}{\sqrt{N_t}}. \tag{6.9}$$

Thus, EGT gives a closed form non-iterative solution that maximizes the SNR, together with distributing the energy efficiently on the propagation paths with considering constructively adding them up.

6.4.3 Hybrid Beamforming

Here the hybrid beamforming architecture is introduced in order to extend the previously proposed analog beamforming algorithms for better performance of RASK. Throughout the chapter, the RF and BB architectures are decoupled as in [120]. Then the equivalent channel $\mathbf{h}^e$ for each receive antenna index R_k, is formed before the digital processing layer as follows:

$$\mathbf{h^e}_k = \mathbf{h}_k \mathbf{F}_{RF}, \tag{6.10}$$

such that, $\mathbf{h}_k \in \mathbb{C}^{1\times N_t}$, $\mathbf{h^e}_k \in \mathbb{C}^{1\times L_t}$ and $\mathbf{F}_{RF} \in \mathbb{C}^{N_t \times L_t}$ represents the analog beamforming matrix and is computed as:

$$\mathbf{F}_{RF} = [\mathbf{f}_{RF,1}, ..., \mathbf{f}_{RF,k}] \tag{6.11}$$

such that $\mathbf{f}_{RF,k}$ is the analog beamforming vector for R_k which can be chosen from $\{\mathbf{f}_{LoS,k}, \mathbf{f}_{EGT,k}\}$.

Then the total equivalent channel $\mathbf{H}_e$ for the N_r receive antennas is represented as:

$$\mathbf{H}_e = \mathbf{H}\mathbf{F}_{RF} = [\mathbf{h}^{eT}_1, ..., \mathbf{h}^{eT}_{N_r}]. \tag{6.12}$$

Finally, we utilize the ZF digital precoding to suppress the inter-antenna element interference. Hence, the digital beamformer is calculated as follows:

$$\mathbf{W} = {\mathbf{H}_e}^H(\mathbf{H}_e{\mathbf{H}_e}^H)^{-1}. \tag{6.13}$$

As a result, the hybrid beamformer $\mathbf{P}$ is calculated as: $\mathbf{P} = \mathbf{F}_{RF}\mathbf{W}$.
At the receiver, the equation (6.1) can be expressed as:

$$\mathbf{y} = f\mathbf{x} + \mathbf{n}. \tag{6.14}$$

6.5 Pure LoS and Sparse Multi-Path Scenarios

In this part, we are providing the performance analysis of the RASK scheme with hybrid beamforming in a pure LoS and sparse multi-path scenarios.

6.5.1 Normalization Factor evaluation

The normalization factor for the two receive antennas f^2 can be represented from equation (6.2) as follows:

$$f = \frac{1}{\sqrt{\mathbb{E}\left\{\mathrm{Tr}\left(\left(\mathbf{F}_{RF}\mathbf{W}\right)^H\mathbf{F}_{RF}\mathbf{W}\right)\right\}}} \tag{6.15}$$

given that the SVD of the equivalent channel $\mathbf{H}_e$ is $\mathbf{H}_e = \mathbf{U}_e\mathbf{\Lambda}_e^{\frac{1}{2}}\mathbf{V}_e^H$, and for ther digital precoder is $\mathbf{W} = \mathbf{V}_e\mathbf{\Lambda}_e^{\frac{-1}{2}}\mathbf{U}_e^H$. Henceforth:

$$\mathbb{E}\{\mathrm{Tr}\left(\left(\mathbf{F}_{RF}\mathbf{W}\right)^H\mathbf{F}_{RF}\mathbf{W}\right)\} = \mathbb{E}\{Tr(\mathbf{F}_{RF}^H\mathbf{F}_{RF}\mathbf{\Lambda}_e^{-1})\} \tag{6.16}$$

For Pure LoS scenario

In this scenario, a deterministic LoS path between the transmitter and each receive antenna R_k is considered. For this specific scenario, where the LoS beamsteering and EGT beamforming are the same, only the phase of the received signal is affected between different antenna, and the pathloss is considered to be equal for all receive antennas. So, the RF beamforming matrix in this specific case is $\mathbf{F}_{RF} = \frac{\mathbf{H}^H}{\sqrt{N_t}}$. Given the fact that the SVD of the propagation channel $\mathbf{H}$ is $\mathbf{H} = \mathbf{U}\mathbf{\Lambda}^{\frac{1}{2}}\mathbf{V}^H$, thus,

$$\begin{aligned}\mathbb{E}\{Tr(\mathbf{F}_{RF}^H\mathbf{F}_{RF}\mathbf{\Lambda}_e^{-1}) &= \mathbb{E}\{Tr(\frac{1}{N_t}\mathbf{H}\mathbf{H}^H\mathbf{\Lambda}_e^{-1})\}\\ &= \mathbb{E}\{Tr(\frac{1}{N_t}\mathbf{\Lambda}\mathbf{\Lambda}_e^{-1})\}\\ &= \frac{\sum_{i=1}^{N_r}\frac{\lambda_i^{\mathbf{H}}}{\lambda_i^{\mathbf{H}_e}}}{N_t}.\end{aligned} \tag{6.17}$$

where $\lambda_i^{\mathbf{H}}$ and $\lambda_i^{\mathbf{H}_e}$ represent the ith eigen-value of the propagation channel $\mathbf{H}$ and the the ith eigen-value of the equivalent channel $\mathbf{H}_e$ respectively. Then from this result, the normalization factor in equation (6.15) for a pure LoS scenario is calculated as follows:

$$f = \sqrt{\frac{N_t}{\sum_{i=1}^{N_r} \frac{\lambda_i^{\mathbf{H}}}{\lambda_i^{\mathbf{H}_e}}}}. \tag{6.18}$$

For Sparse multi-path scenario

In this scenario, the EGT concept is used for the analog beamforming, where $\mathbf{f}_k$ is designed to extract the phases of the sub-channel $\mathbf{h}_k$. In order to evaluate f, we will take the derivations used to calculate the capacity in [115], in order to evaluate the equivalent channel resulted from the analog beamforming $\mathbf{H}_e$. At the diagonal, we have:

$$\mathbf{h}_{k,k}^e = \mathbf{h}_k^H \mathbf{f}_k = \frac{1}{\sqrt{N_t}} \sum_{i=1}^{N_t} |h_{i,k}| \tag{6.19}$$

where $h_{i,k}$ is the ith element of vector $\mathbf{h}_k$. In a sparce rich scattering channel, the elements of $\mathbf{h}_k$ are considered as i.i.d complex gaussian random variables with $h \sim \mathcal{N}(0,1)$, and so $|h|$ follows Rayleigh distribution with mean $\frac{\sqrt{\pi}}{2}$ and variance 1-$\frac{\pi}{4}$. Thus, the central limite theorem indicates that when N_t tends to infinity, we have:

$$\mathbf{h}_{k,k}^e \sim \mathcal{N}(\frac{\sqrt{\pi N_t}}{2}, 1 - \frac{\pi}{4}). \tag{6.20}$$

Moreover, for the off-diagonale terms, i.e. $j \neq k$, we have:

$$\mathbf{h}_{k,j}^e = \mathbf{h}_k^H \mathbf{f}_j = \frac{1}{\sqrt{N_t}} \sum_{i=1}^{N_t} h_{i,k}^* e^{-\phi_{i,j}} \tag{6.21}$$

where $e^{\phi_{i,j}}$ is the phase of the ith element of channel $\mathbf{h}_j$. It has been prooved in Lemma 1 in [115] that the off-diagonal are distributed according to:

$$\mathbf{h}_{k,j}^e \sim \mathcal{CN}(0,1). \tag{6.22}$$

Thus, $|\mathbf{h}_{k,j}^e|$ follows the Rayleigh distribution with mean $\frac{\sqrt{\pi}}{2}$ and variance 1-$\frac{\pi}{4}$, which is negligible compared to the diagonal terms for high N_t. Which mean that the interference between antennas is negligible even without digital preprocessing for high N_t. In this case, the value of f becomes approximately equal to the mean of diagonal term:

$$f = \frac{\sqrt{\pi N_t}}{2}. \tag{6.23}$$

6.5.2 Capacity Analysis

In this chapter we consider the RASK scheme as introduced in chapter 3. Thus, only one receive antenna is targeted per time symbol, and so the system is considered as a MISO system with interference arising from the correlation between the streams. Henceforth, the SE of the channel, that is equal to the capacity, using the hybrid beamforming and RASK is represented as:

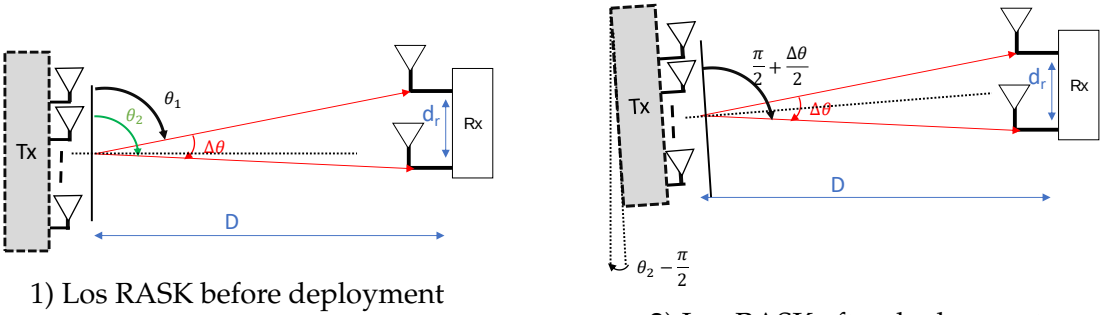

1) Los RASK before deployment optimization

2) Los RASK after deployment optimization

Figure 6.3 – Illustration of the correlation minimization approach adopted for the RASK mmWave framework for two paths

$$\mathcal{C} = \frac{1}{N_r}\log_2\left(\det\left[\mathbf{I}_{N_r} + \rho f^2 \mathbf{H}\mathbf{P}\mathbf{P}^H\mathbf{H}^H\right]\right) \tag{6.24}$$

where ρ represents the received SNR.

In case ZF is used as a digital precoder $\mathbf{W} = \mathbf{H}_e^H(\mathbf{H}_e\mathbf{H}_e^H)^{-1}$, then $\mathbf{H}\mathbf{P} = \mathbf{I}_{N_r}$ and the SE can be represented as:

$$\mathcal{C} = \frac{1}{N_r}\log_2\left(\det\left[\mathbf{I}_{N_r}(1+\rho f^2)\right]\right). \tag{6.25}$$

In the following, our aim is to provide closed form analytic solutions for the SE of the RASK system with hybrid beamforming considering two scenarios: pure LoS scenario and sparse multi-path scenario. As aforementioned, these two scenarios provide boundaries for the performance of realistic mmWave communication systems.

Pure LoS scenario, $N_r = 2$

In this scenario, a deterministic LoS path between the transmitter and each receive antenna R_k is considered. As we mainly focus on small and low complexity IoT devices, the case in which the receiver is equipped with two antennas only ($N_r = 2$) is considered. Thus, in this case two deterministic LoS paths exist between the transmitter and the receiver. The transmit spatial correlation between the two paths is given as follows:

$$\begin{aligned}\bar{\Lambda} &= \left|\mathbf{a}_t^H(\theta_1)\mathbf{a}_t(\theta_2)\right| = \left|\mathbf{a}_t^H(\theta_1)\mathbf{a}_t(\theta_1+\Delta\theta)\right| \\ &= \left|\sum_{i=0}^{N_t-1}\frac{1}{N_t}e^{-j2\pi d_t i(\cos(\theta_1+\Delta\theta)-\cos\theta_1)}\right| \\ &= \left|\frac{\sin(\pi N_t d_t(\cos(\theta_1+\Delta\theta)-\cos\theta_1))}{N_t\sin(\pi d_t(\cos(\theta_1+\Delta\theta)-\cos\theta_1))}\right|.\end{aligned} \tag{6.26}$$

Moreover, it is clear that in this scenario the transmit spatial correlation depends on two parameters, which are the angle of the first path θ_1 and the angular difference

between the two paths $\Delta\theta$. θ_1 is a uniformly distributed random variable such that $\theta_1 \in [0, 2\pi]$ as defined in Section 6.3.2. $\Delta\theta$ is a deterministic value that represents the angular difference between the path arriving at the first receive antenna and the path arriving at the second one as shown in Figure 6.3, and is calculated as follows:

$$\Delta\theta = 2\arcsin(\frac{d_r}{2D}) \tag{6.27}$$

given that d_r is the receive antenna inter-element spacing, and D is the distance between the transmitter and the receiver. In [123], it is shown that the transmit spatial correlation between two paths can be minimized to its lower bound represented as:

$$\bar{\Lambda}_{min} = \begin{cases} 0, & \Delta\theta \geq 2\arcsin(\frac{1}{2N_t d_t}), \\ \left|\frac{\sin(2\pi N_t d_t \sin\frac{\Delta\theta}{2})}{N_t \sin(2\pi d_t \sin\frac{\Delta\theta}{2})}\right|, & \Delta\theta < 2\arcsin(\frac{1}{2N_t d_t}). \end{cases} \tag{6.28}$$

This can be achieved by tilting the antenna array to optimize the deployment of the transmitter in order to minimize the transmit spatial correlation as in [123] (Figure 6.3). The optimum transmit ULA array orientation angle δ for minimizing the transmit spatial correlation in this case after deployment optimization is defined as:

$$\delta = \begin{cases} \arcsin(\frac{p}{2N_t d_t sin\frac{\Delta\theta}{2}}) + \frac{\Delta\theta}{2}, & \Delta\theta \geq 2\arcsin(\frac{1}{2N_t d_t}), \\ \frac{\pi}{2} + \frac{\Delta\theta}{2}, & \Delta\theta < 2\arcsin(\frac{1}{2N_t d_t}), \end{cases} \tag{6.29}$$

such that p is given as:

$$p = 1, 2, .., \left\lfloor 2N_t d_t \sin\frac{\Delta\theta}{2} \right\rfloor, \mathrm{mod}(p, N_t) \neq 0. \tag{6.30}$$

Thus, as shown in equations (6.28) and (6.29), three specific cases exist to be tackled by our framework, which defines our contribution over the existing work in the literature that deals with the SM issues in mmWave systems [106]. The three specific cases are:

- $\Delta\theta = 2\arcsin(\frac{1}{2N_t d_t})$: This is the optimum scenario, in which the transmit spatial correlation $\bar{\Lambda} = 0$ as shown in [106]. In this case, analog beamforming is enough for RSM and no ZF is needed, as the interference/leakage between the antennas doesn't exist. However, this is a very specific case and it is not a realistic assumption for RSM mmWave systems. Henceforth, we provide a solution for the other two cases to introduce a practical RASK framework in mmWave frequencies.

- $\Delta\theta > 2\arcsin(\frac{1}{2N_t d_t})$: In this case, using equation (6.29), the transmit spatial correlation can be nulled by optimizing the deployment of the transmit array, such that $\delta = \arcsin(\frac{p}{2N_t d_t sin\frac{\Delta\theta}{2}}) + \frac{\Delta\theta}{2}$. In this case, again ZF isn't required, since the transmit array deployment optimization is enough to null the interference/leakage

between the antennas. However, this case isn't realistic/favorable in mmWave systems, due to the fact that $\Delta\theta$ has very small values $\Delta\theta \approx 0$ and thus, this condition can only be satisfied by utilizing a massive number of transmit antennas. Henceforth, we move to discuss the third case, which is the most practical one, in more details.

- $\Delta\theta < 2\arcsin(\frac{1}{2N_t d_t})$: This is the most practical and realistic scenario for mmWave RASK systems. In such case, the transmit array deployment optimization provided in equation (6.29) is no longer able to nullify the transmit spatial correlation, but it can minimize it to its lower bound. Thus, hybrid beamforming is required in this case in order to apply ZF in the digital part to nullify the interference between the receive antennas. The transmit array deployment optimization step maximizes the SE achieved by the hybrid beamforming since it minimizes the correlation, and hence ZF can be applied efficiently.

In the rest of the subsection, we will focus on the last scenario, given the fact that it is the most practical and realistic one. Moreover, it is the only scenario that needs hybrid beamforming, while in the other two scenarios analog beamforming is enough.

Now we will provide closed-form analytical models for calculating the SE for RASK in mmWave channels utilizing the hybrid beamforming strategy with LoS beamsteering in the analog domain with ZF in the digital domain.

Driven by the following characteristics of the eigen-values of the channel $\mathbf{H}$ in case of pure LoS environment and $N_r = 2$:

$$\lambda_1^{\mathbf{H}} + \lambda_2^{\mathbf{H}} = N_t N_r = 2N_t \tag{6.31}$$

$$\lambda_1^{\mathbf{H}} \lambda_2^{\mathbf{H}} = (1 - \bar{\Lambda}^2) {N_t}^2 \tag{6.32}$$

where the addition property in equation (6.31) is illustrated in [106] and the multiplication property equation (6.32) is illustrated in [123]. Then, solving equations (6.31) and 6.32 simultaneously, the channel $\mathbf{H}$ eigen-values are calculated as follows:

$$\lambda_1^{\mathbf{H}} = (1 - \bar{\Lambda}) N_t \text{ and } \lambda_2^{\mathbf{H}} = (1 + \bar{\Lambda}) N_t. \tag{6.33}$$

Again, utilizing the fact that the analog beamformer (LoS Beamsteering) in this case (LoS scenario) can be represented as $\mathbf{F}_{RF} = \frac{\mathbf{H}^H}{\sqrt{N_t}}$, thus, the eigen-values of the equivalent channel $\mathbf{H}_e = \mathbf{H}\mathbf{F}_{RF}$ can be related using equations (6.31) and (6.32) in case $N_r = 2$ as follows:

$$\sqrt{\lambda_1^{\mathbf{H}_e}} + \sqrt{\lambda_2^{\mathbf{H}_e}} = \sqrt{N_t} N_r = 2\sqrt{N_t} \tag{6.34}$$

$$\sqrt{\lambda_1^{\mathbf{H}_e} \lambda_2^{\mathbf{H}_e}} = (1 - \bar{\Lambda}^2) N_t. \tag{6.35}$$

Henceforth, solving equations (6.34) and (6.35) simultaneously, the eigen-values of the equivalent channel $\mathbf{H}_e$ can be obtained as follows:

$$\lambda_1^{\mathbf{H}_e} = (1 - \bar{\Lambda})^2 N_t \text{ and } \lambda_2^{\mathbf{H}_e} = (1 + \bar{\Lambda})^2 N_t. \tag{6.36}$$

Moreover, using the expressions of eigenvalues of the propagation channel and the equivalent channel in equations (6.33) and (6.36), the expression of the normalization factor in equation 6.18 becomes:

$$f = \sqrt{N_t(1-\bar{\Lambda})}. \tag{6.37}$$

And as a result, the expression of the SE in equation (6.25) can be expressed as:

$$\mathcal{C} = \log_2\left(1+\rho(1-\bar{\Lambda}^2)N_t\right). \tag{6.38}$$

Pure LoS scenario, $N_r > 2$

In this part, we extend the step of deployement optimization to include more than two antennas by introducing multi-receive antenna and multi-user scenarios as shown in Figure(6.4). From equation (6.29), it is shown that when $\Delta\theta > 2\arcsin(\frac{1}{2N_t d_t})$, the optimal transmit ULA array orientation δ in this case is to be oriented towards the center point of the receive array which is achieved by $\delta = \frac{\pi}{2} + \frac{\Delta\theta}{2}$. We show that this can be extended to multiple receive antennas scenarios, where the optimal orientation is pointing to the center of the receive array also. In Figure (6.4 - 1) we utilize the transmit orientation $\delta = \frac{\pi}{2} + \frac{\Delta\theta}{2}$ from equation (6.29) to solve the correlation minimization problem for each two rays separately resulting in the two green rays in Figure (6.4). Then, as a second recursive step, we again use the orientation optimizing rule $\delta = \frac{\pi}{2} + \frac{\Delta\theta}{2}$ for the two green rays, resulting in the blue ray which points at the center of the receive array. This methodology can be extended to any number of receive antennas. We validate our extension for the optimal transmit ULA orientation for multiple paths using simulation results as shown in Figure 6.7 which will be discussed in more details later.

Sparse multi-path scenario

The SE for hybrid beamforming in sparse multi-path environment (RF: EGT - Digital: ZF) is derived in [115]. It can be modified for RASK based systems, by taking the expression of the normalization factor in equation 6.23 to be used in the equation 6.25, and finally the expression of the SE writes:

$$\mathcal{C} = \log_2(1+\frac{\pi}{4}\rho N_t). \tag{6.39}$$

6.5.3 Analytic BER Performance

From equation (6.14), a given detector has to analyze the following set of signals:

$$\forall j, \quad y_j = \begin{cases} f+\eta_j & \text{if } R_j \text{ is the targeted antenna} \\ \eta_j & \text{otherwise} \end{cases} \tag{6.40}$$

Using the ML detection, referring to [10], the BER performance of the RASK scheme conditioned by $\mathbf{H}$ is approximated by:

$$\text{BER}|\mathbf{H} \approx \frac{N_r}{2} Q\left(f/2\sigma_n\right). \tag{6.41}$$

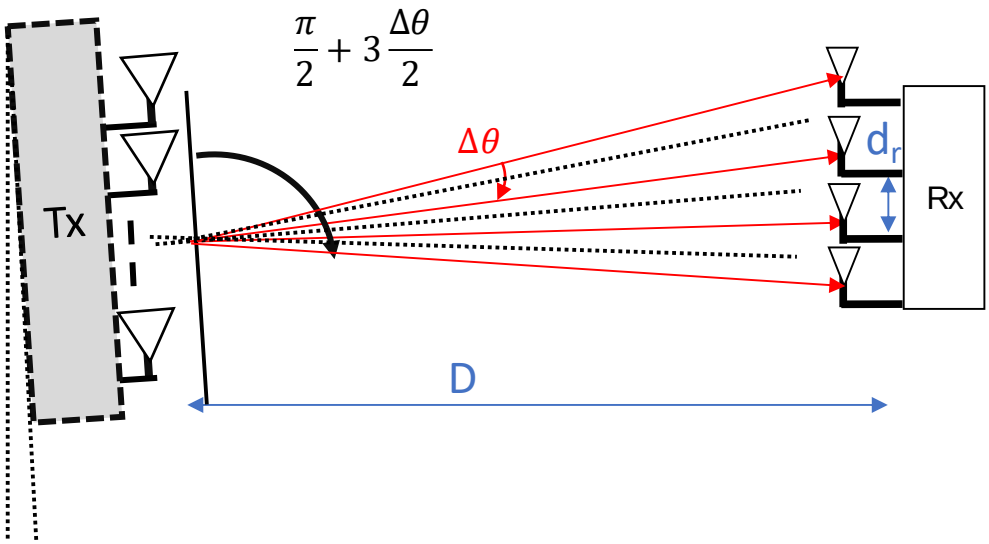

Figure 6.4 – Illustration of the correlation minimization approach adopted for the RASK mmWave framework for multiple receive antennas

In LoS scenario, with optimized deployment of the transmitter to the optimal position as aforementioned for transmit correlation minimization, given a fixed $\Delta\theta$, the channel could be considered as deterministic, and so the conditioned BER is equal to the average BER. Using the expression of the normalization factor in equation (6.37), for two receive antennas ($N_r = 2$), the ABER can be expressed as:

$$\text{ABER}|\mathbf{H}_{LoS} = \frac{N_r}{2} Q\left(\frac{\sqrt{N_t(1-\bar{\Lambda}^2)}}{2\sigma_n}\right). \tag{6.42}$$

For sparse multi-path scenario, also using the expression of the scaling factor in equation 6.23, the ABER of this scenario can be represented as:

$$\text{ABER} \mid \mathbf{H}_{sparce} \approx \frac{N_r}{2} Q\left(\frac{\sqrt{\pi N_t}}{4\sigma_n}\right). \tag{6.43}$$

6.5.4 Simulation Results

In this part, the performance of the introduced hybrid beamforming RASK framework is evaluated in details given the simulation parameters summarized in Table (6.1). Perfect channel estimation is assumed at the transmitter and the receiver sides.

In Figure (6.5), the simulation results show that the optimum orientation of the transmit array is achieved when $\delta = \frac{\pi}{2} + \frac{\Delta\theta}{2}$ in case $\Delta\theta < 2\arcsin(\frac{1}{2N_t d_t})$ as shown in equation (6.29) and proved mathematically in [123] for different numbers of transmit antennas N_t. Similarly in Figure (6.6), equation (6.29) is validated by simulations for

Table 6.1 – Simulation Parameters

Parameter	Value
Channel Model	Sparse Statistical Model [119]
Simulation Type	Monte Carlo (100000 realizations)
Tx Array Architecture	ULA
Tx Inter-antenna spacing	$\lambda/2$
Number of Tx/Rx RF Chains	2

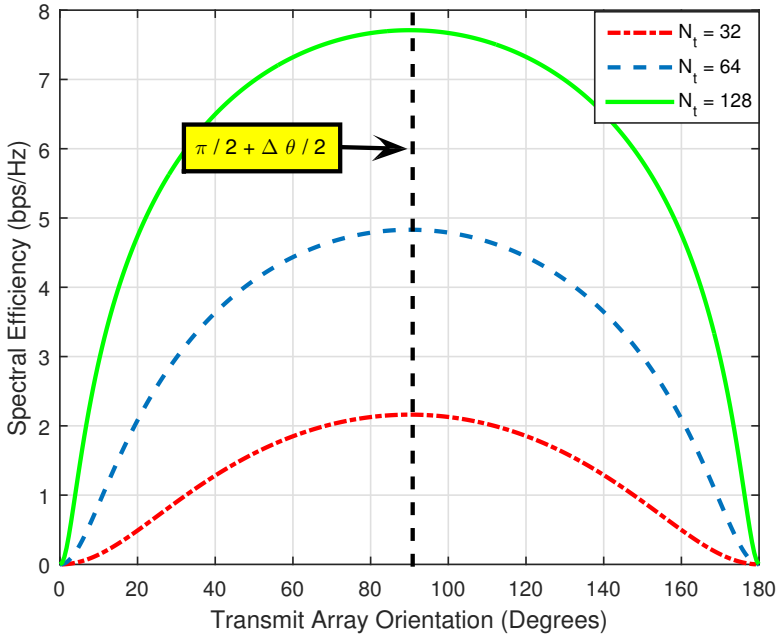

Figure 6.5 – SE versus the ULA transmit array orientation for a given scenario ($N_r = 2, \text{SNR} = 10\text{dB}, d_r = 18\lambda, D = 5000\lambda$) in pure LoS environment

different values of the receiver inter-antenna element spacing d_r. Moreover, in Figure 6.7, it shown that the extension introduced in this paper, compared to [123] that considered only 2 paths, for the transmit ULA array deployment optimization is validated. In this scenario the $\Delta\theta$ is calculated according to equation (6.27) as follows:

$$\Delta\theta = 2\arcsin(\frac{d_r}{2D}) = 2\arcsin(\frac{25\lambda}{1000\lambda}) = 2.8651^{\circ}. \tag{6.44}$$

Henceforth, according to our aforementioned analysis, the optimal ULA transmit array should be pointing towards the center of the receive array for correlation minimization/SE maximization. This will be satisfied given that δ is calculated as follows:

- For $N_r = 4$: $\delta = \frac{\pi}{2} + \frac{3\Delta\theta}{2}$
- For $N_r = 5$: $\delta = \frac{\pi}{2} + 2\Delta\theta$

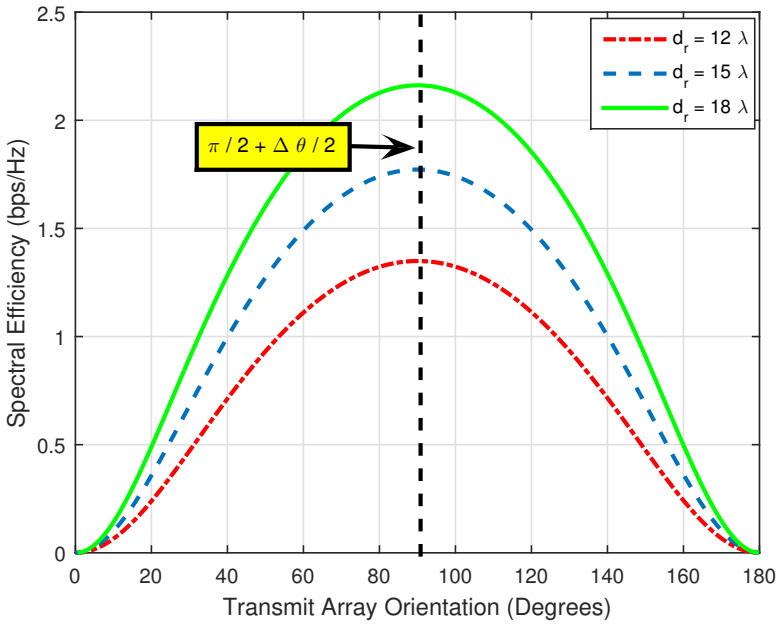

Figure 6.6 – SE versus the ULA transmit array orientation for a given scenario ($N_r = 2, \text{SNR} = 10\text{dB}, N_t = 32, D = 5000\lambda$) in pure LoS environment

- For $N_r = 6$: $\delta = \frac{\pi}{2} + \frac{5\Delta\theta}{2}$
- For $N_r = 7$: $\delta = \frac{\pi}{2} + 3\Delta\theta$

As we can observe from Figure 6.7, the numerical results validate the analysis we did to extend the work presented in [123]. Thus, in this chapter we provide a generic and scalable framework that can be used for practical scenarios and adapt to it.

In Figure 6.8- 1, it is shown that for a highly correlated scenario ($\Delta\theta \approx 0$), after adding the analog beamsteering, the received paths at the two receive antennas are highly correlated. However, when the transmit array is deployed as in equation (6.29), the correlation effect decreases as expected and as shown in Figure 6.9- 1. Moreover, the effect of the deployment optimization on the correlation is more significant after applying the ZF in the digital layer and is significant in the difference between Figure 6.8- 2 and Figure 6.9- 2.

In Figure 6.10, we validate the SE models as it is shown that both the theoretical and numerical SE results match for different deployment scenarios for the LoS channel environment and the sparse multi-path. Note that for this simulation and the other two following, the link budget is not taken into account, and the channel is considered to be normalized to the same power in LoS scenario and sparce multi-path scenario, while in real scenario, it cost much higher transmit power for the multi-path scenario to acheive the same received power as for LoS. Results also shows that the exploitation of diversity enhanced the SE is enhanced when multiple paths exist as these sparse multipath components offered by the channel can be captured by the EGT analog beamforming to add their gains constructively.

In Figure 6.11, similarly, we validate the BER models as it is shown that both the

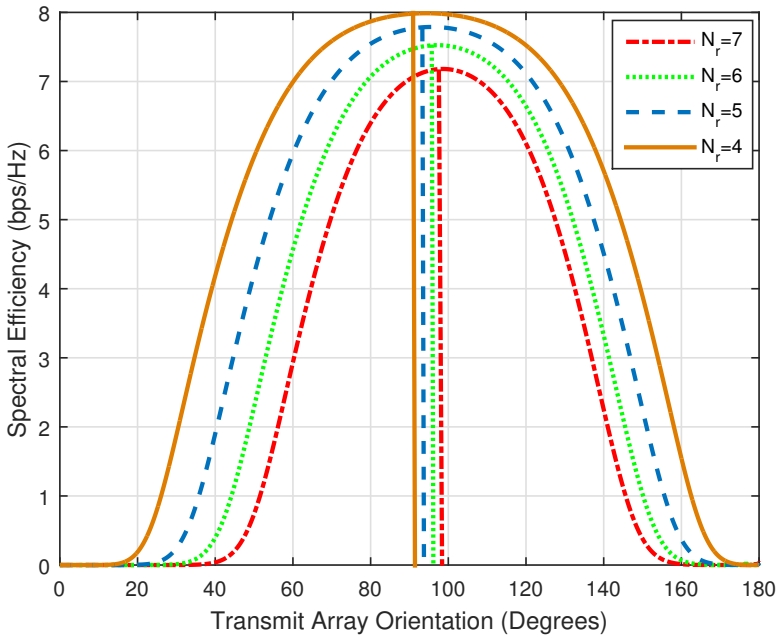

Figure 6.7 – SE versus the ULA transmit array orientation for a given scenario (SNR = 10dB, $N_t = 32, D = 500\lambda, d_r = 25\lambda$) in pure LoS environment

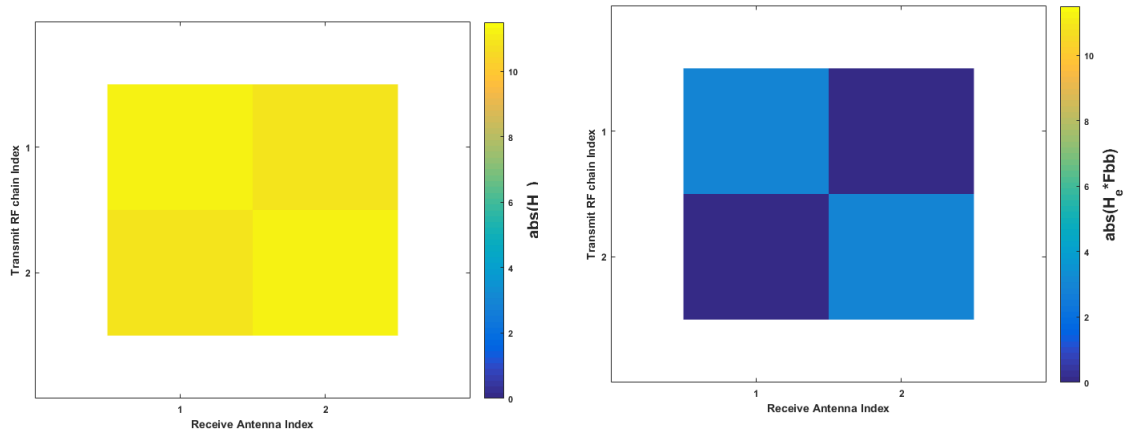

1) The equivalent channel $\mathbf{H}_e \in \mathbb{C}^{N_r \times L_t}$

2) Applying ZF $\mathbf{W}_{ZF}$ on the equivalent channel $\mathbf{H}_e$

Figure 6.8 – Illustration of the effect of applying analog and hybrid beamforming for the RASK mmWave framework in pure LoS environment with transmit ULA for a given scenario ($N_t = 128, N_r = 2, d_r = 25\lambda, D = 5000\lambda$)

theoretical and numerical BER results match for different deployment scenarios for the LoS channel environment and the sparse multi-path. Moreover, it is obvious that decreasing the number of transmit antennas leads to a degradation in BER.

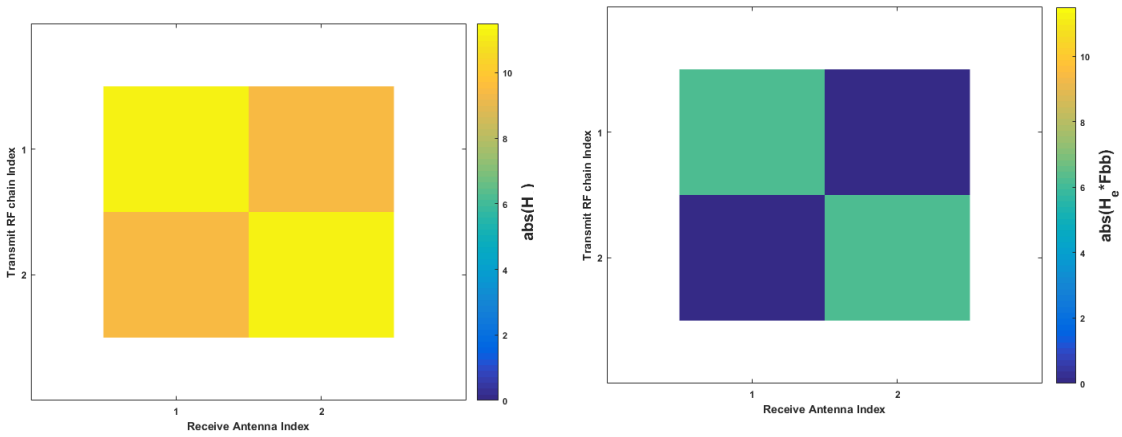

1) The equivalent channel $\mathbf{H}_e \in \mathbb{C}^{N_r \times L_t}$

2) Applying ZF $\mathbf{W}_{ZF}$ on the equivalent channel $\mathbf{H}_e$

Figure 6.9 – Illustration of the effect of applying analog and hybrid beamforming for the RASK mmWave framework in pure LoS environment with transmit ULA for a given scenario ($N_t = 128, N_r = 2, d_r = 25\lambda, D = 5000\lambda$) after applying the transmitter deployment optimization for correlation minimization as illustrated in Figure 6.3

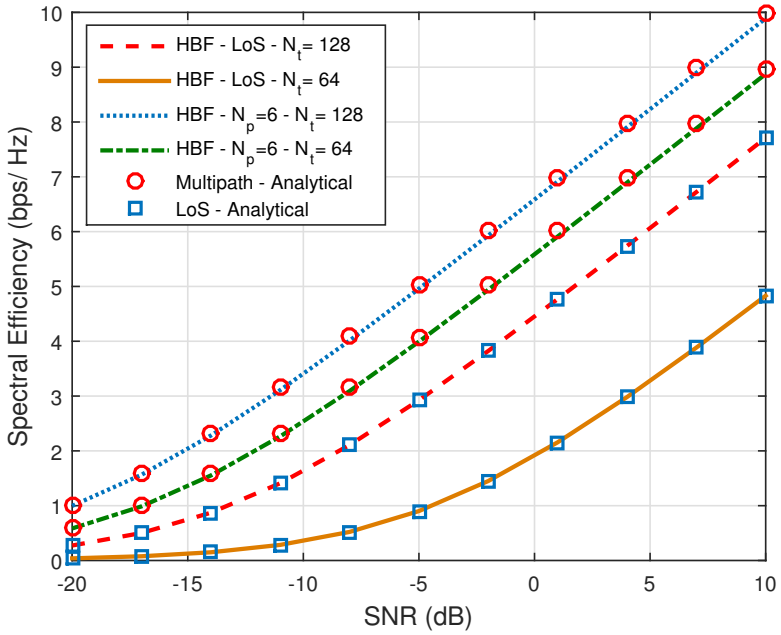

Figure 6.10 – Theoretical and numerical SE versus SNR for a given scenario ($N_r = 2, d_r = 18\lambda, D = 5000\lambda$) in a pure LoS environment and in a sparse multipath environment ($N_p = 6$ paths)

Finally, in Figure 6.12, the theoretical BER is compared for different deployment

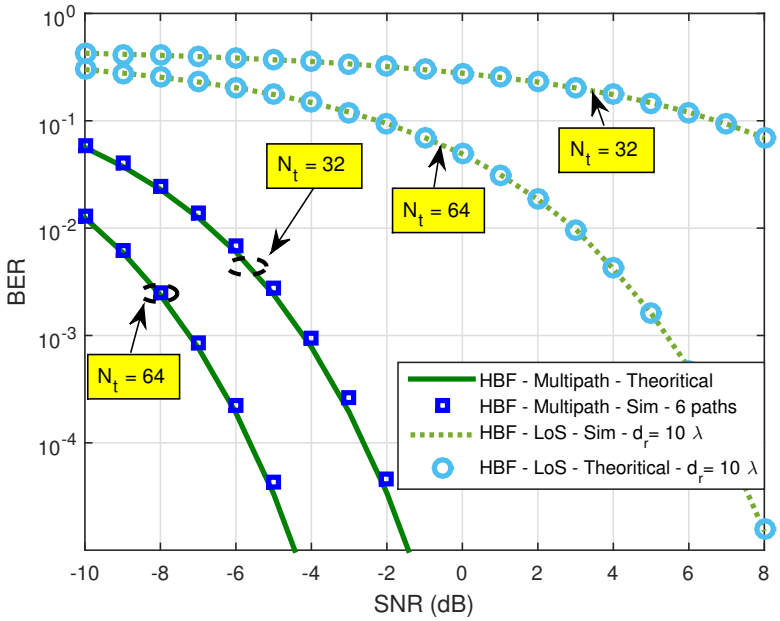

Figure 6.11 – Theoretical and numerical ABER versus SNR for a given scenario ($N_r = 2, d_r = 10\lambda, D = 5000\lambda$) in a pure LoS environment and in a sparse multipath environment ($N_p = 6$ paths)

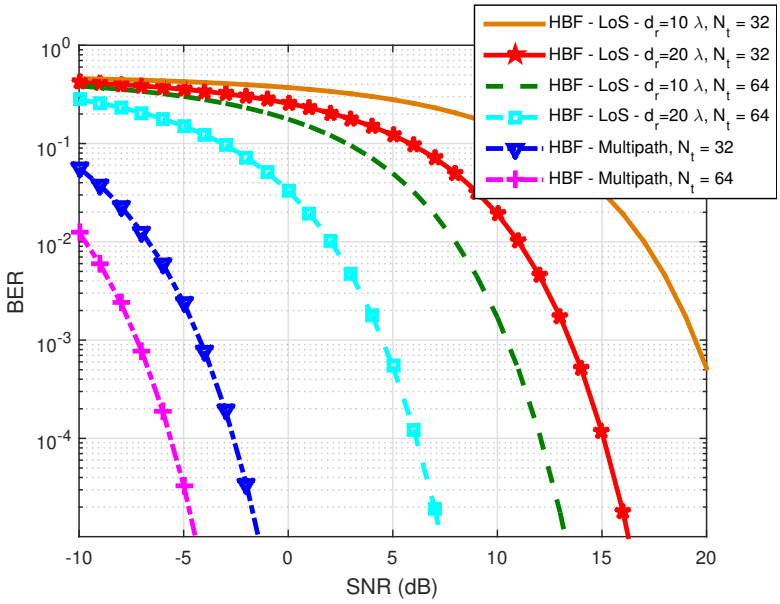

Figure 6.12 – Theoretical ABER versus SNR for different scenarios (given $D = 5000\lambda$) in a pure LoS environment and in a sparse multipath environment

scenarios. We highlight three factors that can affect the BER performance of the system, which is the number of paths of the channel, the receive antennas inter-element spacing, and the number of the transmit antennas. The number of paths is defined by the propagation environment and can't be tuned, but we can only adapt to it using the

suitable analog beamforming algorithm (EGT in case of multipath and LoS beamsteering in case of LoS channels). However, the number of the transmit antennas and the receive antennas spacing can be adjusted given certain deployment constraints.

6.6 Summary

In this chapter, a detailed study for SM in mmWave systems was given, covering all possible scenarios analytically, and numerically compared to the existing work in the literature. We derived closed-form solutions for the SE in case of pure LoS channel environments for any possible deployment scenario, given that two receive antennas exist, and optimal transmit array deployment optimization is applied for correlation minimization. Similarly, we derived closed-form solutions for the BER in case of pure LoS channel environments for any possible deployment scenario, given that two receive antennas exist, and optimal transmit array deployment is applied for correlation minimization. Moreover, a closed form solution for the BER was derived for sparse multipath environments as well to have a complete analysis for the achievable performance of the RSM in mmWave systems. All the introduced models were validated with numerical analysis.

From the analytical and numerical analysis, it is shown that RASK is practically feasible at mmWave frequencies and can achieve considerable SE and BER by carefully applying suitable beamforming and correlation minimization techniques at the transmitter, and increasing the inter-antenna element spacing at the receiver. Henceforth, the low complexity receiver design gain can be completely leveraged at mmWave frequencies.

Chapter 7

Conclusions and Future Work

7.1 Conclusion

In this thesis, we evaluated the performance of SM for low complexity devices. Uplink and downlink transmission schemes were proposed and studied, based on SM concept. The main objective was to minimize the complexity of the connected device while having a good SE and BEP performance. More specifically, we evaluated the performance of RASK scheme using different precoding method and different detection schemes. Also, RASK was studied in Rayleigh and LoS channel, as well as in mmWave environment using hybrid beamforming. Furthermore, an extended scheme of RASK called ERASK was proposed and studied that aims to increase the SE while keeping a low complexity detection at the connected device. Also, an analog scheme to ERASK for uplink transmission, called ESSK, was proposed and studied. In the following, a summary of the main contributions and conclusions of the thesis is provided.

In Chapter 2, performance analysis for the RASK scheme, using MRT or ZF precoding, and different detection schemes, has been provided. For the precoding, we found that the ZF precoding has two benefits compared to MRT: the ZF precoding outperforms the MRT precoding in terms of BER, and the ML based detector in ZF-RASK could be reduced to a single tap receiver. The drawback is that the implementation of ZF at the transmitter is more complex in terms of computational operations. On the other side, for the detection at the receiver, two detection modes has been studied: coherent and non-coherent detection. Obviously, results show that the coherent detection outperforms the non-coherent one, that is made of an envelope detector, but at the cost of additional hardware complexity at the receiver, since a down converter is needed for each receive antenna. Thus, we proposed to use switches at the receiver in order to reduce the hardware complexity of the coherent detector, so that multiple receive antenna are connected to one RF chain. Results show that this method leads to a degradation in performance, because of the degradation in the effective SNR. Thus, depending on the ratio of the number of RF chain to the number of the receive antenna, the non-coherent detector could outperform the coherent detector when switches are used. So, we calculated the equivalence point that gives the minimum number of RF chains needed so that the coherent detector outperforms the non-coherent one.

In addition, for MRT-RASK, the optimal detector couldn't be reduced because of the interference, and a channel estimation at the receiver is needed. And so reducing the

complexity of the detector to use a single tap, leads to a degradation in performance. We find that the detector that measures the maximum real part and minimum imaginary part (MRMI) is the best detector that doesn't need channel estimation. Finally, the practical implementation of the RASK scheme with MRT precoding under LoS channel scenario proofed the concept.

In Chapter 4, the ERASK scheme that extends the concept of RASK is presented, where the number of targeted antennas becomes variable, with all possible combination, resulting in an SE equal to N_r. As for RASK scheme, the ZF precoding is better for ERASK in terms of BER performance, and also the detector remains simple (threshold detector), at the cost of computational complexity. But when the number of transmit antenna increases, the performance of MRT and ZF becomes the same. In addition, the effect of error in channel estimation and the correlation between antennas on the performance of ZF ERASK, has been studied. Results show that ERASK performance degrades when the correlation factor increases, and when channel estimation error is added. Nevertheless, the degradation remains still acceptable for $\rho \leq 0.5$ with a performance degradation of less than 4 dB at a 10^{-3} BER compared to the perfect conditions, and less than 3 dB when only the channel estimation error is included ($\sigma_H = 0.2$, $\rho = 0$). Interestingly, results also indicate that under a given quality of the channel estimation, the antenna correlation has no impact on the performance. Finally, ERSM scheme is presented and studied. In ERSM, the additional M-PSK symbol is transmitted with the ERASK symbol, using two power levels. An optimal power ratio between the two power levels that minimize the total BEP, was derived analytically. Results show that when the optimal ratio is used, the performance of ERSM remains the same if we change the configuration of the symbol, by changing the order of IQ modulation or the number of targeted receive antennas, but keeping the same SE.

In Chapter 5, the ESSK scheme that is analog to the ERASK in uplink was presented and studied. We compare the performance of ML detection with the based equalizer detector. Obviously, the ML outperforms the other detector, but when the number of receive antennas increases, the difference between the two performances decreases. The intrest of using equalization is that the same precoding matrix for ERASK could be used for equalization in ESSK, so that a complete uplink and downlink transmission system between a base station and a connected device has been proposed, with a dual performance.

In Chapter 6, a detailed study for RASK in mmWave systems was given, covering all possible scenarios analytically, and numerically compared to the existing work in the literature. The channel model was described, followed by the beamforming strategies, where a combination of analog beamforming and digital precoding is performed. In analog beamformer, LoS beamsteering and EGT beamforming method where proposed and studied, while the digital precoder is always the ZF precoder. We derived closed-form solutions for the SE in case of pure LoS channel environments for any possible deployment scenario, given that two receive antennas exist, and optimal transmit array deployment optimization is applied for correlation minimization. Results show that the more the channel is multipath, the better the performance of RASK with EGT beamforming is. Similarly, we derived closed-form solutions for the BEP in case of pure LoS channel environments for any possible deployment scenario, given that two receive antennas exist, and optimal transmit array deployment is applied for correlation minimization. Moreover, a closed form solution for the BEP was derived for

sparse multipath environments as well to have a complete analysis for the achievable performance of the RASK in mmWave systems.

7.2 Future Works

In the following, we provides some perspectives for future works that could be done after this thesis. For short term:

- First, some analytical derivations for the BEP for some detectors that has been presented for MRT-RASK, as the ML and the MRMI.
- The proposed ERASK and ESSK scheme in Chapters 3 and 4 represent a dual system based on SM in uplink and downlink, that could be used for the transmission between BS and CD. In a future work, we will try to implement the whole system on National Instrument platform, in order to validate the theoretical study. Also, the implementation will be extended to the multi-user scenario.

Moreover, in long term:

- The waveform of the signal was considered for a flat fading channel. In a future work, we will consider the case of different waveform in single carrier transmission where the frequency selectivity of the channel is taken into account. Also, the robustness of the system in mobility will be evaluated. The object of such work is to study the performance of the SM if it is implemented in well known IoT standard.
- In Chapter 6, we used the hybrid beamforming at the BS only. In future work, we will study the case where the CD is occupied with an analog combiner. In this case, the transmitter exploits the difference between paths to transmit the information, so that different beams are created at the transmitter and detected by the analog combiner at the receiver. This concept is called Beam Index Modulation.

Appendix A

Comparison of n random variables

Let X_1, X_2... X_n be n random variables, where each X_i follows a specific and independent probability distribution $\mathcal{X}_i$. To find the probability $\mathcal{P}\left(Xj, j \neq i < X_i\right)$, we need the probability for each value of x_i that all other variables are less than that value:

$$\text{if } X_i = l, Xj, j \neq i < l \tag{A.1}$$

So that could be calculated by the sum:

$$\mathcal{P}\left(Xj, j \neq i < X_i\right) = \sum_l \mathcal{P}(X_i = l) \times \mathcal{P}(Xj, j \neq i < l). \tag{A.2}$$

For continuous random variable distribution, the equation (A.2) can be expressed by:

$$\mathcal{P}\left(Xj, j \neq i < X_i\right) = \int_{-\infty}^{+\infty} PDF_{X_i}(l) \times \prod_{j=1, j\neq i}^{n} CDF_{X_j}(l) dl. \tag{A.3}$$

Bibliography

[1] C.-X. Wang, F. Haider, X. Gao, X.-H. You, Y. Yang, D. Yuan, H. Aggoune, H. Haas, S. Fletcher, and E. Hepsaydir, "Cellular architecture and key technologies for 5g wireless communication networks", *IEEE Communications Magazine*, vol. 52, no. 2, pp. 122–130, 2014.

[2] L. Atzori, A. Iera, and G. Morabito, "The internet of things: a survey", *Computer networks*, vol. 54, no. 15, pp. 2787–2805, 2010.

[3] M. Di Renzo, H. Haas, A. Ghrayeb, S. Sugiura, and L. Hanzo, "Spatial modulation for generalized mimo: challenges, opportunities, and implementation", *Proceedings of the IEEE*, vol. 102, no. 1, pp. 56–103, 2014.

[4] S. Ganesan, R. Mesleh, H. Ho, C. W. Ahn, and S. Yun, "On the performance of spatial modulation ofdm", in *2006 Fortieth Asilomar Conference on Signals, Systems and Computers*, IEEE, 2006, pp. 1825–1829.

[5] A. Stavridis, S. Sinanovic, M. Di Renzo, H. Haas, and P. Grant, "An energy saving base station employing spatial modulation", in *2012 IEEE 17th International Workshop on Computer Aided Modeling and Design of Communication Links and Networks (CAMAD)*, IEEE, 2012, pp. 231–235.

[6] J. Jeganathan, A. Ghrayeb, and L. Szczecinski, "Spatial modulation: optimal detection and performance analysis", *IEEE Communications Letters*, vol. 12, no. 8, 2008.

[7] Y. A. Chau and S.-H. Yu, "Space modulation on wireless fading channels", in *Vehicular Technology Conference, 2001. VTC 2001 Fall. IEEE VTS 54th*, IEEE, vol. 3, 2001, pp. 1668–1671.

[8] L.-L. Yang, "Transmitter preprocessing aided spatial modulation for multiple-input multiple-output systems", in *Vehicular Technology Conference (VTC Spring), 2011 IEEE 73rd*, IEEE, 2011, pp. 1–5.

[9] D.-T. Phan-Huy and M. Hélard, "Receive antenna shift keying for time reversal wireless communications", in *2012 IEEE International Conference on Communications (ICC)*, IEEE, 2012, pp. 4852–4856.

[10] A. Mokh, M. Crussiere, M. Helard, and M. D. Renzo, "Theoretical performance of coherent and incoherent detection for zero-forcing receive antenna shift keying", *IEEE Access*, 2018.

[11] A. Hashimoto, H. Yoshino, and H. Atarashi, "Roadmap of imt-advanced development", *IEEE Microwave magazine*, vol. 9, no. 4, 2008.

[12] H. Haas, E. Costa, and E. Schulz, "Increasing spectral efficiency by data multiplexing using antenna arrays", in *Personal, Indoor and Mobile Radio Communications, 2002. The 13th IEEE International Symposium on*, IEEE, vol. 2, 2002, pp. 610–613.

[13] E. Telatar, "Capacity of multi-antenna gaussian channels", *Transactions on Emerging Telecommunications Technologies*, vol. 10, no. 6, pp. 585–595, 1999.

[14] G. Tsoulos, *MIMO system technology for wireless communications*. CRC press, 2006.

[15] C. E. Shannon, "Communication in the presence of noise", *Proceedings of the IRE*, vol. 37, no. 1, pp. 10–21, 1949.

[16] Y. G. Li and G. L. Stuber, *Orthogonal frequency division multiplexing for wireless communications*. Springer Science & Business Media, 2006.

[17] N. LaSorte, W. J. Barnes, and H. H. Refai, "The history of orthogonal frequency division multiplexing", in *Global Telecommunications Conference, 2008. IEEE GLOBECOM 2008. IEEE*, IEEE, 2008, pp. 1–5.

[18] R. W. Chang, "Synthesis of band-limited orthogonal signals for multichannel data transmission", *Bell System Technical Journal*, vol. 45, no. 10, pp. 1775–1796, 1966.

[19] G. J. Foschini and M. J. Gans, "On limits of wireless communications in a fading environment when using multiple antennas", *Wireless personal communications*, vol. 6, no. 3, pp. 311–335, 1998.

[20] J. H. Winters, J. Salz, and R. D. Gitlin, "The impact of antenna diversity on the capacity of wireless communication systems", *IEEE transactions on Communications*, vol. 42, no. 234, pp. 1740–1751, 1994.

[21] J. Winters, "On the capacity of radio communication systems with diversity in a rayleigh fading environment", *IEEE journal on selected areas in communications*, vol. 5, no. 5, pp. 871–878, 1987.

[22] E. G. Larsson, O. Edfors, F. Tufvesson, and T. L. Marzetta, "Massive mimo for next generation wireless systems", *IEEE communications magazine*, vol. 52, no. 2, pp. 186–195, 2014.

[23] S. Sinanovic, N. Serafimovski, M. Di Renzo, and H. Haas, "Secrecy capacity of space keying with two antennas", in *Vehicular Technology Conference (VTC Fall), 2012 IEEE*, IEEE, 2012, pp. 1–5.

[24] F. Oggier and B. Hassibi, "The secrecy capacity of the mimo wiretap channel", *IEEE Transactions on Information Theory*, vol. 57, no. 8, pp. 4961–4972, 2011.

[25] J. Barros and M. R. Rodrigues, "Secrecy capacity of wireless channels", in *Information Theory, 2006 IEEE International Symposium on*, IEEE, 2006, pp. 356–360.

[26] S. M. Alamouti, "A simple transmit diversity technique for wireless communications", *IEEE Journal on selected areas in communications*, vol. 16, no. 8, pp. 1451–1458, 1998.

[27] R. U. Nabar, H. Bolcskei, V. Erceg, D. Gesbert, and A. J. Paulraj, "Performance of multiantenna signaling techniques in the presence of polarization diversity", *IEEE Transactions on Signal Processing*, vol. 50, no. 10, pp. 2553–2562, 2002.

[28] L.-U. Choi and R. D. Murch, "A transmit preprocessing technique for multiuser mimo systems using a decomposition approach", *IEEE Transactions on Wireless Communications*, vol. 3, no. 1, pp. 20–24, 2004.

[29] J. G. Proakis, *Digital signal processing: principles algorithms and applications*. Pearson Education India, 2001.

[30] B. Sklar, "Rayleigh fading channels in mobile digital communication systems. i. characterization", *IEEE Communications magazine*, vol. 35, no. 9, pp. 136–146, 1997.

[31] E. Biglieri, J. Proakis, and S. Shamai, "Fading channels: information-theoretic and communications aspects", *IEEE Transactions on Information Theory*, vol. 44, no. 6, pp. 2619–2692, 1998.

[32] T. L. Marzetta and B. M. Hochwald, "Capacity of a mobile multiple-antenna communication link in rayleigh flat fading", *IEEE transactions on Information Theory*, vol. 45, no. 1, pp. 139–157, 1999.

[33] P. J. Smith and M. Shafi, "On a gaussian approximation to the capacity of wireless mimo systems", in *Communications, 2002. ICC 2002. IEEE International Conference on*, IEEE, vol. 1, 2002, pp. 406–410.

[34] M. Chiani, M. Z. Win, and A. Zanella, "On the capacity of spatially correlated mimo rayleigh-fading channels", *IEEE Transactions on Information Theory*, vol. 49, no. 10, pp. 2363–2371, 2003.

[35] L. Brandenburg and A. Wyner, "Capacity of the gaussian channel with memory: the multivariate case", *Bell Labs Technical Journal*, vol. 53, no. 5, pp. 745–778, 1974.

[36] H. Bolcskei, D. Gesbert, and A. J. Paulraj, "On the capacity of ofdm-based spatial multiplexing systems", *IEEE Transactions on communications*, vol. 50, no. 2, pp. 225–234, 2002.

[37] L. Zheng and D. N. C. Tse, "Diversity and multiplexing: a fundamental tradeoff in multiple-antenna channels", *IEEE Transactions on information theory*, vol. 49, no. 5, pp. 1073–1096, 2003.

[38] W. Liu, X. Li, and M. Chen, "Energy efficiency of mimo transmissions in wireless sensor networks with diversity and multiplexing gains", in *Acoustics, Speech, and Signal Processing, 2005. Proceedings.(ICASSP'05). IEEE International Conference on*, IEEE, vol. 4, 2005, pp. iv–897.

[39] S. Sandhu and A. Paulraj, "Space-time block codes: a capacity perspective", *IEEE Communications Letters*, vol. 4, no. 12, pp. 384–386, 2000.

[40] R. Y. Mesleh, H. Haas, S. Sinanovic, C. W. Ahn, and S. Yun, "Spatial modulation", *IEEE Transactions on Vehicular Technology*, vol. 57, no. 4, pp. 2228–2241, 2008.

[41] S. Song, Y. Yang, Q. Xionq, K. Xie, B.-J. Jeong, and B. Jiao, "A channel hopping technique i: theoretical studies on band efficiency and capacity", in *Communications, Circuits and Systems, 2004. ICCCAS 2004. 2004 International Conference on*, IEEE, vol. 1, 2004, pp. 229–233.

[42] J. Jeganathan, A. Ghrayeb, L. Szczecinski, and A. Ceron, "Space shift keying modulation for mimo channels", *IEEE Transactions on Wireless Communications*, vol. 8, no. 7, pp. 3692–3703, 2009.

[43] M. Di Renzo and H. Haas, "Improving the performance of space shift keying (ssk) modulation via opportunistic power allocation", *IEEE Communications Letters*, vol. 14, no. 6, 2010.

[44] P. Liu and A. Springer, "Space shift keying for los communication at mmwave frequencies", *IEEE Wireless Communications Letters*, vol. 4, no. 2, pp. 121–124, 2015.

[45] R. Mesleh, H. Haas, C. W. Ahn, and S. Yun, "Spatial modulation-a new low complexity spectral efficiency enhancing technique", in *Communications and Networking in China, 2006. ChinaCom'06. First International Conference on*, IEEE, 2006, pp. 1–5.

[46] Y. Yang and B. Jiao, "Information-guided channel-hopping for high data rate wireless communication", *IEEE Communications Letters*, vol. 12, no. 4, 2008.

[47] A. Younis, R. Mesleh, H. Haas, and P. M. Grant, "Reduced complexity sphere decoder for spatial modulation detection receivers", in *Global Telecommunications Conference (GLOBECOM 2010), 2010 IEEE*, IEEE, 2010, pp. 1–5.

[48] A. Alshamali and B. Quza, "Performance of spatial modulation in correlated and uncorrelated nakagami fading channel.", *JCM*, vol. 4, no. 3, pp. 170–174, 2009.

[49] R. Mesleh, O. S. Badarneh, A. Younis, and H. Haas, "Performance analysis of spatial modulation and space-shift keying with imperfect channel estimation over generalized fading channels", *IEEE Transactions on Vehicular Technology*, vol. 64, no. 1, pp. 88–96, 2015.

[50] A. Younis, W. Thompson, M. Di Renzo, C.-X. Wang, M. A. Beach, H. Haas, and P. M. Grant, "Performance of spatial modulation using measured real-world channels", in *Vehicular Technology Conference (VTC Fall), 2013 IEEE 78th*, IEEE, 2013, pp. 1–5.

[51] N. Serafimovski, A. Younis, R. Mesleh, P. Chambers, M. Di Renzo, C.-X. Wang, P. M. Grant, M. A. Beach, and H. Haas, "Practical implementation of spatial modulation", *IEEE Transactions on Vehicular Technology*, vol. 62, no. 9, pp. 4511–4523, 2013.

[52] K. Ishibashi and S. Sugiura, "Effects of antenna switching on band-limited spatial modulation", *IEEE Wireless Communications Letters*, vol. 3, no. 4, pp. 345–348, 2014.

[53] R. Rajashekar, K. Hari, and L. Hanzo, "Antenna selection in spatial modulation systems", *IEEE Communications Letters*, vol. 17, no. 3, pp. 521–524, 2013.

[54] A. Stavridis, S. Sinanovic, M. Di Renzo, and H. Haas, "Energy evaluation of spatial modulation at a multi-antenna base station", in *Vehicular Technology Conference (VTC Fall), 2013 IEEE 78th*, IEEE, 2013, pp. 1–5.

[55] R. Mesleh, M. Di Renzo, H. Haas, and P. M. Grant, "Trellis coded spatial modulation", *IEEE Transactions on Wireless Communications*, vol. 9, no. 7, pp. 2349–2361, 2010.

[56] R. Mesleh, I. Stefan, H. Haas, and P. M. Grant, "On the performance of trellis coded spatial modulation", in *Int. ITG Workshop on Smart Antennas*, 2009, pp. 235–241.

[57] E. Basar, U. Aygolu, E. Panayirci, and H. V. Poor, "New trellis code design for spatial modulation", *IEEE Transactions on Wireless Communications*, vol. 10, no. 8, pp. 2670–2680, 2011.

[58] R. Mesleh, S. S. Ikki, and H. M. Aggoune, "Quadrature spatial modulation", *IEEE Transactions on Vehicular Technology*, vol. 64, no. 6, pp. 2738–2742, 2015.

[59] A. Younis, R. Mesleh, and H. Haas, "Quadrature spatial modulation performance over nakagami-*m* fading channels", *IEEE Transactions on Vehicular Technology*, vol. 65, no. 12, pp. 10 227–10 231, 2016.

[60] R. Mesleh, S. S. Ikki, and H. M. Aggoune, "Quadrature spatial modulation–performance analysis and impact of imperfect channel knowledge", *Transactions on Emerging Telecommunications Technologies*, vol. 28, no. 1, 2017.

[61] M. Di Renzo, H. Haas, and P. M. Grant, "Spatial modulation for multiple-antenna wireless systems: a survey", *IEEE Communications Magazine*, vol. 49, no. 12, 2011.

[62] J. Jeganathan, A. Ghrayeb, and L. Szczecinski, "Generalized space shift keying modulation for mimo channels", in *Personal, Indoor and Mobile Radio Communications, 2008. PIMRC 2008. IEEE 19th International Symposium on*, IEEE, 2008, pp. 1–5.

[63] A. Younis, N. Serafimovski, R. Mesleh, and H. Haas, "Generalised spatial modulation", in *2010 Conference Record of the Forty Fourth Asilomar Conference on Signals, Systems and Computers*, IEEE, 2010, pp. 1498–1502.

[64] J. Wang, S. Jia, and J. Song, "Generalised spatial modulation system with multiple active transmit antennas and low complexity detection scheme", *IEEE Transactions on Wireless Communications*, vol. 11, no. 4, pp. 1605–1615, 2012.

[65] R. Y. Chang, S.-J. Lin, and W.-H. Chung, "New space shift keying modulation with hamming code-aided constellation design", *IEEE Wireless Communications Letters*, vol. 1, no. 1, pp. 2–5, 2012.

[66] L. He, J. Wang, and J. Song, "Generalized spatial modulation aided mmwave mimo with sub-connected hybrid precoding scheme", *arXiv preprint arXiv:1704.08824*, 2017.

[67] A. Mokh, M. Hélard, and M. Crussière, "Space shift keying modulations for low complexity internet-of-things devices", in *2017 Global Communications Conference (GLOBECOM)*, IEEE, 2017.

[68] A. Mokh, M. Crussière, M. Hélard, and M. Di Renzo, "Theoretical performance of coherent and incoherent detection for zero-forcing receive antenna shift keying", *IEEE access*, vol. 6, pp. 39 907–39 916, 2018.

[69] Y. Kokar, J.-C. Prevotet, and M. Helard, "Receive antenna shift keying modulation testbed for wireless communications systems", in *Globecom Workshops (GC Wkshps), 2016 IEEE*, IEEE, 2016, pp. 1–6.

[70] A. Mokh, Y. Kokar, M. Hélard, and M. Crussière, "Time reversal receive antenna shift keying on mimo los channel", in *2017 International Conference on Sensors, Networks, Smart and Emerging Technologies (SENSET)*, IEEE, 2017.

[71] A. Stavridis, S. Sinanovic, M. Di Renzo, and H. Haas, "Transmit precoding for receive spatial modulation using imperfect channel knowledge", in *Vehicular Technology Conference (VTC Spring), 2012 IEEE 75th*, IEEE, 2012, pp. 1–5.

[72] X. Li, Y. Zhang, L. Xiao, X. Xu, and J. Wang, "A novel precoding scheme for downlink multi-user spatial modulation system", in *Personal Indoor and Mobile Radio Communications (PIMRC), 2013 IEEE 24th International Symposium on*, IEEE, 2013, pp. 1361–1365.

[73] J. Zheng, "Fast receive antenna subset selection for pre-coding aided spatial modulation", *IEEE Wireless Communications Letters*, vol. 4, no. 3, pp. 317–320, 2015.

[74] N. S. Perović, P. Liu, M. Di Renzo, and A. Springer, "Receive spatial modulation for los mmwave communications based on tx beamforming", *IEEE Communications Letters*, vol. 21, no. 4, pp. 921–924, 2017.

[75] F. Wu, R. Zhang, L.-L. Yang, and W. Wang, "Transmitter precoding-aided spatial modulation for secrecy communications", *IEEE Transactions on Vehicular Technology*, vol. 65, no. 1, pp. 467–471, 2016.

[76] F. Wu, L.-L. Yang, W. Wang, and Z. Kong, "Secret precoding-aided spatial modulation", *IEEE Communications Letters*, vol. 19, no. 9, pp. 1544–1547, 2015.

[77] F. Wu, W. Wang, C. Dong, and L.-L. Yang, "Performance analysis of secret precoding-aided spatial modulation with finite-alphabet signaling", *IEEE Access*, 2018.

[78] R. Zhang, L.-L. Yang, and L. Hanzo, "Generalised pre-coding aided spatial modulation", *IEEE Transactions on Wireless Communications*, vol. 12, no. 11, pp. 5434–5443, 2013.

[79] ——, "Error probability and capacity analysis of generalised pre-coding aided spatial modulation", *IEEE Transactions on Wireless Communications*, vol. 14, no. 1, pp. 364–375, 2015.

[80] ——, "Performance analysis of non-linear generalized pre-coding aided spatial modulation", *IEEE Transactions on Wireless Communications*, vol. 15, no. 10, pp. 6731–6741, 2016.

[81] A. Stavridis, M. Di Renzo, and H. Haas, "Performance analysis of multistream receive spatial modulation in the mimo broadcast channel", *IEEE Transactions on Wireless Communications*, vol. 15, no. 3, pp. 1808–1820, 2016.

[82] A. Stavridis, M. Di Renzo, P. M. Grant, and H. Haas, "Performance analysis of receive space modulation in the shadowing mimo broadcast channel", *IEEE Transactions on Communications*, vol. 65, no. 5, pp. 1972–1983, 2017.

[83] C. Masouros and L. Hanzo, "Dual-layered mimo transmission for increased bandwidth efficiency", *IEEE Transactions on Vehicular Technology*, vol. 65, no. 5, pp. 3139–3149, 2016.

[84] A. Mokh, M. Hélard, and M. Crussière, "Extended receive antenna shift keying", in *2017 IEEE International Conference on Telecommunication (ICT)*, IEEE, 2017.

[85] A. Mokh, M. Crussière, and M. Hélard, "Performance analysis of the maximum ratio transmission preprocessing for extended receive antenna shift keying", in *2017 International Symposium on Wireless Personal Multimedia Communications (WPMC)*, IEEE, 2017.

[86] ——, "Performance analysis of extended rask under imperfect channel estimation and antenna correlation", in *2018 IEEE Wireless Communications and Networking Conference (WCNC)*, IEEE, 2018.

[87] A. Mokh, M. Hélard, and M. Crussiere, "Extended receive spatial modulation mimo scheme for higher spectral efficiency", in *2018 IEEE 87th Vehicular Technology Conference*, 2018.

[88] T. K. Lo, "Maximum ratio transmission", in *Communications, 1999. ICC'99. 1999 IEEE International Conference on*, IEEE, vol. 2, 1999, pp. 1310–1314.

[89] S. Sugiura and L. Hanzo, "Effects of channel estimation on spatial modulation", *IEEE Signal Processing Letters*, vol. 19, no. 12, pp. 805–808, 2012.

[90] A. Forenza, D. J. Love, and R. W. Heath, "A low complexity algorithm to simulate the spatial covariance matrix for clustered mimo channel models", in *Vehicular Technology Conference, 2004. VTC 2004-Spring. 2004 IEEE 59th*, IEEE, vol. 2, 2004, pp. 889–893.

[91] F. Rusek, D. Persson, B. K. Lau, E. Larsson, T. Marzetta, O. Edfors, and F. Tufvesson, "Scaling Up MIMO: Opportunities and Challenges with Very Large Arrays", *IEEE Signal Processing Magazine*, vol. 30, no. 1, pp. 40–60, Jan. 2013, ISSN: 1053-5888.

[92] M.-S. Alouini and A. Goldsmith, "A unified approach for calculating error rates of linearly modulated signals over generalized fading channels", in *Communications, 1998. ICC 98. Conference Record. 1998 IEEE International Conference on*, IEEE, vol. 1, 1998, pp. 459–464.

[93] T. Endeshaw, B. K. Chalise, and L. Vandendorpe, "Mse uplink-downlink duality of mimo systems under imperfect csi", in *Computational Advances in Multi-Sensor Adaptive Processing (CAMSAP), 2009 3rd IEEE International Workshop on*, IEEE, 2009, pp. 384–387.

[94] S. Shi, M. Schubert, and H. Boche, "Downlink mmse transceiver optimization for multiuser mimo systems: duality and sum-mse minimization", *IEEE Transactions on Signal Processing*, vol. 55, no. 11, pp. 5436–5446, 2007.

[95] M. Ding and S. D. Blostein, "Uplink-downlink duality in normalized mse or sinr under imperfect channel knowledge", in *Global Telecommunications Conference, 2007. GLOBECOM'07. IEEE*, IEEE, 2007, pp. 3786–3790.

[96] E. G. Larsson, O. Edfors, F. Tufvesson, and T. L. Marzetta, "Massive mimo for next generation wireless systems", *IEEE Communications Magazine*, vol. 52, no. 2, pp. 186–195, Feb. 2014, ISSN: 0163-6804. DOI: 10.1109/MCOM.2014.6736761.

[97] T. L. Marzetta, "Massive mimo: an introduction", *Bell Labs Technical Journal*, vol. 20, pp. 11–22, 2015, ISSN: 1089-7089. DOI: 10.15325/BLTJ.2015.2407793.

[98] L. Lu, G. Y. Li, A. L. Swindlehurst, A. Ashikhmin, and R. Zhang, "An overview of massive mimo: benefits and challenges", *IEEE Journal of Selected Topics in Signal Processing*, vol. 8, no. 5, pp. 742–758, Oct. 2014, ISSN: 1932-4553. DOI: 10.1109/JSTSP.2014.2317671.

[99] M. Xiao, S. Mumtaz, Y. Huang, L. Dai, Y. Li, M. Matthaiou, G. K. Karagiannidis, E. Björnson, K. Yang, C. Lin, and A. Ghosh, "Millimeter wave communications for future mobile networks", *CoRR*, vol. abs/1705.06072, 2017. [Online]. Available: http://arxiv.org/abs/1705.06072.

[100] T. S. Rappaport, S. Sun, R. Mayzus, H. Zhao, Y. Azar, K. Wang, G. N. Wong, J. K. Schulz, M. Samimi, and F. Gutierrez, "Millimeter wave mobile communications for 5g cellular: it will work!", *IEEE Access*, vol. 1, pp. 335–349, 2013, ISSN: 2169-3536. DOI: 10.1109/ACCESS.2013.2260813.

[101] S. Rangan, T. S. Rappaport, and E. Erkip, "Millimeter-wave cellular wireless networks: potentials and challenges", *Proceedings of the IEEE*, vol. 102, no. 3, pp. 366–385, Mar. 2014, ISSN: 0018-9219. DOI: 10.1109/JPROC.2014.2299397.

[102] A. F. Molisch, V. V. Ratnam, S. Han, Z. Li, S. L. H. Nguyen, L. Li, and K. Haneda, "Hybrid beamforming for massive mimo: a survey", *IEEE Communications Magazine*, vol. 55, no. 9, pp. 134–141, 2017, ISSN: 0163-6804. DOI: 10.1109/MCOM.2017.1600400.

[103] A. Alkhateeb, O. E. Ayach, G. Leus, and R. W. Heath, "Channel estimation and hybrid precoding for millimeter wave cellular systems", *IEEE Journal of Selected Topics in Signal Processing*, vol. 8, no. 5, pp. 831–846, Oct. 2014, ISSN: 1932-4553. DOI: 10.1109/JSTSP.2014.2334278.

[104] O. E. Ayach, S. Rajagopal, S. Abu-Surra, Z. Pi, and R. W. Heath, "Spatially sparse precoding in millimeter wave mimo systems", *IEEE Transactions on Wireless Communications*, vol. 13, no. 3, pp. 1499–1513, Mar. 2014, ISSN: 1536-1276. DOI: 10.1109/TWC.2014.011714.130846.

[105] M. Yüzgeçcioglu and E. A. Jorswieck, "Hybrid beamforming with spatial modulation in multi-user massive MIMO mmwave networks", *CoRR*, vol. abs/1709.04826, 2017. arXiv: 1709.04826. [Online]. Available: http://arxiv.org/abs/1709.04826.

[106] N. S. Perović, P. Liu, M. D. Renzo, and A. Springer, "Receive spatial modulation for los mmwave communications based on tx beamforming", *IEEE Communications Letters*, vol. 21, no. 4, pp. 921–924, Apr. 2017, ISSN: 1089-7798.

[107] Y. Cui, X. Fang, and L. Yan, "Hybrid spatial modulation beamforming for mmwave railway communication systems", *IEEE Transactions on Vehicular Technology*, vol. 65, no. 12, pp. 9597–9606, Dec. 2016, ISSN: 0018-9545.

[108] M. C. Lee and W. H. Chung, "Transmitter design for analog beamforming aided spatial modulation in millimeter wave mimo systems", in *2016 IEEE 27th Annual International Symposium on Personal, Indoor, and Mobile Radio Communications (PIMRC)*, Sep. 2016, pp. 1–6. DOI: 10.1109/PIMRC.2016.7794712.

[109] L. He, J. Wang, and J. Song, "Generalized spatial modulation aided mmwave MIMO with sub-connected hybrid precoding scheme", *CoRR*, vol. abs/1704.08824, 2017. arXiv: 1704.08824. [Online]. Available: http://arxiv.org/abs/1704.08824.

[110] R. Mesleh and A. Younis, "Capacity analysis for los millimeter–wave quadrature spatial modulation", *Wireless Networks*, Jan. 2017, ISSN: 1572-8196. DOI: 10.1007/s11276-017-1444-y. [Online]. Available: https://doi.org/10.1007/s11276-017-1444-y.

[111] J. Wang, L. He, and J. Song, "An overview of spatial modulation techniques for millimeter wave mimo systems", in *2017 IVth International Conference on Engineering and Telecommunication (EnT)*, Nov. 2017, pp. 51–56. DOI: 10.1109/ICEnT.2017.18.

[112] Y. Ding, K. J. Kim, T. Koike-Akino, M. Pajovic, P. Wang, and P. Orlik, "Spatial scattering modulation for uplink millimeter-wave systems", *IEEE Communications Letters*, vol. 21, no. 7, pp. 1493–1496, Jul. 2017, ISSN: 1089-7798. DOI: 10.1109/LCOMM.2017.2684126.

[113] Y. Ding, V. Fusco, A. Shitvov, Y. Xiao, and H. Li, "Beam index modulation wireless communication with analog beamforming", *IEEE Transactions on Vehicular Technology*, pp. 1–1, 2018, ISSN: 0018-9545. DOI: 10.1109/TVT.2018.2819728.

[114] Y. H. Cho and J. J. Kim, "Line-of-sight mimo channel in millimeter-wave beamforming system: modeling and prototype results", in *2015 IEEE 81st Vehicular Technology Conference (VTC Spring)*, May 2015, pp. 1–5. DOI: 10.1109/VTCSpring.2015.7145912.

[115] L. Liang, W. Xu, and X. Dong, "Low-complexity hybrid precoding in massive multiuser mimo systems", *IEEE Wireless Communications Letters*, vol. 3, no. 6, pp. 653–656, Dec. 2014, ISSN: 2162-2337. DOI: 10.1109/LWC.2014.2363831.

[116] T. S. Rappaport, S. Sun, R. Mayzus, H. Zhao, Y. Azar, K. Wang, G. N. Wong, J. K. Schulz, M. Samimi, and F. Gutierrez, "Millimeter wave mobile communications for 5g cellular: it will work!", *IEEE Access*, vol. 1, pp. 335–349, 2013, ISSN: 2169-3536. DOI: 10.1109/ACCESS.2013.2260813.

[117] M. Jacob, S. Priebe, R. Dickhoff, T. Kleine-Ostmann, T. Schrader, and T. Kurner, "Diffraction in mm and sub-mm wave indoor propagation channels", *IEEE Transactions on Microwave Theory and Techniques*, vol. 60, no. 3, pp. 833–844, Mar. 2012, ISSN: 0018-9480. DOI: 10.1109/TMTT.2011.2178859.

[118] P. Karadimas, B. Allen, and P. Smith, "Human body shadowing characterization for 60-ghz indoor short-range wireless links", *IEEE Antennas and Wireless Propagation Letters*, vol. 12, pp. 1650–1653, 2013, ISSN: 1536-1225. DOI: 10.1109/LAWP.2013.2294563.

[119] A. M. Sayeed, "Deconstructing multiantenna fading channels", *IEEE Transactions on Signal Processing*, vol. 50, no. 10, pp. 2563–2579, Oct. 2002, ISSN: 1053-587X. DOI: 10.1109/TSP.2002.803324.

[120] A. Alkhateeb, G. Leus, and R. W. Heath Jr, "Limited Feedback Hybrid Precoding for Multi-User Millimeter Wave Systems", *ArXiv e-prints*, Sep. 2014. arXiv: 1409.5162 [cs.IT].

[121] D. J. Love and R. W. Heath, "Equal gain transmission in multiple-input multiple-output wireless systems", *IEEE Transactions on Communications*, vol. 51, no. 7, pp. 1102–1110, Jul. 2003, ISSN: 0090-6778. DOI: 10.1109/TCOMM.2003.814195.

[122] F. Gholam, J. Via, and I. Santamaria, "Beamforming design for simplified analog antenna combining architectures", *IEEE Transactions on Vehicular Technology*, vol. 60, no. 5, pp. 2373–2378, Jun. 2011, ISSN: 0018-9545. DOI: 10.1109/TVT.2011.2142205.

[123] W. Cai, P. Wang, Y. Li, Y. Zhang, and B. Vucetic, "Deployment optimization of uniform linear antenna arrays for a two-path millimeter wave communication system", *IEEE Communications Letters*, vol. 19, no. 4, pp. 669–672, Apr. 2015, ISSN: 1089-7798. DOI: 10.1109/LCOMM.2015.2401570.

INSA de RENNES
Service des Formations

AVIS DU JURY SUR LA REPRODUCTION DE LA THESE SOUTENUE

Titre de la thèse:
Techniques de Modulations Spatiales à l'Emission et à la Réception pour les Objets à faible Complexité

Nom Prénom de l'auteur : MOKH ALI

Membres du jury :
- Monsieur DI RENZO Marco
- Monsieur CANCES Jean-Pierre
- Madame HELARD Maryline
- Monsieur TERRE Michel
- Madame BAUDOIN Geneviève
- Monsieur CRUSSIERE Matthieu
- Monsieur ROS Laurent

Président du jury : JP CANCES

Date de la soutenance : 15 Novembre 2018

Reproduction de la these soutenue

☒ Thèse pouvant être reproduite en l'état
☐ Thèse pouvant être reproduite après corrections suggérées

Fait à Rennes, le 15 Novembre 2018

Signature du président de jury

Le Directeur,

M'hamed DRISSI

INSTITUT NATIONAL DES SCIENCES APPLIQUÉES - RENNES

Titre : Techniques de Modulation Spatiales à l'Emission et a la Réception pour les Objets a bas Complexité.

Mots clés : Modulation Spatiale, MIMO, Precodage, Space Shift Keying, Receive Antenna Shift Keying

Résumé : Internet of Things est l'un des mots-clés qui représente l'évolution de la 5G capable de connecter les «périphériques connectés» au réseau. Ces CD devraient nécessiter des débits de données modestes et se caractériseront par de faibles ressources en termes de calcul et de consommation d'énergie par rapport aux autres appareils multimédias mobiles. La modulation spatiale (SM) est proposée comme une solution prometteuse pour augmenter le débit de données du CD avec une faible augmentation (ou pas) de la consommation d'énergie. Inspiré par les avantages de SM, l'objectif de cette thèse est d'étudier les performances de différents schémas de transmission basés sur le concept SM au niveau de l'émetteur et du récepteur, respectivement pour une transmission montante et une liaison descendante entre une BS et un CD. Nous avons proposé un système global dont la complexité de calcul supérieure reste à la station de base: le module de transmission est utilisé pour la liaison montante et le module de réception pour la liaison descendante. Il est montré que, avec SM, une activation / désactivation de la liaison montante et du détecteur simple pour la liaison descendante pourrait suffire à la transmission sur le CD. En outre, avec les schémas SM étendus, nous avons augmenté l'efficacité spectrale du SM pour qu'elle soit égale au nombre d'antennes du CD dans les transmissions de liaison montante et de liaison descendante. Un cadre pour la dérivation de la probabilité d'erreur sur les bits (BEP) est développé pour tous les systèmes utilisant différentes méthodes de détection. L'impact de la transmission imparfaite de CSIT a été étudié lorsque le précodage linéaire est implémenté pour la modulation spatiale de réception, ainsi que l'effet des corrélations d'antenne. Enfin, nous avons proposé d'adapter la modulation spatiale au récepteur avec l'environnement mmWave, en utilisant une formation de faisceau hybride au niveau de l'émetteur.

Title: Receive and Transmit Spatial Modulation Techniques for Low Complexity Devices.

Keywords : Spatial Modulation, MIMO, Precoding, Space Shift Keying, Receive Antenna Shift Keying

Abstract: Internet of Things is one of the keyword that represents the evolution in 5G that is able to connect the so-called Connected Devices (CD) to the network. These CDs are expected to require modest data rates and will be characterized by low resources in terms of both computation and energy consumption compared to other mobile multi-media devices. Spatial Modulation (SM) is proposed to be a promising solution to boost the data rate of the CD with a small (or no) increase in energy consumption. Inspired by the advantages of SM, the objective of this thesis is to study the performance of different transmission scheme based on the SM concept at the transmitter and at the receiver, for respectively an uplink and a downlink transmission between a BS and a CD. We proposed a global system where the higher computational complexity remains at the BS: The transmit SM is used for uplink, and the receive SM for downlink.

It is shown that with SM, an ON-OFF keying for uplink and Single Tap detector for downlink could be sufficient for the transmission at the CD. Also, with Extended SM schemes, we increased the spectral efficiency of SM to be equal to the number of antennas of CD in both uplink and downlink transmission. A framework for the derivation of the Bit Error Probability (BEP) is developed for all schemes with different detection methods. Impact of imperfect CSIT transmission has been studied when linear precoding is implemented for the receive spatial modulation, as well as the effect of antenna correlations. Finally, we proposed to adapte the spatial modulation at the receiver with the mmWave environment, using hybrid beamforming at the transmitter.